7-10-2019

Adaptive Closed-Loop Neuromorphic Controller for Use in Respiratory Pacing

Ricardo Siu
Florida International University, rsiu001@fiu.edu

FLORIDA INTERNATIONAL UNIVERSITY

Miami, Florida

ADAPTIVE CLOSED-LOOP NEUROMORPHIC CONTROLLER FOR USE IN RESPIRATORY PACING

A dissertation submitted in partial fulfillment of the

requirements for the degree of

DOCTOR OF PHILOSOPHY

in

BIOMEDICAL ENGINEERING

by

Ricardo Siu

2019

To: Dean John Volakis
College of Engineering and Computing

This dissertation, written by Ricardo Siu, and entitled Adaptive Closed-Loop Neuromorphic Controller for use in Respiratory Pacing, having been approved in respect to style and intellectual content, is referred to you for judgment.

We have read this dissertation and recommend that it be approved.

_____
James J. Abbas

_____
Armando Barreto

_____
Zachary Danziger

_____
David D. Fuller

_____
Jacob McPherson

_____
Ranu Jung, Major Professor

Date of Defense: July 10, 2019

The dissertation of Ricardo Siu is approved.

_____
Dean John Volakis
College of Engineering and Computing

_____
Andrés G. Gil
Vice President for Research and Economic Development
and Dean of the University Graduate School

Florida International University, 2019

ACKNOWLEDGMENTS

I would like to thank the Biomedical Engineering Department and its Coulter Foundation endowment for providing both professional and financial support, and the University Graduate School for awarding me with the Dissertation Year Fellowship to allow me to focus on the authoring of this dissertation. Significant portions of the research reported in this dissertation was supported by the National Institute of Neurological Disorders and Stroke of the National Institutes of Health (R01NS086088). The award also supported my research assistantship.

I would like to thank my advisor, Dr. Ranu Jung, for her support, guidance, and for challenging me to think scientifically throughout the entirety of my tenure in the Adaptive Neural Systems Laboratory. I would like to acknowledge my committee for their support throughout the project and for allowing me to tap into their various fields of expertise. I'd like to especially thank Dr. James Abbas for his immense help in clarifying concepts, providing feedback in all aspects of this dissertation, and light humor. I'd also like to thank my colleagues, Anil, Jefferson, and Brian, who provided assistance, both scientific and technical, throughout different stages of the work presented in this dissertation.

I would like to thank my friends in the Biomedical Engineering Graduate program without whom it would have been impossible to have had such an unforgettable and engaging experience. Finally, I would like to wholeheartedly thank my family for supporting me throughout all stages of my scientific endeavor, from when they ceded to buy a 6-year-old me all the dinosaur magazines they could find, to now.

ABSTRACT OF THE DISSERTATION

ADAPTIVE CLOSED-LOOP NEUROMORPHIC CONTROLLER FOR USE IN RESPIRATORY PACING

by

Ricardo Siu

Florida International University, 2019

Miami, Florida

Professor Ranu Jung, Major Professor

Respiratory pacing can treat ventilatory insufficiency through electrical stimulation of the respiratory muscles, or the respective innervating nerves, to induce ventilation. It avoids some of the adverse effects associated with mechanical ventilation such as risk of diaphragm atrophy and lung damage. However, current respiratory pacing systems provide stimulation in an open-loop manner. This often requires users to undergo frequent tuning sessions with trained clinicians if the specified stimulation parameters are unable to induce sufficient ventilation in the presence of time-varying changes in muscle properties, chest biomechanics, and metabolic demand. Lack of adaptation to these changes may lead to complications arising from hyperventilation or hypoventilation.

A novel adaptive closed-loop neuromorphic controller for respiratory pacing has been developed to address the need for closed-loop control respiratory pacing capable of responding to changes in metabolic production of CO_2, diaphragm

muscle health, and biomechanics. A 3-stage processes was utilized to develop the controller. First, an adaptive controller that could follow a preset within-breath volume profile was developed *in silico* and evaluated *in vivo* in anesthetized rats with an intact spinal cord or with diaphragm hemiparesis induced by spinal cord hemisection. Second, a neuromorphic computational model was developed to generate a desired trajectory that reflects changes in breath volume and respiratory rate in response to arterial CO_2 levels. An enhanced controller capable of generating and matching this model-based desired trajectory was evaluated *in silico* and *in vivo* on rats with depressed ventilation and diaphragm hemiparesis. Finally, the enhanced adaptive controller was modified for human-related biomechanics and CO_2 dynamics and evaluated *in silico* under changes of metabolic demand, presence of muscle fatigue, and after randomization of model parameters to reproduce expected between-subject differences. Results showed that the adaptive controller could adapt and modulate stimulation parameters and respiratory rate to follow a desired model-generated breath volume trajectory in response to dynamic arterial CO_2 levels. *In silico* studies aimed at assessing potential for clinical translation showed that an enhanced controller modified for human use could successfully control ventilation to achieve and maintain normocapnic arterial CO_2 levels. Overall, these results suggest that use of an adaptive closed-loop controller could lead to improved ventilatory outcomes and quality of life for users of adaptive respiratory pacing.

TABLE OF CONTENTS

CHAPTER PAGE

LIST OF TABLES

TABLE PAGE

LIST OF FIGURES

FIGURE PAGE

LIST OF ABBREVIATIONS

Carbon dioxide	CO_2
Oxygen	O_2
End tidal carbon dioxide	$etCO_2$
Partial pressure of arterial carbon dioxide	$PaCO_2$
Central pattern generator	CPG
Respiratory central pattern generator	rCPG
Pattern Generator	PG
Pattern Shaper	PS
Functional electrical stimulation	FES
Spinal cord injury	SCI
Incomplete spinal cord injury	iSCI
Root mean square error	RMSE
Inspiratory root mean square error	iRMSE
Spinal cord hemisection at the second cervical level	C2hX
Spinal cord hemisection at the second cervical level with pacing	C2hXp

CHAPTER 1

INTRODUCTION

The respiratory system carries out one of the main life-sustaining functions in the human body. It allows for delivery of oxygen to tissues and removal of carbon dioxide, a by-product of metabolic activity. Gas exchange between circulation and the outside air is driven by ventilation, the process of cycling outside air to the lungs. Yet, ventilatory insufficiency may occur due to traumatic, pharmacologic, or pathogenic factors affecting the central respiratory center, respiratory motoneurons, or the respiratory muscles. Examples of these include brainstem ischemia due to stroke, congenital central hypoventilation syndrome, and respiratory muscle paralysis due to cervical spinal cord injury. A 2018 report on spinal cord injury statistics in the United States listed that over 4,000 people admitted for hospitalization due to spinal cord injury required ventilatory assistance, with a quarter requiring ventilatory assistance after hospitalization (National Spinal Cord Injury Statistical Center, 2018).

Often, ventilatory insufficiency is treated by mechanical ventilation. Mechanical ventilation is efficient in carrying out gas exchange, however, there are significant drawbacks with chronic use. The diaphragm muscle is passive during mechanical ventilation which can lead to muscle atrophy after prolonged mechanical ventilator use, delaying the time required for recovery and weaning from the ventilator when recovery is possible (Goligher et al., 2015; Levine et al., 2008; Vassilakopoulos, 2012; Zambon et al., 2016). Mechanical ventilators are also often set to

hyperventilate the patients (Slutsky, 1993). Hyperventilation, while acceptable, can lead to lightheadedness and, in severe cases, loss of consciousness (Brown, 1953). Some ventilator modalities can also damage the alveoli by overinflating or by delivering pressures higher than the alveoli can withstand (Ricard et al., 2003; Vassilakopoulos, 2012). In addition, mechanical ventilators are often bulky and require invasive tubing. This reduces the patient's mobility, speech capabilities, and as result, their quality of life.

An alternative to mechanical ventilation is respiratory pacing. Respiratory pacing consists of implanting bilateral stimulating electrodes on either the phrenic nerve or in the diaphragm muscle near the neuromuscular junction and then delivering a current to elicit a diaphragmatic contraction to create a negative pressure and draw air into the lungs. This approach mimics the intrinsic ventilatory biomechanics and thus is less likely to cause exceedingly large pressures that might damage the alveoli (DiMarco, 2005; Khong et al., 2010; Onders, 2012). Atrophy is also ameliorated or avoided through this approach as the muscular contraction recruits muscle fibers, effectively exercising the muscle (Ayas et al., 1999; Garara et al., 2016; Pavlovic and Wendt, 2003; Reynolds et al., 2017).

The respiratory pacing systems currently in the market are open loop systems that require manipulation by a clinician or technician to determine suitable stimulation parameters. Not only does this increase the time required for setup, but the stimulation patterns selected do not account for future changes in diaphragm muscle recruitment requirements that might occur due to factors such as postural

changes, onset of fatigue, and/or electrode encapsulation. Additionally, ventilatory parameters also remain constant throughout normal use of the pacing system unless a technician intervenes and adjusts these parameters. This may lead to hypoventilation or hyperventilation as ventilatory demand can vary due to daily activity, such as during sleep or periods of physical activity. This highlights the need for a closed-loop controller capable of accounting for not only changes in respiratory muscle activation requirements but also to changes in metabolic demand if proper ventilatory function is to be achieved during chronic use of respiratory pacing systems.

An adaptive closed-loop neuromorphic controller was developed for use in respiratory pacing for treatment of hypoventilation. The design of the closed-loop controller is based on the organizational structure of mammalian biological ventilatory control, in which a central pattern generator determines ventilatory behavior while the downstream neural connections and effector muscles determine the resulting breath “shape”. This Pattern Generator (PG) Pattern Shaper (PS) controller was developed and characterized in *in silico* rat and human testbeds and *in vivo* on spinal cord intact and spinal cord injured rats. These studies showed that the PG/PS controller could determine a proper ventilatory response to changes in arterial CO_2 reflected in end-tidal CO_2 ($etCO_2$) and adapt stimulation amplitude and timing to match the proper ventilatory response independent of presence of injury and body weight. The results obtained through these studies suggest that use of this novel PG/PS respiratory pacing controller could reduce the need for monitoring the user, increase the range of activities the

user can perform without falling into hypoventilation, and eliminate the need for long and tedious stimulation tuning sessions.

1.1 Rationale

The work presented here describes the development of a novel closed-loop adaptive controller capable of regulating ventilatory behavior by mimicking the neurophysiological control of ventilation. Biological control of ventilation is a dynamic process controlled by a complex neural network within the lower brainstem that takes into consideration a multitude of factors of mechanical, chemical, and neural origin to generate a corresponding ventilatory pattern (Botros and Bruce, 1990; Molkov et al., 2017; Ogilvie et al., 1992; Smith et al., 1991, 2000, 2009). This central neural network controls activation of the respiratory muscles to elicit a negative pressure in the thoracic cavity, drawing air into the lungs for gas exchange to occur. The adaptive closed-loop controller presented in this work mimics this biological architecture of ventilatory control by implementing a computational model of the respiratory central pattern generator (rCPG) and a model of chest biomechanics to generate a ventilatory pattern appropriate for the current $PaCO_2$ or $etCO_2$ levels. A neural network with learning capabilities then defines and adapts stimulation parameters to eliciting the desired response set by the rCPG model.

Use of an adaptive closed-loop controller addresses the issues pertaining to open-loop control respiratory pacing systems. By being able to dynamically modulate ventilation, the adaptive PG/PS controller can respond to changes in metabolic

production of CO_2 that may result from change in activity levels. This expands the range of activities the user can engage in without suffering from inadequate ventilation, improving quality of life. Meanwhile, the adaptive PG/PS controller's ability to adapt stimulation parameters to match the desired ventilatory profile allows for the controller to always elicit the adequate breath volume profile independent of onset of fatigue, disease affecting ventilatory lung compliance or resistance, postural effects, or changes in diaphragm muscle mass due to stimulation-induced recovery from atrophy. These improvements over open-loop respiratory pacing systems may eventually allow chronic use of respiratory pacing technology that is analogous to biological ventilatory control, effectively restoring lost or impaired ventilatory function.

1.2 Design Goals

The overall goal of the thesis presented in this document is the development, characterization, and testing of a closed-loop adaptive respiratory pacing controller able to adapt on a breath-by-breath basis to changes in metabolic rate, muscle activation, and respiratory biomechanics. The adaptive closed-loop controller should be able to autonomously:

- Adapt stimulation parameters to elicit a desired breath volume profile independent of the system's intrinsic biomechanical properties.
- Maintain the desired elicited breath volume profile regardless of changes in muscle properties, such as fatigue.

- Determine an appropriate “desired” breath volume shape and duration based on a measure of the patient’s arterial CO_2 levels.
- Update the desired breath volume and time profile in response to dynamic changes in $PaCO_2$ levels to achieve and maintain normocapnia.

The specific aims listed below serve to accomplish these goals and further translation of the adaptive closed-loop controller for clinical use.

1.3 Specific Aims

1.3.1 Specific Aim 1

Specific Aim 1 is to develop a closed-loop adaptive respiratory pacing controller capable of autonomously defining the stimulation waveform required to achieve a previously defined breath volume at a fixed breathing frequency. This specific aim can be subdivided into the following sub aims:

a) Development of a computational platform based on rat ventilatory biomechanics in which the controller can be developed, optimized, and assessed prior to *in vivo* implementation.
b) *In vivo* assessment in spinal cord intact rats to assess the controller’s ability to match a desired ventilatory profile.
c) *In vivo* assessment in rats with spinal cord hemisection at the C2 level to assess the controller’s ability to match a desired ventilatory profile in the presence of diaphragm hemiparesis.

1.3.2 Specific Aim 2

Specific Aim 2 is to include in the closed-loop adaptive controller the ability to replicate the physiological ventilatory response to dynamic $PaCO_2$ changes by modulating breath volume and respiratory rate and to evoke this response through adaptation of stimulation parameters. This is accomplished as per the following sub aims:

a) Incorporation of an rCPG mathematical model into the closed-loop adaptive controller to mimic the physiological ventilatory response and integration of rat CO_2 dynamics into the previously developed computational platform to expand, optimize, and assess the controller's ability to respond to dynamic $PaCO_2$ levels prior to *in vivo* implementation.
b) *In vivo* evaluation of the adaptive closed-loop controller's ability to achieve and maintain normocapnia in a rat model of central ventilatory deficiency through anesthesia-induced ventilatory depression.
c) *In vivo* evaluation of the adaptive closed-loop controller's ability to achieve and maintain normocapnia after diaphragm hemiparesis in rats with spinal cord injury through spinal cord hemisection at the C2 level.

1.3.3 Specific Aim 3

Specific Aim 3 is to modify the adaptive closed-loop controller to make it suitable for human use in order to prepare the technology for human clinical trials. The results obtained in this aim serve to narrow the bridge between the preclinical

studies developed in Aims 1 and 2 and future clinical assessment of the PG/PS controller. Specific Aim 3 is subdivided into the following sub aims:

a) Development of a computational testbed based on human ventilatory biomechanics and CO_2 dynamics and conversion of the closed-loop adaptive controller to human use.
b) Computational assessment of the adaptive closed-loop controller's response to changes in CO_2 production due to metabolic demand changes in an integrated human computational testbed.
c) Computational assessment of the adaptive closed-loop controller's response to differences in muscle activation due to fatigue of the diaphragm muscle in an integrated human computational testbed.
d) Computational assessment of the adaptive closed-loop controller's ability to adapt to variations in ventilatory biomechanics and CO_2 dynamics in an integrated human computational testbed.

1.4 Organization of the dissertation

Chapter 1 serves as an introduction to the dissertation and discusses the rationale, design goals, specific aims, and organization of the dissertation.

Chapter 2 consists of a review of the pertinent literature, computational model selection, and rationale for the controller design.

Chapter 3 describes the design of the PS controller for diaphragmatic pacing and its assessment *in silico* and *in vivo*.

Chapter 4 presents the implementation of an adaptive PG into the PS controller and its development and assessment *in silico* and *in vivo*.

Chapter 5 focuses on the translational aspect of the adaptive PG/PS controller and its adaptation to a human implementation. It also presents a human computational testbed capable of assessing temporally acute and chronic factors that are of significance in a clinical setting.

Chapter 6 describes the significance of this thesis, its impact, limitations, and the future work to be addressed prior and during clinical implementation.

CHAPTER 2

LITERATURE REVIEW

2.1 The ventilatory control loop

Ventilation, when not under voluntary control, originates from complex neural networks in the lower brainstem, is determined by input from physiological sensors around the body, and is placed into action through respiratory muscle activity. From an engineering standpoint, the ventilatory control loop can be simplified and broken down into three main components: The effector muscles that activate to initiate gas exchange, the sensors consisting of central and peripheral chemoreceptors that detect changes in blood gas concentrations as a result of gas exchange, and the controller which resides in the brainstem and dictates the activity of the effectors based on input from the sensors. These three components work together to form a closed-loop system capable of maintaining proper levels of pH, pCO_2, and pO_2. An introduction to each of these components will follow in this section

2.1.1 Biomechanical action of respiratory muscles

While gas exchange in the alveoli is a passive process, cycling the air in the alveoli is not. The process through which air is cycled through the lungs is called ventilation. Ventilation occurs as the inspiratory muscles contract, expanding the thoracic cavity and thus creating negative pressure, drawing air into the lungs. When required, expiratory muscles also play a role by reducing the thoracic

volume and, through positive pressure, expel air out of the lungs. The muscles driving inspiration can be classified into three main groups. A large diameter dome-like internal muscle called the diaphragm located between the thoracic and abdominal cavity which when contracted flattens and thus increasing thoracic volume. Several smaller muscles within the rib's interspace which elevate the ribs and thus expand the thorax outwards called the external intercostal muscles. And a variety of smaller muscles collectively known as accessory inspiratory muscles. As for expiration, abdominal muscles serve to contract the abdominal wall, increasing abdominal pressure and pushing the diaphragm muscle towards the thorax while the internal intercostal muscles oppose the action of the external intercostal muscles (De Troyer et al., 2005; Sauleda et al., 1998).

The main inspiratory muscle, the diaphragm, normally performs the majority of the ventilatory work, contributing with up to 65% of the total inspiratory force (Jarosz et al., 2012). However, synergistic activation of inspiratory muscles leads to an effect greater than a simple additive contribution (De Troyer et al., 2005). The prime example being diaphragm and external intercostal coactivation. Studies have shown that activation of just the diaphragm can lead to a paradoxical movement of the rib cage as it is drawn into the thorax by the negative pressure exerted by the diaphragm. However, when coactivation between the diaphragm and external intercostals occur, this inverse movement of the rib cage does not occur and is instead moving in an outward motion, increasing thoracic space and thus negative pressure (De Troyer and Estenne, 1984). This activation between separate muscle groups also allows for other non-ventilatory behaviors such as

sighing, coughing, and sneezing to occur. However, these are beyond the scope of this thesis and will not be expanded up on.

Besides muscle activation patterns, there are several factors that influence how respiratory muscle contractions affect the resulting breath volume. From a mechanical perspective, these properties include chest compliance, airway resistance, and inertance. Chest compliance refers to the distensibility of the lung tissue. Stiff lung tissue, due to diseases such as fibrosis, lead to reduced compliance and thus require more work from the respiratory muscle to evoke adequate breath volumes (Nagels et al., 1980; Plantier et al., 2018). Likewise, increased airway resistance will require more work to draw air into the lungs, such is the case with asthma (Nagels et al., 1980). Inertance relates to the acceleration of gas during respiration. Studies have shown that if high, as may occur in obesity, elevated pulmonary pressures are required to evoke maximal ventilatory maneuvers (Nagels et al., 1980; Sharp et al., 1964).These factors, along with the force generated by the respiratory muscles, have an effect on the breath's volumetric profile.

2.1.2 Respiratory feedback sensors

As the respiratory muscles contract and drive gas exchange within the body, changes in blood gas levels occur throughout the vasculature and are detected by central and peripheral chemoreceptors. Peripheral chemoreceptors in the carotid and aortic bodies respond to changes in arterial O_2, and arterial CO_2. Likewise, central chemoreceptors located in the ventrolateral surface of the medulla

oblongata respond mostly to changes in pH of the cerebrospinal fluid (Barnett et al., 2017; MacLeod, 1925; Ursino and Magosso, 2002).

To prevent over-inflation of the lungs that might cause tissue damage, peripheral mechanoreceptors called pulmonary stretch receptors (PSR) provide mechanical feedback which serves as a crucial indicator for the termination of inspiration (Burnet and Hilaire, 1999; Rybak et al., 1997). This reflex is referred to as the Hering-Breuer reflex. PSRs also play a significant role in synchrony of the respiratory drive to an external source. Several studies in animals and humans have shown that removal of this feedback leads to an inability to synchronize intrinsic ventilation to mechanical ventilation (Abu-Shaweesh et al., 1999; Harris and St John, 2003; Simon et al., 2000).

For an extensive and comprehensive review of chemoreceptors and role in regulation of breathing please see (Guyenet, 2014).

2.1.3 Respiratory central pattern generator

The respiratory central pattern generator (rCPG) integrates a variety of neural inputs, including those from the chemoreceptors and mechanoreceptors discussed in the previous section, to generate a ventilatory pattern capable of maintaining adequate respiratory function. The rCPG has been shown to consist of several neuronal populations distributed along the pons and medulla that mutually interact to create a cyclical behavior from which respiratory rhythmogenesis arises (Kam et al., 2013; Ogilvie et al., 1992; Smith et al., 1991, 2009). Activity from some of these populations then travel through motor pathways to activate specific effector

muscles at specific phases of the respiratory cycle, providing fine temporal tuning of activation to elicit a specific ventilatory response.

Most respiratory rhythmogenesis models consist of a group of 5 or more mutually interacting neuronal populations where each is more active than the others at specific phases in the respiratory cycle. One of the earlier neural network models based on the cat respiratory central pattern generator consisted of five neuronal populations: pre-inspiratory, early-inspiratory, inspiratory, post-inspiratory, and expiratory neurons (Botros and Bruce, 1990). This activity-based model showed behavior that was comparable to that of experimental data and was able to predict responses typical to hypercapnic behavior when chemoreceptor drive was increased. The latest models have followed a similar trend and have been able to replicate behaviors ranging from ventilatory response to hypoxia (Rubin et al., 2011) to active expiration (Molkov et al., 2014a).

2.2 Impairments in respiratory control

The process of ventilation is dependent on a variety of components within the respiratory system. These being the central controller found in the medulla, the effector muscles that provide the mechanical action, and the chemoreceptors that assess the level of CO_2 or O_2 found in the arterial bloodstream and feed into the central controller. If any of these components or the links between them are compromised, ventilatory activity will be depressed or cease completely, leading to hypoventilation. Hypoventilation can lead to hypoxia, which can lead to cell death in extreme cases, and to hypercapnia, which can cause cerebral damage,

respiratory acidosis, and cardiac tissue damage. Hypoventilation can be the result of a variety of conditions. Among them are spinal cord injury (Brown et al., 2006; Linn et al., 2000; Zimmer et al., 2007), congenital central hypoventilation syndrome (Berry-Kravis et al., 2006; Kasi et al., 2016), and Pompe disease (Fuller et al., 2013; Smith et al., 2016).

Damage to the cervical region of the spinal cord above the level of C5, where the phrenic motoneurons exit the spinal cord, might cause damage to the phrenic motoneurons and descending respiratory pathways (Gonzalez-Bermejo et al., 2015). Trauma at this level can lead to weakening or paralysis of the respiratory muscles (Gardner et al., 1986; Linn et al., 2000). The 2018 National Spinal Cord Injury Statistical Center report indicates that 19.9% of individuals with tetraplegia in the USA are dependent on mechanical ventilation immediately after injury, with roughly 30% of this population unable to produce sufficient tidal volume for independent ventilation after rehabilitation (National Spinal Cord Injury Statistical Center, 2018).

Congenital Central Hypoventilation syndrome (CCHS) is a rare congenital disorder affecting the autonomic nervous system attributed to mutation of the PHOX2B gene (Trang et al., 2005; Weese-Mayer et al., 2003, 2009). CCHS presents itself with symptoms characteristic of autonomic nervous system dysregulation. These include hypoventilation, which becomes more severe during sleep, sporadic sweating, severe constipation, dysphagia, attenuated heart rate response to exercise, and decreased basal body temperature (Weese-Mayer et al., 1999). To

prevent hypoventilation, individuals with mild CCHS are often on assisted nocturnal ventilation, with more severe cases being on continuous ventilatory support (Berry-Kravis et al., 2006; Kasi et al., 2016).

Pompe disease is a muscular disease that results from lack of a glycogen hydrolyzing enzyme, leading to accumulation of glycogen in many tissues but most prominently muscle tissue leading to disfunction and, eventually, complete loss of function (Fuller et al., 2013; Kishnani et al., 2006; Smith et al., 2016). Pompe disease is characterized by rapid degradation of ventilatory function due diaphragm dysfunction. While enzyme replacement therapy treatments are available, these are unable to reach the central nervous system, which have been shown to be affected by glycogen depositions and significantly affect ventilatory function (Fuller et al., 2013).

2.3 Ventilatory support for ventilatory insufficiency

Hypoventilation, particularly chronic hypoventilation, can be a debilitating condition. Fortunately, there are several approaches for treatment of hypoventilation that have proven effective. These approaches differ in their mechanism of action, target demographic, and overall effect on patient health.

2.3.1 Mechanical ventilation

Mechanical ventilation is the gold standard in the clinical setting when concerned with ventilatory support. In the aforementioned cases, mechanical ventilators are widely used to maintain proper ventilation. Mechanical ventilators function by

creating a positive pressure that causes air to flow into the lungs. While mechanical ventilators have a clear and effective role in intensive care units and in acute respiratory assistance, chronic mechanical ventilator usage has considerable drawbacks (Claxton et al., 1998; Ricard et al., 2003). Due to forceful inflation of the lungs, alveolar damage might occur due to the high air pressures (Ricard et al., 2003). Another major concern with chronic mechanical ventilation is respiratory muscle atrophy (Andrew Shanely et al., 2002; Levine et al., 2008; Powers et al., 2002; Zambon et al., 2016). This has severe implications if ventilatory rehabilitation is expected. If the diaphragm muscle is weak, then weaning from a mechanical ventilator becomes difficult and the time to recovery severely increases (Powers et al., 2002). Other drawbacks of mechanical ventilators are the presence of intrusive tubing that affects speech, the size of the device makes it harder to transfer the patient, and there also exists a social stigma associated with mechanical ventilators (DiMarco, 1999). These factors may lead to a significant reduction in the quality of life of the ventilated individual.

2.3.2 Respiratory pacing

Respiratory pacing can serve as an alternative to mechanical ventilation. This approach relies on functional electrical stimulation (FES) to cause a contraction of the diaphragm muscle to create negative pressure within the thoracic cavity and thus draw air into the lungs, effectively eliciting a breath (Chervin and Guilleminault, 1994; DiMarco, 2009; Glenn et al., 1988; Onders, 2012). FES triggers neural activity in the affected neural tissue by delivering pulse trains. Pulse

trains are delivered to the phrenic nerve directly via a cuff electrode surrounding the nerve itself, or indirectly via intramuscular stimulation through stimulating electrodes in the proximity of the phrenic innervation site of the diaphragm.

FES used for artificial ventilation circumvents several of the problems found with mechanical ventilators. Negative pressure produced by diaphragmatic contraction reduces the likelihood of alveolar damage and atelectasis. Atrophy is also ameliorated or avoided due to repetitive diaphragmatic contraction. Even in cases where atrophy has already occurred, respiratory pacing was shown to have caused some recovery in diaphragm muscle fiber size (Ayas et al., 1999). Given that air is no longer being delivered to the patient through the mouth or trachea, tubing is no longer a concern. This improves mobility of the user, speech, removes the stigma associated with intubation, along with other benefits (Brown et al., 2006; DiMarco, 2009; Masmoudi et al., 2017; Onders, 2012; Onders et al., 2007).

2.3.3 Contraindications of respiratory pacing

While respiratory pacing has been shown to have a positive effect on respiratory outcome in patients with spinal cord injury (DiMarco, 2005, 2018; Garara et al., 2016; Glenn et al., 1984; Le Pimpec-Barthes et al., 2011; Onders, 2012), such has not been the case in all clinical trials. Respiratory pacing is only possible when the phrenic nerve is intact and the diaphragm is properly innervated for the neural signals to be transmitted to the muscle fibers to cause a contraction (Chervin and Guilleminault, 1994; Gonzalez-Bermejo et al., 2015; Jarosz et al., 2012; Lucangelo et al., 2008). An example of respiratory pacing failing to improve respiratory

outcomes was seen in a controversial study assessing effectiveness and safety of pacing on patients with Amyotrophic Lateral Sclerosis (ALS) (Gonzalez-Bermejo et al., 2016; McDermott et al., 2015). This study showed that, unlike during mechanical ventilation, respiratory pacing was associated with decreased survival in patients with ALS. The study raised the possibility of pacing induced neuromuscular damage seen in animal models of ALS, which differs from healthy models (Amirjani et al., 2012; Lepore et al., 2010). Additionally, given that ALS causes degeneration of the neural and muscular tissue, electrical stimulation of this damaged tissue likely adversely affects the behavior of the neuromuscular system, either by decreased conductivity at the phrenic nerve level or reduced contractile force capacity at the diaphragm level. Thus, selection criteria must be clearly defined and followed prior to selection for respiratory pacing.

2.4 Stimulation approaches for respiratory pacing

Currently, three major approaches to respiratory pacing have been explored: diaphragmatic stimulation, phrenic nerve stimulation, and spinal cord stimulation. Each approach have their own benefits and drawbacks; however, increased, however, increased performance comes with the cost of increased risk. Diaphragm pacing poses a low surgical risk but requires multiple stimulating electrodes to elicit the same response as observed in the other modalities. Phrenic nerve stimulation introduces risk of phrenic nerve damage, which may permanently compromise ventilatory function. However, if the stimulating electrodes are implanted properly, widespread diaphragm contraction is likely to occur at a much lower charge than

diaphragmatic stimulation (Onders, 2012). Finally, spinal cord stimulation poses the greatest risk as damage to the spinal cord can affect function in several other areas, however, by stimulating the premotor neurons, the muscle fibers are recruited in a physiological manner, producing a more natural contraction. Additionally, spinal cord stimulation of several muscles might lead to better synergistic activation between the muscle sets, improve ventilatory capacity (DiMarco et al., 2005, 2018).

2.5 Current respiratory pacing technology

Current phrenic pacing systems in the market are the Astrostim (Astrotech, Tempere, Finland) and the Vienna phrenic pacemaker (Medimplant, Vienna, Austria) in Europe and the Avery Breathing Pacemaker System (Avery Biomedical Devices, NY, USA) (Khong et al., 2010), in the United States; these systems vary mostly in their electrode technology (Onders, 2012). Only one system is available commercially for diaphragmatic pacing, the NeuRx RA/4 System (Synapse Biomedical, OH, USA). All four of these systems rely on an external stimulator on which stimulation parameters are manually configured for open-loop stimulation.

The characteristic pulse amplitude, pulse width, and pulse frequency dictate the level of muscular contraction in FES. These parameters along with cycle period are often set by a technician or clinician to obtain a desired tidal volume and respiratory rate. This implies that a technician/clinician must be consulted whenever changes to these stimulation parameters are required. Aside from adding to the cost of the treatment, this open-loop configuration does not account

for changes such as changes in postural loading to the diaphragm, onset of pacing-induced muscle fatigue, and changes in electrode properties. Thus, a closed-loop respiratory pacing controller that can account for these changes is desired.

2.6 Closed-loop FES control schemes

Despite clear limitations on open-loop strategies for control of FES of skeletal muscle, lack of reliability, robustness, and sub-optimal performance have led to limited availability of closed-loop FES control systems. Furthermore, most proposed FES closed-loop control algorithms target control of limb movement (Abbas and Chizeck, 1991; Cienfuegos et al., 2017; Davoodi and Andrews, 1998; dos Santos et al., 2016; Feng Wang and Andrews, 1994; Ferrante et al., 2016; Ferrarin et al., 2001; Freeman et al., 2009; Ibrahim et al., 2011; Kim et al., 2009; Resquín et al., 2016; Wassink and Keller, 2004), with only a few studies addressing closed-loop control of respiratory pacing (Mercier et al., 2017; Zbrzeski et al., 2016). However, these closed-loop respiratory pacing approaches were still in their infancy and required further investigation prior to clinical consideration.

Respiratory pacing poses additional demands on robustness and reliability of the control algorithm as failure may lead to lung damage, severe hypoventilation, or complete cessation of breathing. Traditional PID controllers may provide acceptable tracking performance for short periods of time and are often resistant to perturbations, but are slow to adapt and fail to account for non-linear and time-dependent muscular and biomechanical changes (Resquín et al., 2016; Riess and Abbas, 2000). Adaptive model-based closed-loop control approaches require

extensive model configuration for each user, requiring extensive parametrization and affecting performance over time if those parameters do change (Ferrarin et al., 2001; Gwo-Ching Chang et al., 1997). Fuzzy logic approaches (Davoodi and Andrews, 1998; Ibrahim et al., 2011) require delineation of control rules and may not be able to account for unforeseen perturbations to the system.

Respiratory pacing adds another dimension of complexity compared to other FES applications since residual intrinsic ventilatory activity may influence controller performance. The presence of intrinsic muscle activation requires for the control algorithm used to be able to account for the presence of the intrinsic drive and either entrain to the intrinsic drive or cause entrainment of the intrinsic drive. Otherwise, tracking errors are likely to occur as these two would conflict with one another and adversely affect controller performance.

2.7 Pattern Generator Pattern Shaper control

Previously, an adaptive neuromorphic paradigm for FES closed-loop control had been developed for cyclic lower limb locomotion (Abbas and Chizeck, 1991; Abbas and Triolo, 1997; Fairchild et al., 2010; Ichihara et al., 2009; Kim et al., 2009; Riess and Abbas, 2000). This adaptive neuromorphic controller consists of a pattern generator (PG) and a pattern shaper (PS). The PS is a single layer neural network with weighted, time-shifted, overlapping activation profiles. The output of the PS at each time step is then obtained as a weighted summation of the neuron outputs at that time step.

Studies done to assess the PG/PS controller's performance in lower limb control included computational studies for parametrization of controller variables (Stites and Abbas, 2000), comparisons against PID controller performance (Riess and Abbas, 2000), and experimental studies in both animal and humans that showed that the PG/PS controller was capable of producing muscle contractions that followed the physiological movement pattern while adapting to muscle fatigue (Abbas and Chizeck, 1995; Abbas and Triolo, 1997; Fairchild et al., 2010; Ichihara et al., 2009; Kim et al., 2008).

The adaptive ventilatory controller developed in this dissertation is based on this previously developed adaptive controller for locomotion. The following chapters of this dissertation will explicitly describe how the controller has been adapted and improved for the purpose of controlling ventilatory function through FES and its assessment both *in silico* and *in vivo*.

CHAPTER 3

CONTROL OF BREATH VOLUME THROUGH THE USE OF AN ADAPTIVE CLOSED-LOOP PATTERN SHAPER

3.1 Introduction

When the autonomic control of ventilation is compromised, such as with cervical spinal cord injury or central hypoventilation syndrome, means of artificial ventilation are often needed. Dependence on mechanical ventilation to treat hypoventilation can cause a considerable impact on quality of life. Although mechanical ventilators are widely used to treat respiratory insufficiency (Kacmarek, 2011), mechanical ventilation can in itself have detrimental effects on lung health.(Claxton et al., 1998; Ricard et al., 2003) Positive pressure mechanical ventilators have been reported to cause alveolar damage and lead to diaphragm muscle atrophy, with studies indicating onset of atrophy after 18 hours of mechanical ventilation.(Andrew Shanely et al., 2002; Levine et al., 2008; Ricard et al., 2003; Zambon et al., 2016)

Restoration of ventilation through electrical stimulation (pacing) is an alternative to mechanical ventilators in cases where the phrenic nerve is intact, but the pre-motor neurons have been damaged or when the respiratory central pattern generator (rCPG) has been compromised. Pacing can be accomplished through stimulating cuff electrodes on the phrenic nerve, intramuscular electrodes in the diaphragm muscle, or catheter-based transvenous electrodes.(Reynolds et al., 2017) A series of stimulating pulses delivered to the target cause contraction of the diaphragm

muscle and thus elicit a functional breath.(Chervin and Guilleminault, 1994; DiMarco, 1999, 2009; Glenn et al., 1988; Onders, 2012) Pacing approaches have the benefit of neural activation of the diaphragm to produce negative pressure ventilation, eliciting a breath in a more physiological manner. Pacing could also slow or reverse the development of muscle atrophy, and possibly promote central neuroplasticity for improved recovery.(DiMarco, 2009; Masmoudi et al., 2017; Onders, 2012; Onders et al., 2007)

Current commercially-available systems operate in an open-loop manner, in which the clinician must determine and set stimulation parameters that are suitable for ventilatory pacing for a given individual.(Onders, 2012) However, there is a need to adjust the stimulation parameters for pacing at a short time-scale in response to physiological and metabolic demand, postural load changes,(Winslow and Rozovsky, 2003) and stimulation-induced muscle fatigue. Changes over the long time-scale such as electrode encapsulation or muscle atrophy, should also be accounted for.

The limitations of an open-loop system could be addressed by an adaptive closed-loop bioelectronic control system that adjusts stimulation to provide sufficient ventilation to the user. To achieve efficient and responsive ventilation, the controller should be able to automatically and repeatably produce a suitable breath volume profile and adapt respiratory rate with minimal technician intervention. As an initial step to develop an adaptive ventilatory controller for diaphragmatic pacing, the aims of the present study were the design and development of a

neuromorphic closed-loop adaptive controller capable of achieving and maintaining a desired breath volume profile at a pre-determined fixed respiratory rate.

An adaptive ventilatory pacing controller, shown in Figure 1, was developed following a neuromorphic pattern generator/pattern shaper (PG/PS) architecture.(Abbas and Triolo, 1997; Jung, 2018; Kim et al., 2009) A computational model for the chest and diaphragm in the adult rat was used for initial development of the controller and for selection of suitable PS parameters. A rodent model of incomplete spinal cord injury was used to assess the ability of the controller to ameliorate hypoventilation. Hemisection of the spinal cord at the C2 level causes hemiparesis of the ipsilateral hemidiaphragm and leads to significant reduction in tidal volume.(Doperalski et al., 2008; Dougherty et al., 2012a; Sandhu et al., 2009) *In vivo* studies in both spinal cord intact and left C2-hemisected (left C2hX) animals confirmed that PS-controlled adaptive pacing could achieve and maintain a desired volume profile. In left C2hX animals, tidal volume was restored to values observed prior to the hemisection. Pacing also caused a decrease in the elevated end-tidal CO_2 ($etCO_2$) values that resulted from the reduced ventilation after hemisection. Because breathing itself is dynamic, the development of a similarly dynamic neuromorphic controller for ventilation represents an important step in expansion of neurotechnology that is able to, ultimately, replicate and replace autonomic function after ventilatory impairment.

3.2 Methods

3.2.1 Animal care and surgical procedure

In vivo studies were conducted on spontaneously breathing, adult, male Sprague Dawley rats (open loop stimulation *n = 1*, 415 g, 4.3 months old, adaptive stimulation spinal cord intact *n = 9*, 372 ± 74 g, 4.1 ± 0.9 months old; adaptive stimulation left C2hX *n = 7*; 419 ± 121 g, 4.4 ± 1.2 months old) with the approval of the Institutional Animal Care and Use Committee of Florida International University. Rats were initially anesthetized with intraperitoneal pentobarbital (50 mg/kg) followed by supplemental inhaled isoflurane (1.0 – 2.5%) in 100% O_2. The plane of anesthesia was assessed via a toe-pinch reflex. Body temperature was maintained between 36-38 °C via a heating lamp. A pulse oximeter sensor monitored SpO_2. A tracheal tube was inserted after a tracheostomy and sutured to the trachea. A small animal pneumotachometer (PTM Type HSE-73-0980, Harvard Apparatus, Holliston, MA) connected directly to the tracheal tube measured air flow. Flow was integrated (PI-1000, CWE Inc., Ardmore, PA) to obtain breath volume. A capnograph (CapStar-100, CWE Inc., Ardmore, PA) monitored end-tidal CO_2 ($etCO_2$) throughout the experiment. 30G stainless steel needle electrodes were inserted subcutaneously to monitor cardiac activity via electrocardiogram. Stainless steel wire intramuscular recording electrodes (SS-304, 44 AWG, AM-Systems, Carlsborg, PA) were inserted below the tongue for recording of genioglossus (GG) muscle activity in some animals (n=2). GG activity

was recorded to assess synchrony between the intrinsic inspiratory drive and paced breaths.

A ventral incision provided access to the caudal aspect of the diaphragm muscle. A handheld stimulator (DigiStim 3 plus, Neuro Technologies) with a blunted needle delivered constant current pulses at 1 Hz to map the location of the neuromuscular junction. Stimulation electrodes were implanted near this location. The peritoneal incision remained open to provide visualization of the diaphragm during assessment of muscle twitch thresholds, after which the incision was sutured closed.

A lateral C2 hemisection was performed prior to stimulation in 7 rats to use as an incomplete spinal cord injury (iSCI) model. A dorsal C2 laminectomy was performed to expose the cervical spinal cord. Once exposed, a microscalpel was used to perforate the dura and to sever the left half of the spinal cord at the C2 level. Observing a considerable decrease in tidal volume provided a functional assessment of a proper hemisection. Spinal tissue was also collected for histological assessment to ensure that the hemisection resulted in severance of all descending phrenic pathways.

3.2.2 Diaphragmatic stimulation

Diaphragmatic pacing was conducted using single stranded, stainless steel electrodes (SS-304, 44 AWG, AM-Systems, Carlsborg, PA) implanted bilaterally through the abdominal fascia of the diaphragm or through the muscle itself with the use of a suture needle (10 mm, 3/8th circle, cutting, Havel's Inc., Cincinnati,

OH). Stimulation was performed using a constant-current programmable stimulator (FNS-16, CWE Inc., Ardmore, PA) delivering cathodic first, biphasic current pulses of 200 μs/phase at 75Hz with amplitude modulated every 40 ms by the adaptive PS controller. The 75 Hz stimulation frequency was shown to provide tetanic contractions in rat skeletal muscle.(Fairchild et al., 2010; Jung et al., 2009) Pulses delivered at 75 Hz were also found to consistently elicit effective tetanic contractions of the diaphragm during preliminary trials and thus this pulse frequency was maintained for all trials in this study. In all experimental trials the initial current pulse amplitude was set to zero which automatically changed once the PS controller was initiated. Current amplitude was determined by scaling the PS controller output to the maximum limit for current amplitude set for each stimulating channel. The maximum current amplitude was set for each stimulating channel at 4 times the twitch threshold amplitude observed for each hemidiaphragm during open-loop stimulation. Maximum current amplitude values for the stimulated hemi-diaphragms ranged from 0.5 mA to 4.0 mA; the FNS-16 stimulator resolution for the current amplitude is 0.001 mA.

3.2.3 Experimental protocol

To assess the controller's ability to achieve a desired ventilatory profile in both spinal cord intact and left C2hX rats, the controller was set to modulate stimulation to match a desired breath volume profile with a constant cycle period. The desired breath volume profile and cycle period were obtained from baseline ventilatory data recorded for at least one minute prior to stimulation in each trial in spinal cord

intact animals and in multiple intermittent recordings prior to injury for the trials in left C2hX animal. The desired breath volume profile was defined by averaging all recorded breathing cycles except for sighs. The averaging algorithm automatically excluded breaths identified as sighs based on preliminary data and literature that describes sighs as being breaths with a tidal volume of at least twice the normal tidal volume.(Wilhelm et al., 2001)

To illustrate the ability of the controller to modulate breath volume in spinal cord intact animals, the desired breath volume profile was scaled by 120%. This scaling factor was selected to match the approximately 20% increase in tidal volume observed in preliminary studies on anesthetized spinal intact rats that were exposed to a hypercapnic challenge. In left C2hX animals, the desired breath volume profile was maintained at pre-hemisection values unless an increase in desired breath volume was required to promote in-phase synchronization. The duration of the desired breath cycle was set to match the duration of the breath cycle prior to the trial; if required to improve the likelihood of synchronization, this value was adjusted (within ± 10%). The desired breath volume profile was maintained constant throughout the trial.

In trials in spinal cord intact animals, each trial consisted of at least one minute of spontaneous breathing, followed by at least 100 cycles of pacing with an increased desired breath volume of 120% of the baseline breath volume. There were one to eight trials per spinal cord intact animal. In animals with iSCI, prior to hemisection, trials were defined as multiple recordings of one minute each of spontaneous

breathing (*n=3* per rat, with the exception of rat 11 where *n=2*). After hemisection, trials were defined as at least one minute of spontaneous breathing followed by at least 200 pacing cycles. There were two to six trials post-hemisection per animal.

Expiratory muscles were not stimulated and therefore expiration was passive. A rest period of 15 minutes was allowed between trials to allow the diaphragm to recover from stimulation-induced fatigue. In left C2hX animals, a mechanical ventilator was used to maintain proper ventilation during these rest periods and to maintain $etCO_2$ at nominal levels.

3.2.4 Performance measures

The adaptive controller adapts the stimulation output to the magnitude of the error between the desired volume and the measured volume at a given instant. To quantify the deviation from the desired volume and the achieved volume traces over the portion of the respiratory cycle directly affected by inspiratory muscle activation, the inspiratory root mean square error (iRMSE) % for each pacing cycle was defined as

$$iRMSE = \frac{100}{\max(V_D)} \sqrt{\frac{1}{q} \sum_{i=i_{insp}}^{q} ei^2} \qquad (1)$$

Where $max(V_D)$ is the peak value for the desired volume, i_{INSP} denotes the time step at the start of inspiration, q the number of time steps in the inspiratory phase of the desired breath volume profile, and e_i the instantaneous error at time step i.

The basis of this error value across several pacing cycles has been used as an indicator of controller accuracy in previous studies regarding evaluation of the PG/PS controller (Abbas and Triolo, 1997; Riess and Abbas, 2000; Stites and Abbas, 2000). In the current study, the number of pacing cycles required for iRMSE % to fall below a certain threshold and maintain it for at least 10 pacing cycles served as an indicator of controller speed of adaptation. A threshold of 5% iRMSE was selected for simulation studies. In animal studies, due to inherent breath-to-breath variability in the inspiratory volume profile, the iRMSE threshold was elevated to 10%. The mean and standard deviation of the iRMSE of the last 40 pacing cycles of the pacing period were used to assess controller performance.

In addition to the iRMSE measures, the effectiveness of pacing in left C2hX animals was assessed by evaluating tidal volume and $etCO_2$ during pacing. Values for these measures were tabulated under pre-hemisection, post-hemisection without pacing, and post-hemisection with pacing conditions from 40 pacing cycles for tidal volume and 10 pacing cycles for $etCO_2$ per condition. Analyzing tidal volume over 40 cycles allowed assessment of the controller's ability to maintain a constant tidal volume over a large number of cycles, while selecting 10 cycles of $etCO_2$ allowed assessment of the transient response of $etCO_2$ to pacing.

For tidal volume, the breath cycles post-hemisection without pacing were obtained just prior to initializing pacing. For $etCO_2$, the breath cycles post-hemisection were collected after synchronization between the pacing and intrinsic breathing occurred. This was done to utilize tidal volumes similar to eupnea, thus minimizing

the potentially confounding effect of expiratory breath volume on $etCO_2$ values. Post-hemisection with pacing cycles were obtained prior to the end of the 200-pacing cycle pacing period in both cases.

3.2.5 Histology

After completion of the experimental protocols each left C2hX animal was perfused with phosphate buffer solution followed by 4% paraformaldehyde. The spinal cord was extracted from the atlas to the C7 vertebra and placed in 4% paraformaldehyde and then transferred to 30% sucrose for dehydration. Spinal cords were then frozen and cryosectioned to obtain 10 µm longitudinal sections. The presence of a gap in the ventrolateral tissue observed under light microscopy of unstained sections was used to indicate completeness of the spinal cord hemisection.

3.2.6 Experimental design and statistical analysis

A post-hoc t-test power analysis was performed to assess whether the number of spinal cord intact (n = 9) and spinal cord left C2hX (n = 7) animals provided sufficient power for statistical analysis of the number of pacing cycles required to achieve 10% iRMSE or less. Based on descriptive statistics obtained for this measure (spinal cord intact = 16.06 ± 6.66 pacing cycles, left C2hX = 58.8 ± 27.25 pacing cycles) and an alpha of 0.05, the test provided a power of 0.98 (Df = 14). A repeated measures ANOVA power analysis was also performed post-hoc to assess if 40 pacing cycles was sufficient to identify a difference in tidal volume amongst the pre-hemisection, post-hemisection without pacing, and post-

hemisection with pacing conditions in the left C2hX rats. A similar analysis was done to determine if 10 pacing cycles of $etCO_2$ were sufficient. The resulting power was 1.00 and 0.95 for tidal volume and $etCO_2$, respectively. All power analysis was performed using G*Power 3.1.9.2.(Faul et al., 2007) Descriptive statistics were obtained using SPSS (IBM, Armonk, NY).

To assess the effect of pacing on tidal volume and $etCO_2$ after hemisection, a general linear mixed model (Cnaan et al., 1997) was used with fixed effects of trial number and condition (spinal cord intact, hemisection without pacing, and hemisection with pacing) and random intercept effects of both trial number and measurement occasion (last 40 breath measurements within each trial for tidal volume and last 10 breath measurements for $etCO_2$). The generalized linear mixed model was performed using SAS 9.4 (SAS Institute Inc., Cary, NC).

3.2.7 PG/PS controller design

The PG/PS controller utilized in this study is based on the original PG/PS controller that was designed and used to control cyclic limb movements using functional neuromuscular stimulation. The PG/PS controller had the ability to compensate for muscle fatigue by adapting stimulation pulse parameters and charge delivery to achieve the desired functional outcome.(Abbas and Chizeck, 1991; Abbas and Triolo, 1997; Fairchild et al., 2010; Ichihara et al., 2009; Jung et al., 2009; Riess and Abbas, 2000; Stites and Abbas, 2000) The PG module generates the pacing cycle period while the PS module adapts to define stimulation parameters that elicit a desired action. In the current study, a fixed frequency oscillator was used as the

PG to produce a fixed respiratory frequency that did not change from breath-to-breath. The PS module consisted of a single-layer neural network with the output profile of each neuron being a raised cosine function; the outputs of the neurons in the set are time-shifted with respect to each other. In its current implementation, the number of neurons was set as 25, with one reaching its peak every 40 ms (which matched the frequency at which the controller sends an update to the stimulator). To create a stimulation pulse train with frequency of 75 Hz, each update to the stimulator resulted in the production of three pulses of identical amplitude. Each neuron reaches its peak activity at a specific time-step but its temporal profile overlaps across a specified number of neighboring neurons. The width of the temporal profile determines the number of overlapping activation profiles and is defined in the controller by the parameter n_a. The output, *z(t)*, of the PS at each time step is the weighted summation of the non-zero neuron outputs at that time step and is given by

$$z(t) = \sum_{j=1}^{n_a} w_j(t) y_j(t) \quad (2)$$

Where the output of a neuron *j* at time *t* is defined as $y_j(t)$, with the weight for that specific neuron set as $w_j(t)$. The output, $z(t)$, is restricted to the range of values between 0 and 1 and then scaled by the maximum current amplitude defined for each channel.

Each scaling factor, or weight, for each neuronal output is modified based on an instantaneous error between a pre-established target breath volume cycle profile

and the measured volume signal. The controller works in a feedforward manner by modifying each neuron's weight at each time step based on the measured value of error at that time. The change in weights for neuron *j* is

$$\Delta w_j(t) = \eta e(t) \sum_{i=1}^{n_p} \frac{1}{n_p} y_j(t - tT) \quad (3)$$

Where η is the learning rate, $e(t)$ is the instantaneous error at time *t*, *T* is the update period, n_p is number of past activations over which the error is averaged, and *i* the n_p index.

Computer simulations were carried out to elucidate the range of parameters over which adaptation would be stable and errors minimized. These ranges were then used in animal studies to assess *in vivo* implementation of the controller.

3.2.8 Musculoskeletal diaphragm model

A computational model of diaphragm and chest biomechanics was used as a testbed to design and develop the PG/PS adaptive controller prior to *in vivo* evaluation. The musculoskeletal model and PG/PS controller were implemented in the LABVIEW programming environment using the Control Design and Simulation module (National Instruments Inc., Austin, TX). The chest model is a biomechanical model in which the mechanical action of diaphragm muscle displacement is assumed to correspond linearly to breath volume.(Lessard, 2009; Milhorn, 1966) A proportionality constant, k_p, was implemented to calculate breath volume from muscle displacement. The mechanical action of the diaphragm is defined by the inertance of the chest system, m_L, the elastance of the system, K_L,

and the damping coefficient of the system, B_L. Chest biomechanics was described mathematically as a function of diaphragm contractile force via the following equation,

$$k_p F_{dia} = m_L \frac{d^2x}{dt} + B_L \frac{dx}{dt} + K_L x \quad (4)$$

Where the input to the model is the force exerted by the diaphragm muscle, F_{dia}, and the output is the displacement of the diaphragm, x. The mechanical circuit is shown in Figure 2(A).

The diaphragm muscle model was based off the multiplicative quadriceps muscle model with reverse recruitment shown in Figure 2(B).(Abbas and Chizeck, 1991; Teixeira et al., 1991) Briefly, the total force exerted by the muscle, F_{dia}, is given by the product of a dynamic muscle activation model output A_k, force-length factor A_{FL}, and a force-velocity factor A_{FV}.

$$F_{dia}(t) = A_k(t) A_{FL}(t) A_{FV}(t) \quad (5)$$

Intrinsically, fatigue-resistant fibers are recruited first while fast-fatigable fibers are recruited later when there is a higher demand for recruitment of muscle fibers. However, due to the nature of extraneural electrical stimulation in which larger fibers have a lower threshold, the larger fast fatigable fibers are recruited before the slow fatigue-resistant fibers are activated resulting in reverse recruitment.(Peckham and Knutson, 2005) This reverse recruitment produces nonlinear input/output properties that were modeled using

$$r(t) = \gamma_0 + \gamma_1[Stim(t) - D] + \gamma_2[Stim(t) - D]^2 + \gamma_3[Stim(t) - D]^3 \quad (6)$$

in which muscle recruitment, *r(t),* is calculated to mimic the intrinsic recruitment curve observed experimentally in previous studies in rats.(Mantilla et al., 2010) *D* represents the dead band, or the pulse amplitude below which no fibers are recruited, and the constants, γ_0, γ_1, and γ_3 were modified to obtain a cubic curve that fit these experimental results.

The force generated as fiber recruitment increases is a dynamic process which was modeled using a second-order autoregressive, moving average (ARMA) model with input and output delays.(Abbas and Chizeck, 1991)

$$a_k(t) = a_1 A_k(t - T) + a_2 A_k(t - 2T) + b_0 r(t - T) \quad (7)$$

Constants a_1 and a_2 define the linear dynamics of the model, while b_0 defines the muscle input gain. The delay T, was based on the model update period of 14 ms.

The force-length component, A_{FL}, and force-velocity component, A_{FV}, serve as scaling factors to the force generated by the dynamic model. Force-length factor was estimated with a quadratic equation,

$$A_{FL}(t) = 1 - \frac{[L(t) - L_0(t)]^2}{L_w^2} \quad (8)$$

with L being the length at instant t, L_o the reference length, and L_w the maximum length of the muscle.

The force-velocity factor was obtained via

$$A_{FV}(t) = \frac{K_V[V_{max} - V(t)]}{K_V[V_{max}] + V(t)} \quad (9)$$

with K_V being the force-velocity slope and V_{max} the maximum shortening velocity. Constants for all equations and their values can be found in Table 1.

3.2.9 Computational trials for parametrization of suitable controller parameters

A previous study has illustrated the ability of the PS controller to adapt across a wide range of controller parameters.(Stites and Abbas, 2000) However, in this study the PS was assigned to follow a trajectory for limb movement that differs considerably in profile, amplitude, and duration from one derived from respiratory volume. A LabVIEW implementation of the PS controller and musculoskeletal model was used to carry out the computer simulations. All simulations utilized a predetermined desired trajectory from a baseline volume profile obtained from experimental data.

The controller parameters varied in computer simulation studies were: number of active neurons at any one time-step, number of past neuron activations over which to average the instantaneous error, and learning rate. The controller update frequency was set at 25 Hz and the number of neurons was set to 25. Learning rate values tested were 0.0001, 0.0005, 0.001, 0.002, 0.003, and 0.004. The values tested for the number of active neurons tested ranged from 1 to 19 (in steps of 2) and the values tested for the number of past activations ranged from 2 to 20 (in steps of 2). Each of these simulated trials were done for a length of 100 pacing cycles.

To determine the controller parameters suitable for fast, accurate, and stable performance, only parameter triads that would pass selection criteria were selected. These criteria were: iRMSE below 5% within 20 pacing cycles, mean iRMSE below 5% and a standard deviation below 2.5% iRMSE after <5% iRMSE was attained. Processing of trial results for parameter set selection was performed using MATLAB (Mathworks Inc., Natick, MA).

3.3 Results

3.3.1 Simulations demonstrate the pattern shaping capabilities of the controller

Using the musculoskeletal model as a developmental testbed, a closed-loop PG/PS controller capable of adapting and modulating the stimulation output to elicit a desired breath volume profile was developed. Results from a sample simulation trial using 3 active neurons with 6 past activation values with a learning rate of 0.001 are presented in Figure 3. In Figure 3(A, B), volume and stimulation traces for the first ten pacing cycles show how the controller can adapt the stimulation levels so that the measured volume profile matches a pre-set desired volume profile. Figure 3(C) shows that in pacing cycles 91-100 the measured and desired volume profiles still match closely. Figures 3(E) and 3(F) show how iRMSE and charge delivered changed over a 100-pacing cycle trial period. When the trial starts, a decrease in iRMSE to a value below 5% iRMSE by pacing cycle # 5 is seen. For the rest of the trial, iRMSE remains well below 5% and finally decreases to an average of 0.96% in the last 10 pacing cycles of the simulation trial. Charge delivered per pacing cycle increases initially as the controller adapts to increase

the elicited breath volume profile and match the desired profile. Given that the controller is continuously adapting, charge delivered then decreases as the controller fine tunes the neuronal weights to further reduce iRMSE. Once the error is at a minimum, the charge delivered remains constant for the rest of the trial unless there is a change in the error.

3.3.2 Synchronization between intrinsic breaths and paced breaths *in vivo*

In vivo trials demonstrated the ability of the controller to adapt to fatigue and reduce inspiratory RMSE in both spinal cord intact and left C2hX anesthetized rats. However, unlike in computational studies, the residual intrinsic respiratory drive interacts with the controller in a manner that significantly affects the controller's performance. Figure 4, which shows the first 100 seconds of a trial, depicts how the intrinsic respiratory drive interacts with the pacing after it is initiated. Initially stimulation is set to zero as the controller has yet to adapt and increase stimulator output. However, as the error values increase due to the mismatch in timing between the intrinsic breaths and the paced breaths, the controller adapts gradually increasing charge delivered during each pacing cycle. Eventually, the intrinsic breaths synchronize with the pacing induced breaths.

3.3.3 Adaptive current modulation is able to achieve and maintain a desired volume profile

After successful adaptation, the measured volume profile closely matches the desired profile, as demonstrated by low iRMSE, and that performance is maintained for the remainder of the trial (Figure 5). Figure 5(A) – 5(B) shows a

comparison of the volume profile between a breath elicited using an open loop approach with a square-shaped burst and a breath elicited using pulse amplitudes determined by the PS controller after adaptation. The open-loop approach in Figure 5(A), other than lacking adaptation to extrinsic factors, elicits a breath that differs significantly from a natural breath. However, the breath elicited by the adaptive PS controller in Figure 5(B) matches the desired breath closely. Trials in three rats in a different study (data not provided here) showed a similar inability to match the desired volume profile under open-loop control.

A summary of the iRMSE and charge per pacing cycle for all spinal cord intact animal trials is presented in Figures 5(C) and 5(D), respectively. Entrainment with synchronization usually occurred by pacing cycle 20 and, within 5 pacing cycles, this resulted in an iRMSE of 10%. As seen in Figure 5(C), iRMSE remained below 10% for most of the trials, with the exceptions of periods where intrinsic perturbations occurred. These events are marked by a sudden rise and drop in iRMSE. In seven trials, pacing was performed for an extended duration of up to 15 minutes (not shown). These extended trials also showed iRMSE below 10% throughout the trial when in synchrony. As shown in Figure 5(D), charge delivered per pacing cycle increased substantially until entrainment and synchronization occurred. After this initial period, the controller fine-tuned the stimulator output to obtain the desired volume profile. The charge delivered remained relatively steady for the rest of the trial, changing only when intrinsic perturbations occur.

Figures 5(E) and 5(F) show a summary of the data from Figure 5(C). Figure 5(E) shows the average number of pacing cycles each animal took to achieve the 10% iRMSE threshold and maintain it for at least 10 pacing cycles. This value is heavily dependent on how fast and robustly the intrinsic respiratory rhythm entrains to the pacing.

Given that some of the factors that affect entrainment and synchronization differed between animals, the variability in this value was high. However, the number of pacing cycles required to reach this value among all spinal cord intact animals were 16.06 ± 6.66 pacing cycles.

Figure 5(F) shows the average iRMSE % for the last ten pacing cycles of the 100-pacing cycle trials for each animal ($iRMSE_{10}$). On one trial with animal 9, desynchronization occurred once during this ten- pacing cycle period; this resulted in the outlier observed. All other trials remained with consistently low $iRMSE_{10}$ for the last ten pacing cycles across all trials.

In left C2hX animals, the adaptive controller was able to elicit breath volume profiles that were comparable to those observed prior to the injury. Figure 6 shows the initial 100 seconds of a trial showing the adaptive pacing's effect in a left C2hX animal with the target breath volume being the breath volume profile collected pre-hemisection. Despite a considerable reduction in the rodent's breath volume with only the impaired intrinsic drive, the controller could adapt to sufficiently stimulate the diaphragm muscle to attain the breath volume profile observed pre-hemisection. This breath volume profile was maintained for the duration of the trial.

Nine trials across multiple animals were extended to last over 25 minutes to assess longer periods of ventilatory pacing (not shown). Except for periods of desynchronization between the paced and intrinsic breaths, iRMSE remained below 10% in these extended trials.

Overall controller performance and stimulation results for left C2-hemisected animals can be seen in Figure 7 and Figure 8. Across all left C2hX animals, iRMSE after entrainment and synchronization remained at 10% or less as seen in Figure 7(A). The number of pacing cycles required to achieve an iRMSE of less than 10% for more than 10 pacing cycles is shown in Figure 7(B). Overall, 58.8 ± 27.25 pacing cycles were required across all left C2hX animals to reach 10% iRMSE and maintain it within the 200- pacing cycle trial period. This value exceeded 200 pacing cycles in two trials for animal 16 and thus those trials were excluded from this average. The pacing cycle number to threshold in left C2hX animals was higher in comparison to those of spinal cord intact animals, suggesting that spinal cord injury has a detrimental effect on promotion of respiratory synchronization.

Results across all left C2hX animals and across all trials are shown in Figure 8. The effect on tidal volume is shown in Figure 8(A). Tidal volume across all animals was significantly higher during post-C2 hemisection with pacing (post-C2hXp) than that during postC2 hemisection without pacing (post-C2hX) for the last 40 pacing cycles of each trial (0.59 ml increase, p=<0.0001). Pre-hemisection (pre-C2hX) tidal volume was not significantly different from post-C2 hemisection with pacing

(0.05 ml difference, p=0.39). This shows the controller's ability to closely match a desired volume profile despite injury.

In most trials, pacing had an effect on $etCO_2$ as shown in Figure 8(B). All three conditions were mutually significantly different, with pre-hemisection values lowest, post-C2 hemisection with pacing values higher, and post-C2 hemisection after synchrony (post-C2hXs) values highest (pre-C2hX vs post-C2hXs difference = 1.42%, p=<0.0001; pre-C2hX vs post-C2hXp difference = 0.75%, p=0.0001; post-C2hXs vs post-C2hXp difference = 0.67%, p<0.0001). While the resulting $etCO_2$ was still well above the normal $etCO_2$ range, this reduction does show that adaptive pacing is able to have an effect on $etCO_2$. It is likely that $etCO_2$ can be further reduced to normative values with respiratory rate modulation once $etCO_2$ feedback is implemented.

Controller parameters differed to a certain extent amongst spinal cord intact animals; however, this further shows the robustness of the controller under multiple controller parameters. Table 2 shows the controller parameters across all spinal cord intact animals. Controller parameters for all left C2hX animals were set to n_a=3, n_p = 6, and η=0.001.

Figure 9(A) shows 15 seconds of a trial in a left C2hX rodent in which synchronization was lost. The desired and actual volume profile for each breath are shown in the top row. The muscle activity recorded from the genioglossus (GG) muscle reflects the intrinsic respiratory drive,(Brouillette and Thach, 1980; Fregosi

and Fuller, 1997; John et al., 2005) while the stimulation trace shows the timing at which pacing occurred.

Synchronization between the desired and actual volume profiles is lost after the fourth pacing cycle, with the GG muscle activating half a pacing cycle after pacing occurs. However, this mismatch rapidly corrects itself after a few pacing cycles. De-synchronization causes an increase in the error signal to the controller and thus current amplitude delivered (not shown) increases.

Histological analysis confirmed injury to the descending respiratory pathways in all left C2hX animals; a sample ventral spinal cord section from one animal is shown in Figure 9(B). Ventilatory function was also assessed by functional comparison of tidal volume prior to and after the hemisection. Hemisection led to an average decrease in tidal volume of 0.64 ml ($p<.0001$).

3.3.4 Number of past activations, number of active neurons, and learning rate determine controller stability, performance, and adaptation speed

A total of 500 computer simulation trials were completed, each with a different permutation of learning rate, number of neurons, and past activations, to determine suitable combinations of these controller parameters that would allow for fast, accurate, and stable controller performance. Of these trials, a total of 39 parameter sets matched the selection criteria of mean iRMSE of less than 5% within 20 pacing cycles with a standard deviation of less than 2.5% iRMSE after 5% iRMSE had been achieved. Figure 10(A) shows these parameters along with number of pacing cycles required to lower iRMSE to less than 5%.

Results from the simulations showed that faster learning rates increased adaptation speed and thus reduce number of pacing cycles to reach the threshold. However, faster learning rates also showed a decrease in stability. As learning rate was increased, the number of acceptable parameter combinations decreased from 21 sets to only one set. The iRMSE standard deviation values of the last ten paced cycles of each trial ($iRMSE_{10}$), which are assumed to be inversely proportional to stability, also showed an overall increase as learning rate increased (Figure 10(B)). When selecting a learning rate to use in the experiments, it is necessary to consider that decreased stability could pose a problem given the inherent variability of the system and presence of non-ventilatory behavior. Thus, for *in vivo* verification of the controller parameters, a learning rate that is low enough to provide stability, yet high enough to provide sufficient adaptability, is desired.

These simulations determined a suitable range of parameters for various learning rates. For the *in vivo* studies, a low learning rate capable of maintaining robustness and stability is desired to prevent errors from propagating. Thus, a learning rate of 0.001 was deemed suitable. For this learning rate, 3 to 5 active neurons and 4 to 8 past activation values, were considered suitable parameter values as they had the lowest values for $iRMSE_{10}$ % while still showing low standard deviation values. These ranges were found under the assumptions that muscle mechanics remain constant over time, i.e. that there was no fatigue, and that the breath volume profile selected as the desired trajectory is an ideal trajectory.

The controller parameters that were ultimately implemented in the spinal cord intact animal studies differed from those found computationally as the presence of an intrinsic respiratory drive affected controller performance. This required controller parameter tuning to improve synchronization and entrainment with the intrinsic respiratory drive. However, the controller parameter trends that were observed computationally were generally maintained across animals. Controller parameters used can be found in Table 2

3.4 Discussion

The present study presents a novel neuromorphic closed-loop, adaptive controller for ventilatory pacing capable of modulating stimulation parameters to elicit a breath volume profile that follows a desired profile over hundreds of breaths. A computational platform facilitated development of the controller and provided a range of controller parameters that achieved satisfactory performance, accuracy, and stability. Evaluation in spinal cord intact and left C2-hemisected rats validated the parameters determined computationally. The Pattern Shaper (PS) controller successfully reduced the error between measured and desired breath volume profiles in the presence of a competing intrinsic respiratory drive and/or diaphragm muscle fatigue. In left C2hX rats, the PS controller successfully restored breath volume to levels observed prior to the injury while also reducing $etCO_2$ values. These studies support the use of the closed-loop adaptive PS controller for ventilatory pacing to achieve breath-by-breath control after spinal cord injury or central hypoventilation syndrome.

3.4.1 Computational studies provided a testbed for controller development and characterization

The simulations carried out using biomechanical computational models illustrate the benefits of utilizing computational models as test-bed platforms for the development of neurotechnological algorithms prior to utilization in *in vivo* studies. Here, the computational models ensured that the neuromorphic algorithm for ventilatory control was able to properly adapt and maintain a desired breath volume profile before any animal study was performed, substantially decreasing development time and use of experimental resources. These computational studies identified ranges of controller parameter values that resulted in fast, accurate, and stable performance and identified interactions between these parameters that affect adaptation performance.

The PS controller determines the amplitude of upcoming stimulation pulses as the weighted summation of the output of all neurons in the network, however, only neurons that have a non-zero output at any particular instant contribute to a stimulation pulse. Since each neuron has non-zero output for a portion of the breath cycle and the output profiles are shifted in time, the width of the output profile is directly related to the number of active neurons. Low values for this parameter localize the influence of each neuron but might also lead to unstable behavior. However, stability can be improved by selecting an appropriate value for the number of past-activations included in the summation term of the adaptation algorithm. As shown in Figure 10, when using a low value for the number of active

neurons, selecting a high value for the number of past activations was more likely to meet performance specifications.

The learning rate, η, directly scales the change in neuronal weight in response to each error measurement. While fast adaptation is generally desired, high learning rates can produce large and rapid changes in weights that can compromise stability or produce an under-damped response. With a low value for learning rate, the controller reaches the target iRMSE more slowly, but then the system performance remains stable.

These simulations suggest that for clinical deployment the controller would benefit from a learning rate that is fast enough to adapt to provide sufficient ventilation while being slow enough to remain stable.

3.4.2 Controller provided autonomous and individualized ventilatory pacing

Animals in this study varied in weight, stimulation twitch threshold, presence of injury, and ventilatory drive as defined by $etCO_2$ levels. Irrespective of these differences the PS controller autonomously adapted to achieve the desired ventilatory profile for each individual. In rodents with partial diaphragm function due to left C2 spinal cord hemisection, the controller adapted stimulation values to elicit tidal volume profiles that matched those observed pre-hemisection. Furthermore, the controller was able to elicit the same desired breath volume profile despite differences in the un-paced breath volume between trials. This shows that the adaptive controller can automatically personalize treatment regardless of the efficacy of the intrinsic respiratory drive after injury.

The incomplete spinal cord injury model used in this study also helps to highlight the adaptive properties of the controller in that the desired breath volume profile was attained regardless of a non-paralyzed hemidiaphragm contralateral to the C2 spinal hemisection. Stimulation, scaled to each hemidiaphragm's twitch threshold, was delivered to both left and right hemidiaphragms without differentiating between paralyzed and non-paralyzed hemidiaphragms. This may have led to increased activation of the hemidiaphragm contralateral to the injury. Despite this asymmetrical activation, the controller was able to fine tune stimulation in such a way that the desired breath volume profile was still attained and maintained. In cases where both hemidiaphragms are affected, we expect the controller to behave as in the spinal cord intact animals given that both hemidiaphragms would be activated and contributing to ventilation.

Experiments shown here consisted only of acutely spinal C2-hemisected animals. Thus, the effect of recovery from phenomena such as spinal shock, or neuroplasticity in the form of the crossed-phrenic phenomenon, and respiratory muscle atrophy after chronic injury were not addressed. However, inferences regarding the controller's advantages with regards to these conditions can be made. The PS controller is able to adapt on a breath-by-breath basis and is thus able to adapt in a matter of breaths to transient biomechanical changes that occur after the spinal injury. The controller's ability to adapt ventilation is not based on explicit knowledge of the system's mechanics, using only the elicited breath volume as its controlled variable. Since changes in biomechanics affect the elicited breath volume, these changes would be reflected in the breath volume signal

sampled by the controller. The PS controller would then adapt stimulation output to compensate for these changes, thus maintaining a desired breath volume profile regardless of transient changes that might occur.

Previous animal studies (Kowalski et al., 2013; Nochomovitz et al., 1983; Walter et al., 2011) have shown the feasibility of ventilatory pacing, while a number of other studies have assessed viability and safety of ventilatory pacing in humans for hypoventilation after spinal cord injury.(Chervin and Guilleminault, 1994; DiMarco, 2009; DiMarco et al., 2002; Garara et al., 2016; Onders et al., 2011; Posluszny et al., 2014; Zimmer et al., 2007) However, these animal and human studies considered only the use of pulse trains with fixed stimulation parameters. While open-loop controllers might elicit a desired tidal volume at the time of pacing calibration, this fixed stimulation waveform must be manually selected for each individual. The selected stimulation may not be suitable after muscles fatigue, possibly leading to insufficient ventilation, discomfort, or pain. The PS controller addresses this issue with its adaptive shape-defining abilities. The PS controller achieves personalized pacing by using real-time measurements of performance (volume) to adapt pulse amplitude within the pulse train, thus allowing it to activate the diaphragm to elicit the breath volume profile desired.

In open-loop paradigms, manual adjustment of stimulation parameters is required to maintain a constant tidal volume during short and long-term changes to the muscle or electrode interface, such as muscle fatigue or electrode encapsulation.(Akers et al., 1997; Grill and Mortimer, 1994) The PS controller

continuously adapts to achieve a fixed ventilatory pattern regardless of any change that might occur. Fatigue was not directly quantified in this study, but the presence of a gradual increase in stimulation charge delivered and a constant low iRMSE throughout the trial suggests that the controller was able to account for stimulation-induced fatigue of the diaphragm muscle. This effect was described in more detail in previous studies in both rodents and humans concerning use of the PS controller architecture for lower limb control.(Abbas and Triolo, 1997; Fairchild et al., 2010; Kim et al., 2009) Additionally, electrical stimulation has shown to cause fatigue onset on a faster time-scale than intrinsic neural activation.(Ratkevičius et al., 1998) This ability to adapt diminishes or eliminates the need for clinical intervention to adjust the stimulation parameters, reducing the cost, attendant time, and inconvenience to the patient. Such consistency in ventilation might also expand the range of activities that could be performed without increasing the risk of hypoventilation or discomfort.

For the controller to be clinically viable in the presence of any degree of intact respiratory drive, the paced and intrinsic breaths should be synchronized to achieve effective and efficient ventilation. The onset of breaths produced by diaphragmatic contraction due to stimulation may or may not coincide with the onset of breaths due to the intrinsic respiratory drive. This is illustrated in figure 9, where GG activity that reflects respiratory drive (Brouillette and Thach, 1980; Fregosi and Fuller, 1997; John et al., 2005) is not synchronized with the pacing signal.

Although the PS controller does not have an explicit mechanism to achieve synchronization, it was observed that the adaptive algorithm's intrinsic adaptation to error can promote entrainment and synchronization. This behavior occurred both at the initiation of pacing and sporadically throughout pacing. Errors that result from the temporal mismatch between the elicited and desired volume profile cause an increase in stimulation output. When the increased stimulation in the paced cycle matches an intrinsic inspiratory phase, a comparatively stronger diaphragmatic contraction occurs, causing an overshoot of the peak volume elicited. The increased pulmonary stretch receptor feedback likely triggers the Hering-Breuer reflex through vagal afferents, which resets the phase of the breathing cycle and produces entrainment and synchronization.(Muzzin et al., 1992; Simon et al., 1999)

Loss of synchrony was observed in both spinal cord intact and left C2hX rats; however, left C2hX animals also showed a higher incidence of these events and required more pacing cycles to re-synchronize. In contrast with spinal cord intact animals, all left C2hX animals had difficulty achieving initial phase synchronization; with pacing cycles to 10% iRMSE lasting an average of 53 pacing cycles, compared to 17.5 pacing cycles in spinal cord intact animals. One possible reason for difficulty in entrainment and synchronization is that pacing in spinal cord intact animals targeted a breath volume that was 20% higher than baseline, increasing stretch receptor input to the rCPG thus strengthening the coupling between the paced and intrinsic breaths. Meanwhile, the desired breath volume in left C2hX animals was the same as their baseline breath volume leading to baseline levels

of stretch receptor feedback to the rCPG and thus weaker coupling than in spinal cord intact animals. Additionally, In left C2hX animals, the hemisection unilaterally disrupts diaphragm stretch receptor-mediated feedback to the rCPG via phrenic afferents,(Nair et al., 2017) possibly reducing the strength of the primary signal mediating entrainment of the intrinsic drive by the electrical pacing.

The interaction between intrinsic respiratory drive and respiratory pacing is also evident after cessation of pacing. In most animals, after cessation of pacing, a reduction in tidal volume and increase in cycle period are observed. This reduction in minute ventilation was considerably more pronounced immediately after cessation and gradually returned to values similar to baseline in a period of 30 to 60 seconds. This suggests a decreased neuro-respiratory drive due to stimulation-induced hyperventilation and thus decreased chemoreceptor feedback to the central drive. It was observed that this decrease in minute ventilation was less pronounced in trials that experienced a large number of loss of entrainment events, suggesting that a highly active intrinsic respiratory drive is the cause of loss of entrainment to ventilatory pacing.

Future work assessing chronic respiratory pacing should consider the interplay between pacing and a dynamic intrinsic respiratory drive, if one is present. Previous studies have suggested technology that can be used to synchronize artificial ventilation with intrinsic respiratory drive or to replicate its function. These methods include development of a controllable stimulator with an update frequency higher than the stimulation frequency and a real-time processing

controller,(Castelli et al., 2017) implementation of a bio-inspired spiking neural network model that follows intrinsic respiratory rate,(Zbrzeski et al., 2016) predictive algorithms using body temperature and heart rate,(Kimura et al., 1992) and breath-triggering through the use of genioglossus muscle activity.(Mercier et al., 2017) However, these approaches have not yet been sufficiently developed or investigated.

3.4.3 Dynamic control of $etCO_2$ can lead to further control of ventilation

The observed decrease in $etCO_2$ was lower than expected likely due to pacing that elicited baseline levels of ventilation after spinal hemisection, which may have been sufficient to avoid further increases in CO_2, but not sufficient to completely expel excess CO_2. This effect was observed more sharply in animals which had low baseline tidal volumes and as a result, lower paced ventilation. Thus, a greater change in overall ventilation may be required to achieve a more pronounced decay in $etCO_2$. This could be achieved by automatic adjustments to respiratory rate. In the current implementation of the controller, the PG portion of the controller produced a fixed oscillatory pattern. A PG that responds to changes in $etCO_2$ and adjusts the respiratory frequency could be developed, as a respiratory pattern-generator inspired model-based PG.

Future work will focus on developing a variable closed-loop PG capable of responding to changes to $etCO_2$ and integrating it with the PS controller presented here. The PG would be based on a model of the biological rCPG to dictate the desired ventilatory pattern. A chemoreceptor model would convert the incoming

$etCO_2$ signal into a neural drive that would feed into this rCPG model. The PS portion of the controller would then proceed to adapt stimulation to achieve this new ventilatory pattern. This approach would allow for a comprehensive respiratory pacing controller capable of providing proper ventilation regardless of metabolic demand variations, muscle-related changes, and individual differences (Jung, 2018).

Although ventilatory pacing has been under development for over 70 years, and has already been used clinically, there has been a lack of closed-loop controllers for ventilatory pacing. Open-loop control has the potential to lead to inadequate ventilation as the patient undergoes changes in their physiological state, such as changes in metabolic demand and postural load, and changes in the electrode-tissue interface, such as electrode encapsulation. The automation of initial stimulation parameter selection and consequent adaptation on a breath-by-breath basis allows for individualized closed-loop control of ventilatory pacing on a long-term time scale with adaptability to short-term changes.

Furthermore, this adaptive closed-loop control strategy would allow for gradual reduction of stimulation following respiratory rehabilitation, eventually leading to automatic weaning, thereby decreasing time spent in rehabilitative therapy and potentially improving ventilatory outcome measures. The PS controller modulates stimulation as a function of the error between the desired and measured volumes, increasing stimulation if the measured volume is lower than the desired volume and decreasing stimulation if the measured volume is larger. If the diaphragm

muscle is gradually strengthened as a result of repeated electrical activation and its contribution to the overall breath volume increases, the controller would respond to the increased breath volume by decreasing stimulation output. If the trend continues, the controller would eventually decrease stimulation until the patient could independently maintain sufficient ventilation, thus autonomously weaning the patient from ventilatory support.

3.5 Clinical significance

Respiratory pacing can serve an alternative to mechanical ventilation in cases of respiratory insufficiency. Each patient, depending on their weight, requires different breath volumes for adequate ventilation and breath-to-breath modulation of ventilation to account for changing metabolic states. Current commercially-available respiratory pacing systems are open-loop and require manual calibration by a clinician or technician to set the stimulation levels to achieve the desired breath volume. We present a closed-loop respiratory pacing controller that can automatically determine the stimulation parameters needed to achieve a desired breath volume and adapt this stimulation during an on-going breath. Experimental studies in rodents show that the adaptive controller can achieve a desired breath volume profile for a wide range of body weights, even after diaphragmatic hemiparesis caused by spinal cord injury. This adaptive approach offers multiple clinical advantages over current systems. The approach allows for a streamlined automated set-up process that provides the required pacing regardless of patient specific ventilatory biomechanics. During ongoing use, there would be a reduced

risk of inadequate ventilation as the controller would adapt and respond to physiological changes such as those on muscle fatigue or alteration in posture. Furthermore, the adaptive controller could be used as a respiratory rehabilitation tool to strengthen inspiratory muscles and allow automatic weaning from mechanical ventilation.

Tables

Table 1: Chest and diaphragm biomechanical model parameters

m_L	1.8 g	a_1	0.6679
B_L	8.4 g·s^{-1}	a_2	-0.1001
K_L	11.5 g·s^{-2}	b_0	20
k_p	7 g·cm^3·s^{-2}	L_w	6 cm
γ_0	0	L_0	0 cm
γ_1	0.01909	V_{max}	48 cm·s^{-1}
γ_2	-0.0001152	K_V	0.2
γ_3	2.6 x 10^{-7}	D	3.5%

Table 2: Controller parameters utilized in spinal cord intact animals

Animal #	***Active Neurons***	***Past Neurons***	***Learning Rate***
1	13	6	0.0003
2	7	2	0.001
3	7	4	0.0001
4	7	4	0.0001
5	11	6	0.0003
6	7	4	0.001
7	7	4	0.001
8	3	6	0.001
9	3	6	0.001

Figures

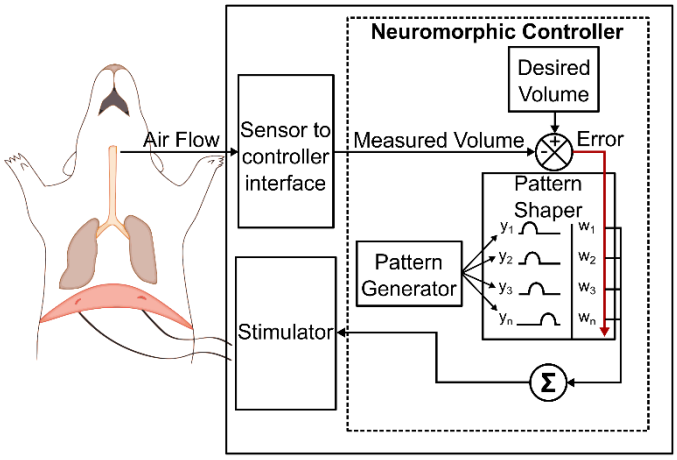

Figure 1. Closed-loop controller architecture for use in experimental studies for diaphragmatic control. The pattern generator sets a fixed respiratory cycle period. The pattern shaper neural network adapts as a function of the instantaneous error between the desired and measured breath volume profiles. The summation of time-shifted neuronal outputs from the pattern shaper dictate controller output to the stimulator.

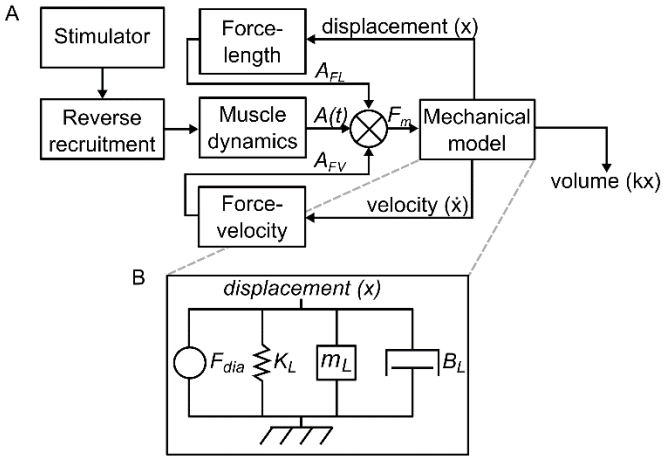

Figure 2. A diaphragm muscle model (A) and chest biomechanical model (B) are used for simulation of closed-loop pacing of the diaphragm muscle. The mechanical model output is the displacement of the diaphragm (*x*), which then translates to volume through a conversion factor (*k*). The displacement and velocity are delivered back into the muscle model to factor into the force-length and force velocity contributions. The controller modulates stimulation delivered based on the error between a desired volume and the output of the model.

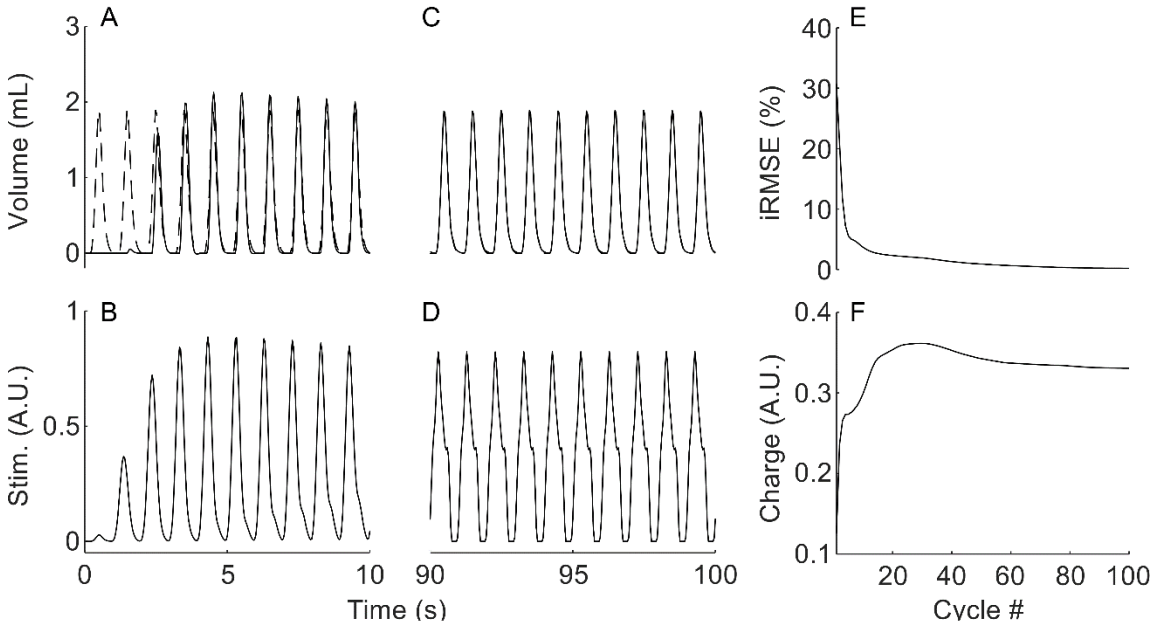

Figure 3. Adaptive PS controller effect in breath volume in a simulated trial. Example of a simulation trial showing the controller adapting the stimulation output (**B, D**) to match the measured volume (**A,C**, solid) to the desired volume (**A,C**, dashed) during the initial stimulation (pacing cycles 1-10) and at end (pacing cycles 91-100) of a 100 second trial.(**E**) Inspiratory RMSE throughout 100 pacing cycles in a simulated trial using controller parameters obtained from parametrization (η=0.001, n_a = 3, n_p = 6). (**F**) The corresponding normalized charge delivered by the controller as it adapted the stimulation output to match the targeted volume profile.

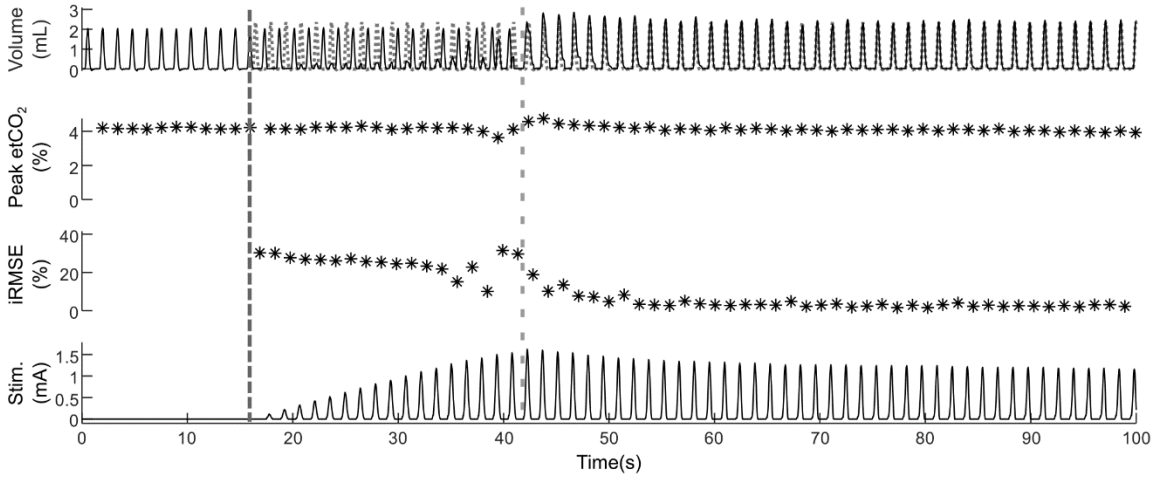

Figure 4. Adaptive PS controller implementation in a spinal intact animal. The controller adapts stimulation output to match the measured volume (solid line) to the desired volume (dotted line). The controller was turned on at 10 seconds (dark grey vertical dashed line) with controller parameters ($n_a = 3$, $n_p = 6$, $\eta = 0.001$). The controller was able to cause successful synchronization after 14 pacing cycles (light grey vertical dashed line) and maintained low iRMSE thereafter.

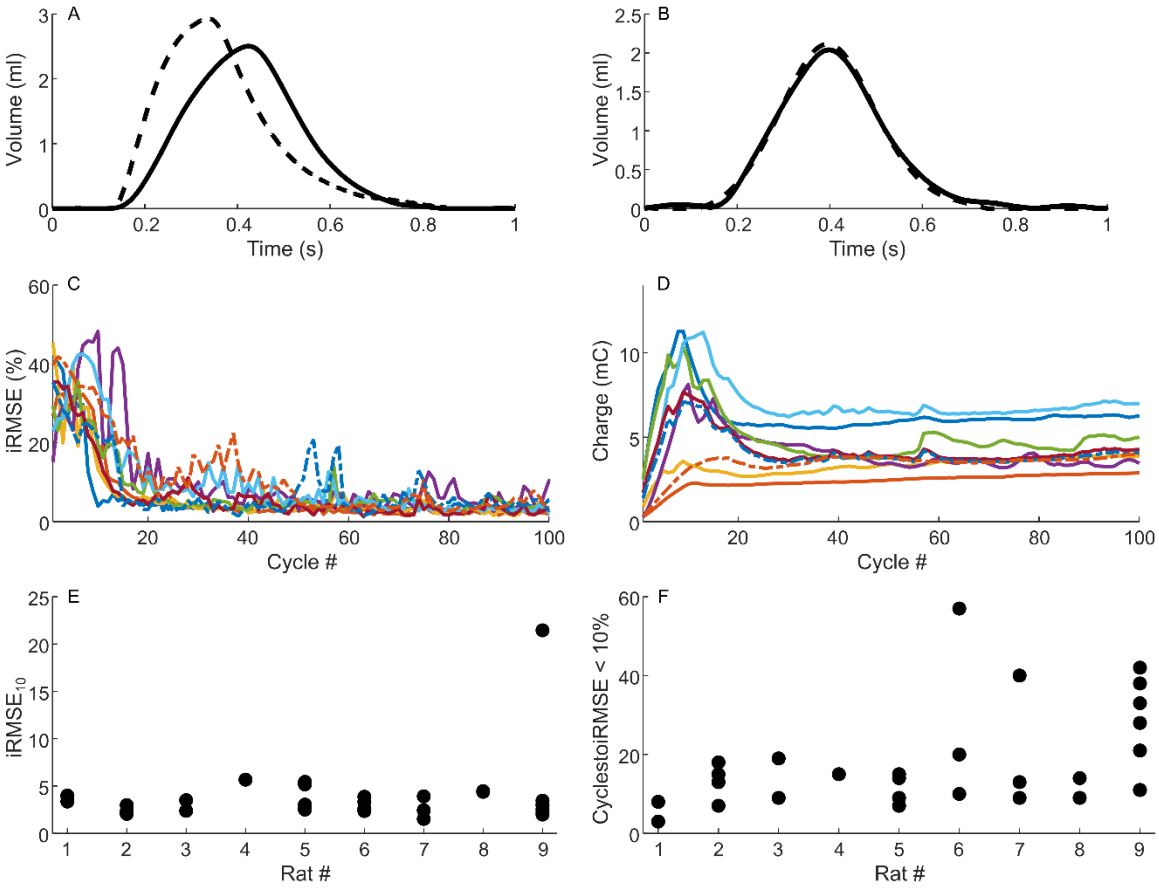

Figure 5. Ability of adaptive PS control to achieve a desired breath volume profile in spinal intact animals. (**A**) Open-loop stimulation using a square-shaped stimulation burst elicited a breath profile (solid line) different from that of a spontaneous breath (dashed line). (**B**) The adaptive controller modulated stimulation to elicit a breath profile similar to a desired breath profile derived from a spontaneous breath. (**C**) Average inspiratory Root Mean Square Error (iRMSE) between the desired and measured breath volume profiles for each animal. iRMSE is elevated at the initiation of the pacing due to lack of synchrony between the breaths produced during intrinsic respiration and those elicited by pacing. After synchrony, the controller is able to reduce and maintain a low iRMSE across all animals. (**D**) Average charge delivered per pacing cycle per animal. The controller tended to trigger entrainment by increasing stimulation output until synchronization occurred. (**E**) Average iRMSE in the last 10 pacing cycles per trial for all animals. $iRMSE_{10}$ was maintained below 10% except for one trial for animal 9, in which a desynchronization occurred during the last 10 pacing cycles. (**F**) Number of pacing cycles per trial required to achieve the desired 10% threshold, including the pacing cycles required to reach synchronization.

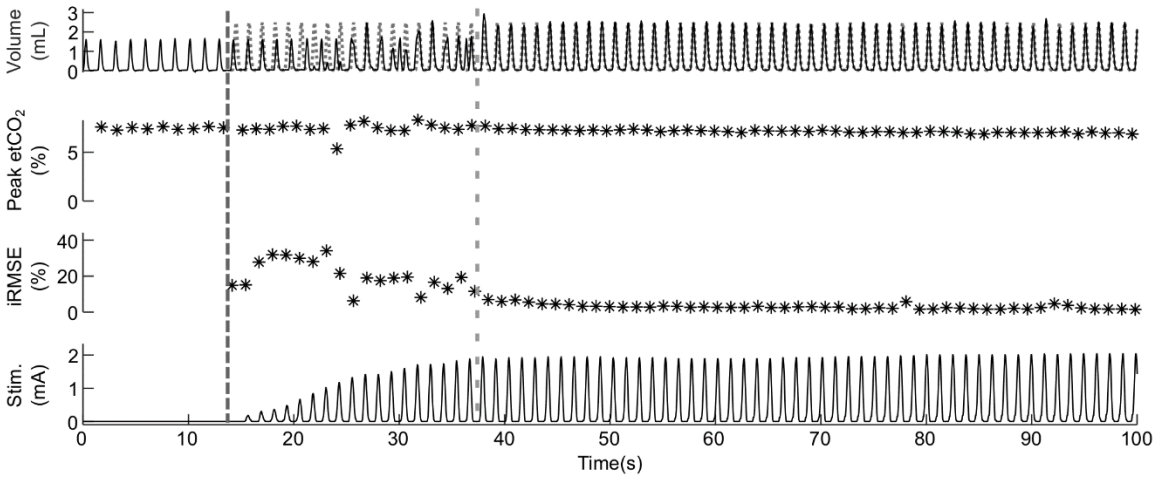

Figure 6. Adaptive PS controller implementation in an animal with left C2 spinal cord hemisection. The dark grey dashed line depicts controller initiation. The rodent is spontaneously breathing at a tidal volume of 1.8 ml before stimulation while the desired tidal volume was set to 2.5 ml. After the 20 pacing cycles required for entrainment and synchronization (light grey dashed line), the elicited volume profile quickly matched the desired volume profile (dotted line). This increased volume was maintained for the rest of the rest of the stimulation trial.

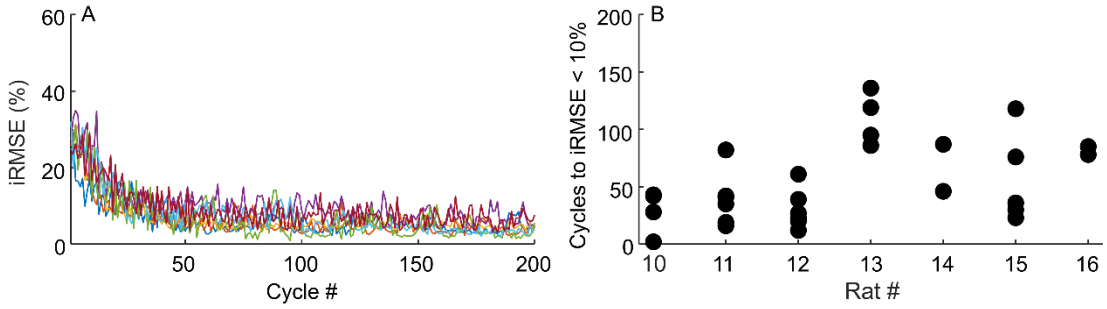

Figure 7. Ability of adaptive PS control to achieve a desired breath volume profile in animals with left C2 spinal cord hemisection. Left C2 spinal cord hemisected animals took longer to achieve entrainment and synchrony between the paced and spontaneous breaths than observed in intact animals. This effect can be seen in (**B**) where the iRMSE was not reduced below 10% until very late in the trial in some instances. However, as can be seen in (**A**), iRMSE averaged around 10% for the duration of the trial.

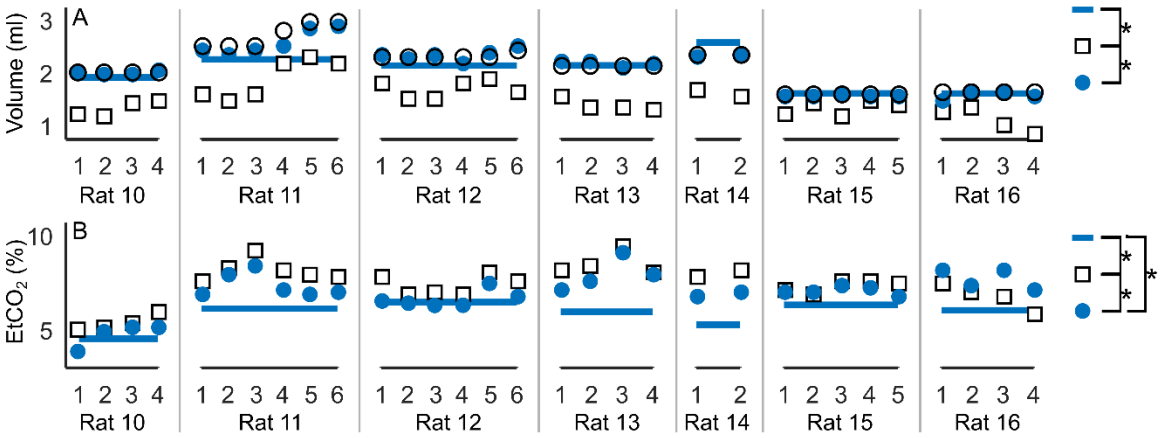

Figure 8. Effect of pacing on tidal volume and end-tidal CO_2 across trials for all left C2 spinal cord hemisected animals. Tidal volume and $etCO_2$ pre-hemisection (pre-hX; solid line), post-hemisection without pacing (post-hX; empty square), and post-hemisection with pacing (post-hXp, solid circle) conditions in each trial for each animal. Pacing was able to restore tidal volume to target values (empty circle) similar or larger than those observed prior to the injury (pre-hX vs. post-hX difference = 0.64 ml, p<.0001; post-hXp vs. post-hX difference = 0.59 ml, p<.0001). $EtCO_2$ was also reduced in most cases during post-hemisection with pacing. However, the amount reduced was not sufficiently large to match the $etCO_2$ values observed when pre-hemisection values were recorded (pre-hX vs post-hXp difference = 0.73%, p=.0002; pre-hX vs. post-hX difference = 1.46%, p<.0001; post-hX vs post-hXp difference = 0.73%, p<.0001). Pre-hemisection values obtained from n = 3 trials, with the exception of rat 11 (n = 2 trials).

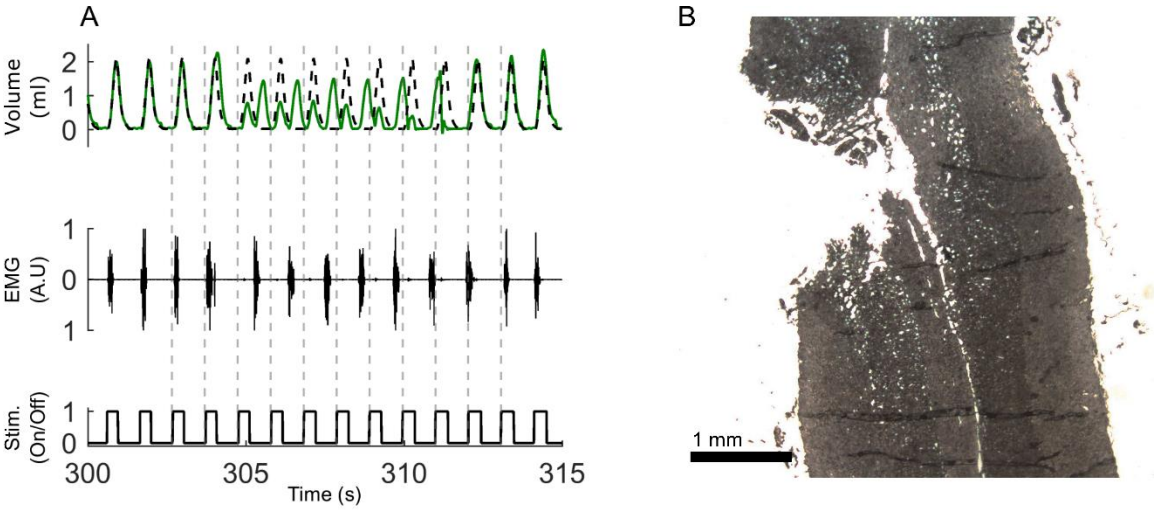

Figure 9. Resynchronization between intrinsic respiration and diaphragm pacing after a C2 spinal cord hemisection. (**A**) Loss and recovery of synchronization between intrinsic respiration (breath volume, genioglossus EMG) and diaphragm pacing (stimulation on/off, bottom, stimulation onset denoted by grey dashed lines). De-synchronization leads to elevated error between measured (solid) and desired (dashed) breath volume. The controller is capable of re-establishing synchronization after de- synchronization due to phase shift timing between inspiratory timing of GG and pacing. (**B**) Sample histological section of the ventral spinal cord following C2 lateral spinal cord hemisection. Spinal cord tissue of injured animals was longitudinally cryosectioned in 15 µm sections and analyzed to assess exactness of hemisection. Hemisection was also assessed functionally by observing changes in tidal volume post-injury.

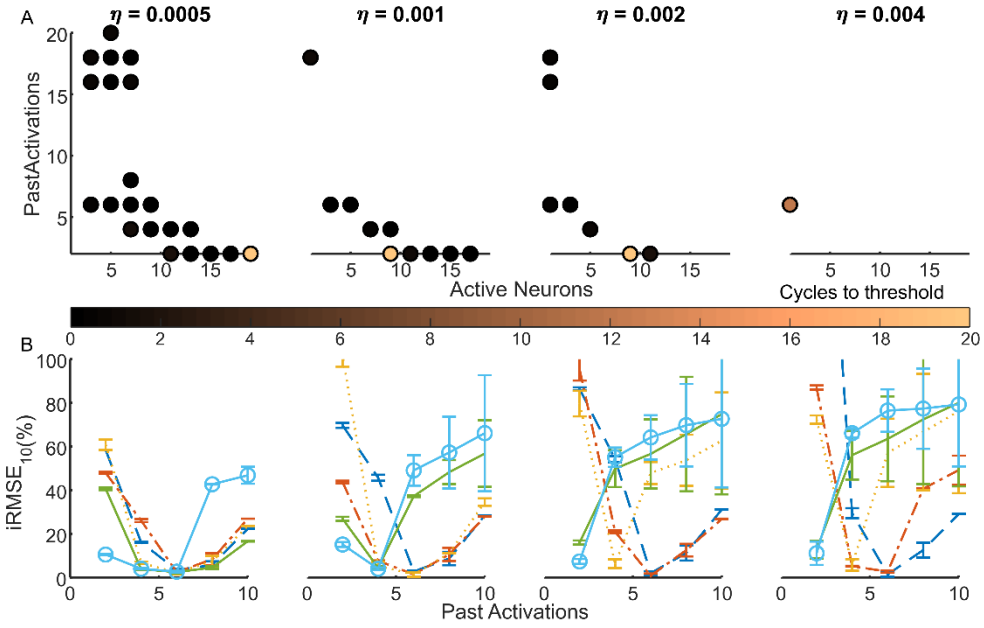

Figure 10. Effects of varying learning rate, number of active neurons, and number of past activations on PS controller performance as determined by simulations. (**A**) Solid dots indicate suitable parameter configurations led to adaptation that met the acceptance criteria of achieving and maintaining a 5% inspiratory RMSE within 20 pacing cycles while maintaining a standard deviation below 2.5% throughout 100 pacing cycles for several learning rates (η). Dot color denotes number of pacing cycles required to meet an inspiratory RMSE value of 5%. (**B**) Parameter trends obtained from simulation studies. Plots show effect on $RMSE_{10}$ with respect to number of past activation values (n_p) for several widths of the activation function given by n_a (1 n_a = blue dashed; 3 n_a = orange dashed dotted; 5 n_a = yellow dotted; 7 n_a = green solid; 9 n_a =light blue)

CHAPTER 4

CONTROL OF BREATH VOLUME AND RESPIRATORY RATE THROUGH THE USE OF AN ADAPTIVE CLOSED-LOOP PATTERN GENERATOR PATTERN SHAPER CONTROLLER

4.1 Introduction

Ventilation is a highly dynamic process through which the mammalian brain maintains adequate respiration. However, disease, trauma, or disorders in the brainstem, spinal cord, or effector muscles and their innervating nerves, may bring about impairment of ventilation or complete inability to control the ventilatory process and lead to hypoventilation. Hypoventilation often leads to hypoxia and hypercapnia, which in severe cases may disrupt homeostasis, cause brain damage, and eventually lead to death (Cragg and Drysdale, 1983; Roussos and Koutsoukou, 2003; Tiruvoipati et al., 2017; West and Luke, 2016). Mechanical ventilation is usually the de-facto approach to restore and maintain proper ventilatory function and prevent hypoventilation. Mechanical ventilation is effective in that air is constantly and reliably delivered to the pulmonary airways independent of the person's indigenous ventilatory capabilities. However, mechanical ventilation poses some drawbacks. Positive pressure from the mechanical ventilator cycles air through the alveoli. Under this process, a decreased respiratory drive reduces activity of the respiratory muscles, which may lead to muscle atrophy. Atrophy may increase the time required for weaning from

mechanical ventilation in cases where recovery is possible (Andrew Shanely et al., 2002; Levine et al., 2008; Vassilakopoulos, 2012; Zambon et al., 2016). Furthermore, a risk of alveolar damage due to elevated positive air pressure is present during mechanical ventilation as shown by several studies (Claxton et al., 1998; Levine et al., 2008; Zambon et al., 2016).

Respiratory pacing which consists of electrically stimulating the diaphragm or its innervating nerve, the phrenic nerve, has been shown to be an alternative to mechanical ventilation. Appropriate stimulation causes a contraction of the diaphragm eliciting inspiration and can elicit a functional breath (DiMarco, 2005, 2018; Le Pimpec-Barthes et al., 2016; Nochomovitz et al., 1983; Onders, 2012; Peterson et al., 1986). Respiratory pacing overcomes the drawbacks of mechanical ventilation. Respiratory pacing ameliorates atrophy since the muscle is recruited electrically at every breath, reduces risk of lung damage since electrically-driven diaphragm activation draws air into the alveoli through negative pressure (Brown et al., 2006; DiMarco, 2005; Onders, 2012), and does not require intubation. However, commercially available respiratory pacing systems lack the ability to adjust the stimulation parameters in response to changes in the user's chest biomechanics and/or physiological metabolic changes. The stimulation parameters are set in a clinic by a clinician or medical technician familiar with the pacing technology (Jarosz et al., 2012). Furthermore, changes in the tissue-electrode interface or mechanical properties of the ventilatory system over days or weeks require re-tuning the system (Glenn et al., 1976). Most importantly, the pre-set stimulation parameters preclude the ability of the pacing to automatically

change in response to altered respiratory demands consequent to metabolic changes.

An adaptive closed-loop controller for respiratory pacing that is able to modulate stimulation parameters to ensure a desired breath volume pattern is maintained has been previously developed and described in Chapter 3 (Siu et al., 2019). The controller utilized an Pattern Shaper (PS) scheme based on an adaptive artificial neural network originally designed for lower limb locomotor control in rodents and in humans (Abbas and Chizeck, 1991, 1995; Fairchild et al., 2010; Ichihara et al., 2009; Kim et al., 2009; Riess and Abbas, 2000). This adaptive PS controller was modified for diaphragm pacing use and was able to evoke a desired breath-volume, restoring eupnic ventilation in rats with diaphragm hemiparesis. However, eupnic ventilation was unable to account for the increased arterial CO_2 levels that resulted from decreased ventilation. Thus, it is required for the controller to be able to elicit a proper hypercapnic response, where both breath volume and respiratory rate increase in comparison to eupnic ventilation, to achieve normocapnia.

For unimpaired breathing, the respiratory central pattern generator (rCPG), a network of interconnected neuronal populations located in the brainstem, generates a ventilatory pattern in response to CO_2 chemoreceptor activity, lung mechanoreceptors and other neural inputs originating from the cortex and amygdala (Feldman and Kam, 2015; Molkov et al., 2017; Richter and Smith, 2014). The generated ventilatory pattern contains information about both breath volume and breath cycle duration. In hypercapnia, an elevated arterial CO_2 concentration

causes an increase in CO_2 chemoreceptor activity. This increase in chemoreceptor activity increases rCPG activity, resulting in elevated breath volume and decreased cycle duration (Molkov et al., 2014a, 2014b). The rise in ventilation improves the efficacy at which CO_2 is removed from circulation, eventually causing arterial CO_2 concentration to decrease, reducing chemoreceptor activity, and finally reducing ventilation to eupneic values (West and Luke, 2016).

The objective of the work presented here was to develop a closed-loop controller capable of, through respiratory pacing, modulating ventilation in a manner that is similar to that of physiological control of ventilation. This was accomplished by developing a neuromorphic closed-loop adaptive controller that generates an appropriate ventilatory pattern automatically in response to changes in partial pressure of arterial CO_2 ($PaCO_2$) levels and then evokes this response through modulation of the stimulation parameters as needed. This approach allows for generation of the desired dynamic volume profile within a given breath, allowing the user to be properly ventilated whenever they are in a situation in which respiratory demand differs from when the system was tuned.

Similar to a previously developed version of the controller, the closed-loop PG/PS controller implements a single layer neural network, described in Chapter 3 (Siu et al., 2019), to serve as a pattern shaper module. However, in this study, a mathematical model of the rCPG (Botros and Bruce, 1990)serves as the basis for the pattern generator module to determine the appropriate ventilatory response to changes in $PaCO_2$. The rCPG model was replicated, modified, and integrated with

a chemoreceptor model and a pulmonary stretch receptor model to complete the PG module. The PG module was then coupled with the existing PS controller. The PG/PS controller was assessed *in silico* to ensure adequate functionality prior to *in vivo* studies. The controller's ability to control for changes in $PaCO_2$ was assessed *in vivo* in two animal models of increased $PaCO_2$ caused by hypoventilation. Hypoventilation was induced either by repressing central control of ventilation through use of supplementary isoflurane anesthesia (Dardai and Heavner, 1987; Imai et al., 1999; Sollevi and Lindahl, 1995) or by reducing inspiratory capacity through paresis of the left diaphragm via a left C2 spinal cord hemisection (left C2hX) (Doperalski et al., 2008; Dougherty et al., 2012b; Gill et al., 2014; Sandhu et al., 2009; Siu et al., 2019). These *in vivo* studies confirmed that the controller was able to adequately respond to changes in $PaCO_2$ by generating a proper ventilatory response and matching that response through modulation of stimulation parameters to eventually reduce $PaCO_2$ to normocapnic values.

This biologically-inspired adaptive closed-loop respiratory pacing controller is the first ever approach for management of $PaCO_2$ for respiratory pacing applications. Closed-loop control of $PaCO_2$ in people with ventilatory impairments would not only permit patients with respiratory pacers to alleviate concerns about inadequate ventilation during everyday tasks but may also allow patients without ambulatory impairments to lead a more active lifestyle without risk of hypoventilation; leading to improvements in health and quality of life.

4.2 Methods

4.2.1 Animal care and surgical procedure

Spontaneously breathing, adult, male Sprague-Dawley rats were used to assess PG/PS controller performance in spinal cord intact rats (n = 7, 411 ± 91 g., 3.6 ± 0.9 months) and left C2hX rats (n = 6, 390 ± 80 g., 3.4 ± 0.8 months). Animal use was approved by the Institutional Animal Care and Use Committee of Florida International University. Rats were anesthetized via subcutaneous delivery of urethane (1.5 g/kg) and supplemental isoflurane (0.2 – 1.5% in 100% O_2). The plane of anesthesia was evaluated via the toe-pinch reflex and assessment of breathing rate and heart rate. A closed-loop heating plate (TCAT-2AC, Physitemp, Clifton, NJ) maintained body temperature at 37-38°F by monitoring temperature through a rectal probe. A tracheostomy was performed to monitor air flow through the lungs and measure it using a small in-line animal pneumotachometer (PTM Type HSE-73-0980, Harvard Apparatus, Holliston, MA). Integration of air flow (0.2 s time constant) through a hardware integrator (PI-1000, CWE Inc, Ardmore, PA) provided a measure of volume. End-tidal CO_2 ($etCO_2$) served as a measure of $PaCO_2$ and was monitored through a side-stream capnograph (CapStar-100, CWE Inc., Ardmore, PA). Electrocardiography was performed using 30G stainless steel needles inserted subcutaneously in the chest and abdomen for monitoring of plane of anesthesia and overall rat health. To assess controller performance after hemiparesis induced hypoventilation, a left C2 spinal cord hemisection was performed on one subset of rats (*n* = 6). To assess completeness of injury,

electromyograms (EMG) of the hemidiaphragm ipsilateral to the injury were obtained during the spinal cord hemisection procedure and for several minutes later. Spinal cord tissue was processed for visual assessment of completeness of spinal cord hemisection through light microscopy as described in Chapter 3.

4.2.2 Diaphragm stimulation

The diaphragm muscle was stimulated bilaterally through single-stranded, stainless steel electrodes (SS-304, 44 AWG, AM-Systems, Carlsborg, PA) implanted intramuscularly in each hemidiaphragm as described in Chapter 3. A constant-current stimulator (FNS-16, CWE Inc., Ardmore PA) delivered biphasic cathodic-first stimulation pulses at a current amplitude determined by the controller, a fixed pulse width of 200 µs/phase, inter-phase interval of 80 µs, and pulse frequency of 72 Hz as described in Chapter 3. The current amplitude determined by the controller is scaled based on the muscle fiber twitch threshold collected during electrode implantation. Twitch threshold was obtained through visual observation of minimal twitch using a single biphasic pulse with the stimulation parameters mentioned above. Trials lasted for 900 sec or more.

4.2.3 Experimental protocol

Two groups of hypoventilated rats were utilized to assess whether the PG/PS could autonomously control breath volume and respiratory rate to regulate $PaCO_2$. One group consisted of spinal cord intact animals undergoing ventilatory depression via delivery of supplemental isoflurane. Given that isoflurane is a respiratory depressant (Dardai and Heavner, 1987; Eikermann et al., 2008; Imai

et al., 1999), supplemental isoflurane was delivered (+1.5% in 100% O_2) to suppress ventilation and thereby induce hypercapnia. Once 7% $etCO_2$ or more was reached, the PG/PS controller was initiated and its ability to respond to hypercapnia and reduce $etCO_2$ closer to normocapnia (5 ± 0.5%) was assessed. The PG/PS controller was considered to be successful if it reduced and maintained $etCO_2$ to within the normocapnic range.

To assess controller performance when hypoventilation resulted from a traumatic spinal cord injury (SCI), we used a left C2 spinal hemisection model (Doperalski et al., 2008; Lane et al., 2009; Sandhu et al., 2009; Siu et al., 2019). Spinal hemisection from the C2 to C5 leads to hemiparesis of the hemidiaphragm ipsilateral to the injury. This results in hypoventilation due to reduced inspiratory muscle activity. After each trial, left C2 spinal cord hemisected rats were allowed to rest for at least 30 minutes between trials to both recover from electrical stimulation-induced muscle fatigue and for them to become hypercapnic due to reduced inspiratory capacity after hemiparesis. If hypercapnia exceeded 7% before 30 minutes had elapsed, mechanical ventilation was applied to prevent $etCO_2$ from exceeding 7%. Mechanical ventilation was required twice for rat 2 prior to trial 3 and 5.

In all animal trials, the desired ventilatory pattern was determined by the PG module of the controller based on $etCO_2$ feedback and animal body weight as described in the following section.

4.2.4 Performance measures

The performance of the PG/PS controller was evaluated in terms of its ability to determine and evoke an adequate ventilatory behavior in response to elevations in the sampled $etCO_2$ values, and in its ability to reduce $etCO_2$ values towards normocapnic levels and maintain normocapnia throughout the trial. The PG/PS controller's ability to determine and evoke a desired ventilatory output was assessed by observing whether the elicited minute ventilation was directly proportional to the measured $etCO_2$. The PG/PS controller performance and its ability to achieve and maintain the desired ventilatory pattern was determined by measuring the inspiratory root mean square error (iRMSE) values throughout the trial. Finally, $etCO_2$ values after pacing indicated whether the model-guided ventilatory profile generated by the PG could be used to control $PaCO_2$. The first 20 cycles of iRMSE after entrainment and the last 20 cycles of the trial were compared to assess whether controller performance declined over time. The controller's ability to decrease $PaCO_2$ and achieve normocapnia was determined by average decrease in $etCO_2$ from the 10 breath cycles obtained after pacing was initiated and entrainment had occurred to the last 10 cycles of the 1000 cycle trial.

4.2.5 Statistical analysis

A general linear mixed model (Cnaan et al., 1997) was used to assess the effect of PG/PS controlled pacing on $PaCO_2$. Fixed effects of trial number and condition (prior to pacing and after pacing) and random intercept effects of both trial number and measurement occasion (last 20 breath measurements within each trial). All

descriptive statistics are given in the form of mean ± standard deviation. The generalized linear mixed model was performed using SAS 9.4 (SAS Institute Inc., Cary, NC).

4.2.6 PG/PS Controller design

The PG/PS controller design is based on the biological ventilatory control scheme, where the PG generates a model-based ventilatory pattern and the PS adapts stimulation parameters to evoke the desired ventilatory pattern in response to dynamic changes in $PaCO_2$ levels. The design of the PG/PS controller can be seen in Figure 11. For this adaptive ventilatory controller the PG module utilizes a triphasic oscillatory network developed by Botros and Bruce to model the respiratory central pattern generator (Botros and Bruce, 1990). This network is composed of five interconnected neuronal populations; most of the synapses are inhibitory. The activity of each of these populations is maximal at different phases of the respiratory cycle, these being early inspiratory, inspiratory, late-inspiratory, post-inspiratory, and expiratory. These populations receive mostly inhibitory input from each other as well as from other external inputs depending on the population, such as chemoreceptors and pulmonary stretch receptors. The equations for this oscillating respiratory network are,

$$\frac{dI}{dt} = -a_I I - W_{EI}S(E) - W_{PI}S(P) - W_{LI}S(L) + W_{II}S(I) + n_{CO_2}B_I \quad (10)$$

$$\frac{dL}{dt} = -a_L L + W_{IL}S(I) - W_{EL}S(E) - W_{RL}S(R) + W_{LL}S(L) + B_L + W_{vL}v \quad (11)$$

$$\frac{dP}{dt} = -a_P P - W_{EP}S(E) - W_{RP}S(R) + W_{PP}S(P) + n_{CO_2}B_P \quad (12)$$

$$\frac{dE}{dt} = -a_E E - W_{IE}S(I) - W_{RE}S(R) - W_{EE}S(E) + n_{co2}B_E \quad (13)$$

$$\frac{dR}{dt} = -a_R R - W_{IR}S(I) - W_{PR}S(P) + W_{RR}S(R) + n_{CO_2}B_R + W_{vR}v \quad (14)$$

Where *I*, *L*, *P*, *E*, and *R* represent the inspiratory, late-inspiratory, post-inspiratory, expiratory, and early inspiratory neuronal populations, respectively, while *v* represents the input from the vagus nerve which carries pulmonary stretch receptor information. The self-decay term denoting the rate of decay is defined by a_i, where *i* is the respective neuronal population. This term allows for silencing of the *i*-population when no input is present. W_{ji} refers to the gain of the signal, or weight, of the *j* neuron to the *i* neuron, whereas W_{ii} is the self-activation factor. B_i refers to the weight of the chemoreceptor signal, n_{CO2}, which is considered to change linearly with $PaCO_2$. To convert firing frequency of the neuronal population to population activity, a sigmoid function, *S*, is used. This *S* function is as follows,

$$S(X) = K \cdot \alpha + (1 - K) \cdot \beta \quad (15)$$

$$\alpha(X) = \begin{cases} \min(X, 4) & \geq 0 \\ 0 & < 0 \end{cases} \quad (16)$$

$$\beta(X) = \frac{4}{1 + e^{-1.75 \cdot (X-2)}} \quad (17)$$

Where X is the firing frequency and *K* is a constant that determines the steepness of the function.

The chemoreceptor input, n_{CO2}, is given as a linear step-wise function of $PaCO_2$:

$$n_{CO_2} = \begin{cases} P_aCO_2 > 35 & n_{CO_2} = 0.2 \\ 45 < P_aCO_2 < 35 & n_{CO_2} = (PaCO_2 \cdot 0.072) - 2.32 \\ P_aCO_2 < 45 & n_{CO_2} = 1.72 \end{cases} \quad (18)$$

The limits of 0.2 and 1.72 were set as a result of a set of preliminary simulations performed on the rCPG model to obtain the minimum and maximum n_{CO2} values at which a physiologically-relevant response was obtained. The linear function constants were set so that a linear response between a P_aCO_2 of 35 to 45 mmHg is maintained.

An exponential moving average of the peak $PaCO_2$ value sampled by the PG/PS controller each cycle is used by the chemoreceptor model to derive neural CO_2 input. To prevent instability caused by abrupt changes in $PaCO_2$ due to non-eupnic breaths such as sighs or gasps, a long time constant of 8 sec was used. This was determined through simulations which are described in later sections.

To represent the pulmonary stretch receptor input, *v*, a one-dimensional model of chest biomechanics was used (Lessard, 2009; Milhorn, 1966). This model is as below,

$$k_dN = m_L\ddot{x} + B_L\dot{x} + K_Lx \quad (19)$$

Where *x* is diaphragm displacement, m_L corresponds to diaphragm mass, B_L to a damping constant, and K_L to elastance. *N* refers to neural input from the inspiratory population of the rCPG, and k_d is a proportionality constant that translates displacement to mechanoreceptor output. Aside from providing the vagal feedback

necessary to birth the oscillatory behavior, this biomechanical model continuously provides a desired trajectory for the PS module.

The PS module for respiratory control has been described in Chapter 3. The PS module aims to determine adequate stimulation parameters to elicit a specified breath volume profile. In previous studies, this desired profile was preset based on baseline breath volumes and profiles for each rat; here, the desired profile was generated by the previously described PG module. Briefly, the PS consists of a single-layered neural network with time-shifted activation profiles. The output of the controller is a value from 0 to 1 which is multiplied by the maximum allowed current amplitude. The controller output to the stimulator, z, is given by

$$z(t) = \sum_{j=1}^{n_a} w_j(t) y_j(t) \quad (20)$$

The output is defined by the summation of the output of all weighted active neurons, n_a. Neuronal weights are given by w_j.

The PS uses a comparator to define the error at any time *t*, *e(t)*, between the desired volume trajectory defined by the PG module and the measured volume profile. The change in weight, Δw_j, for all neurons at time *t* is defined by

$$\Delta w_j(t) = \eta e(t) \sum_{k_p=1}^{n_p} \frac{1}{n_p} y_j\left(t - k_p T\right) \quad (21)$$

Where η is the learning rate, n_p is the number of past activations over which the error will be time averaged to account for delays in activation, and $y_j(t-k_pT)$ is the output of neuron *j* at previous times. Hence, the error at time *t* affects all neurons

that are currently active, with the most active neuron at time t receiving the largest alteration in weight.

The PG/PS controller was programmed and implemented in LabVIEW (National Instruments, Austin, TX) for both experimental and computational studies. All controller constants can be found in Table 1. In animal studies, the output of the controller was scaled to four times the twitch threshold and sent to a programmable stimulator as described in Chapter 3.

4.2.7 Computational platform for controller development

The PG/PS controller was developed and validated computationally though a software-in-loop approach (SIL) approach prior to *in vivo* assessment. A comprehensive rat computational model containing biomechanical, muscular, and CO_2 dynamics was developed based on a previously published model for rat biomechanical and muscular responses as in Chapter 3. A computational model for CO_2 generation in humans (Lessard, 2009; Milhorn, 1966; Topor et al., 2007) was adapted and scaled to match rat normative values found in literature (Molkov et al., 2014a; Whitehead et al., 1999) and integrated with the biomechanical model. The organization of these models and their integration with the adaptive PG/PS controller is illustrated in Figure 12. A list of constants and variables used for these models can be found in Table 1.

The model describing CO_2 dynamics is based on a CO_2 compartmental model containing a general body tissue compartment, a brain compartment, and a lung compartment with appropriate CO_2 transport delays (Molkov et al., 2014a). The

body tissue and brain compartments produce CO_2 based on compartment volumes and a rate of CO_2 production as described below

$$V_T \frac{dC_T}{dt} = M_T + Q(C_{AT} + C_T) \quad (22)$$

Where *T* represents brain tissue or body tissue, depending on the compartment. The concentration of CO_2 of the compartment, C_T, is given by volume of the compartment, metabolic rate of the compartment, $\dot{M}$, given as CO_2 production rate, perfusion through the compartment, Q, and CO_2 concentration from the arterioles to the compartment tissue, C_{AT}. The concentration from both compartments is then scaled by their respective perfusion rates and summed to represent total venous CO_2 concentration, C_V. This value is then sent to the lung compartment defined by

$$\frac{dVC_a}{dt} = \begin{cases} Q(C_V - C_a) + \dot{V}C_{in} & \dot{V} \geq 0 \\ Q(C_V - C_a) + \dot{V}C_a & \dot{V} < 0 \end{cases} \quad (23)$$

Where arterial CO_2 concentration is given by the difference between arterial CO_2 concentration and venous CO_2 concentration multiplied by total perfusion, Q, and during inspiration added to the inspired CO_2 concentration or, at any other point, arterial CO_2 concentration.

4.2.8 Computational studies for PG/PS development

Assessment of the controller was carried out in the computational testbed previously described. To first ensure the PG module responded appropriately to changes in $PaCO_2$, a range of $PaCO_2$ values from 20 to 60 mmHg were delivered to the PG through the chemoreceptor model. $PaCO_2$ remained constant

throughout a given simulation run. A proportional increase in minute ventilation for each increase in $PaCO_2$ would indicate that the PG module is able to respond accordingly to changes in CO_2.

The stability of the response to CO_2 is dependent on the stability of the measured signal. To reduce the possibility of controller instability due to sighs, shallow breaths, airway occlusion, or apnea, an exponential moving averager (EMA) was implemented. The time constant of the EMA was selected via simulated trials assessing the controller's response to two different physiological scenarios, sudden increase in metabolic demand and apnea. The sudden increase in metabolic demand was modelled by increasing CO_2 production in the tissue by 50% at 180 sec after pacing initiation. Apnea was simulated by setting diaphragm activation to zero for one cycle 300 sec after pacing initiation. Time constants of 1, 2, 4, 6, 8, 10, 15, 20, 25, and 30 sec were used for the EMA. The response was assessed by calculating the root mean square error (RMSE) between the measured $PaCO_2$ response and a desired CO_2 response from 5 sec prior to the increase in CO_2 rate production to 60 sec after the apnea is induced. A low standard deviation in RMSE would imply better stability after perturbation.

To assess the controller's ability to control ventilation reliably in response to changes in $PaCO_2$ in a closed-loop manner, simulations were carried out where a change in CO_2 was induced by modulating CO_2 production rate in the tissue. The baseline value for CO_2 production rate was modified to be 10% - 200% of baseline CO_2 production after 180 seconds to simulate changes in respiratory demand due

to metabolic activity. These simulations were performed to test the controller's ability to adapt to changes in baseline CO_2 production and to observe its ability to elicit the desired ventilatory pattern to maintain normocapnia. $PaCO_2$ at the end of the trial would be used to assess the controller's ability to regulate $PaCO_2$ to prevent hypocapnia or hypercapnia. The adaptive PG/PS controller was compared to a version of the controller with a constant PG output, but with adaptable PS, allowing matching of breath volume profile, but lacking ability to respond to $PaCO_2$.

4.3 Results

4.3.1 Adaptive closed-loop controller responds to changes in metabolic demand by adapting breath volume and breathing rate in computational studies

Computational studies showed that the controller, when provided with a wide range of $PaCO_2$ values, can compute a ventilatory pattern with an elevated minute ventilation, elicit the desired ventilation through modulation of stimulation parameters, and modulate this ventilation to control the rate of elimination of CO_2 within the body to maintain normocapnia. Figure 13(A) shows that with increasing $PaCO_2$ in the computational model, the controller responds by increasing tidal volume and decreasing cycle period.

Simulations were carried out to select a time constant that resulted in a stable controller response to sudden changes in $PaCO_2$. Controller stability was assessed by analyzing the responses to a sudden increase in CO_2 production and an apneic event. The results of these simulations using different time constants for the EMA in the chemoreceptor module are shown in Figure 13(B). After a 50%

increase in CO_2 production in the body tissue compartment, low values of τ led to a fast response but unstable oscillatory behavior long after the perturbation. Larger values, however, achieved stability but caused a significant overshoot in $PaCO_2$ after apnea. Overall, a τ of 8 sec led to a small overshoot with minimal underdamping as represented by the lowest $PaCO_2$ RMSE.

Simulations compared a fixed-PG version of the controller with one with an adaptive PG while varying CO_2 production rates across a range of 10% to 200% of the baseline CO_2 production rates. The fixed PG controller was only able to maintain normocapnia within 80% to 110% of the baseline CO_2 production rate, while the adaptive PG controller was able to achieve normocapnia within a range of 20% to 180% of the baseline CO_2 production rate. Thus, while the $PaCO_2$ did not always achieve normocapnia, when compared to a version of the controller with a fixed PG, the adaptive PG/PS showed a much wider range over which CO_2 tissue production rate could vary, as seen in Figure 13(C).

4.3.2 The adaptive PG/PS controller modulated ventilation to reduce $etCO_2$ after anesthesia-induced hypoventilation

The adaptive closed-loop controller was able to provide pacing that altered ventilation appropriately thereby alleviating hypercapnia in spinal cord intact animals that had undergone anesthesia-induced respiratory depression. Hypoventilation in these animals occurred due to suppression of the ventilatory response to hypoxia and hypercapnia (Dahan and Teppema, 2003; Sollevi and Lindahl, 1995). This resulted in a reduction in respiratory rate, as seen in Figure

14(A), which decreased minute ventilation, resulting in hypercapnia. Figure 14(B) shows how the adaptive closed-loop controller autonomously altered respiratory rate and breath volume in response to hypercapnia. Initially, the controller modulated pacing to increase minute ventilation, which led to a drop in $etCO_2$. As the trial progressed, the controller adapted and responded to a decrease in $etCO_2$ values by generating and evoking a ventilatory pattern with reduced minute ventilation, eventually leading to normocapnia throughout the trial as seen in Figure 14(C). The PG/PS controller was also able to maintain a low iRMSE throughout the duration of the trial, showing that the PS module was able to adapt and closely match the paced breath volume profile to the desired ventilatory pattern set by the PG module.

Similar results were observed across multiple animals, where the controller was able to generate and achieve a model-based ventilatory pattern that led to an overall decrease in $etCO_2$ after ventilatory depression. A summary of the effects of pacing on $etCO_2$ and iRMSE in all trials for all spinal cord intact animals can be seen in Figure 14(D) and Figure 14(E). Overall, $etCO_2$ decreased by 1.1% ($p < 0.05$) from controller initiation to the end of the trial. An average iRMSE of less than 15% also shows that the PS module of the controller was able to adapt despite variations in desired ventilatory patterns set by the PG module throughout the cycle as a response to changes in $PaCO_2$. Overall, these trials illustrate that, on a reduced ventilatory drive due to central respiratory depression, the PG/PS controller was able to respond appropriately and provide an adequate ventilatory

pattern. The PG/PS controller was able to elicit and maintain this constantly updating pattern by continuously modulating stimulation parameters.

4.3.3 The controller reduced and maintained $etCO_2$ close to normocapnic levels after trauma-induced hypoventilation in spinal cord injured rats

In animals with SCI-induced hypoventilation, the PG/PS controller was also able to generate and evoke a ventilatory pattern that could normalize $PaCO_2$ as it did in the anesthesia-induced hypoventilation group. In contrast to the effect of isoflurane, hemisection at the C2 level of the spinal cord leads to diaphragm hemiparesis, significantly decreasing inspiratory capacity without affecting the rCPG response to hypercapnia. This leads to a ventilatory pattern with lower tidal volume, decreasing overall ventilation which then causes hypercapnia. A comparison of the ventilatory pattern and ipsilateral diaphragm EMG before and after left C2 hemisection is shown in Figure 15(A). The EMG trace shows cessation of ipsilateral diaphragm activity after C2 spinal cord hemisection, verifying diaphragm hemiparesis. Figure 15(B) shows how the PG/PS controller responded after controller initiation at the start of the trial, shortly after entrainment onset, and at the end of the trial. After initiation, the adaptive PG/PS controller is able to elicit a breath volume profile with a tidal volume similar to or larger than that observed prior to injury and with a short breath cycle duration. The increase in tidal volume and decrease in cycle duration led to an increase in minute ventilation which caused a decrease in $etCO_2$ towards normocapnia. Once $etCO_2$ decreased to values close to normocapnia, the PG/PS controller updated the desired ventilatory

pattern to one with a reduced minute ventilation to remain within a normocapnic range and prevent hypocapnia. Figure 15(C) shows how the controller continuously updated the ventilatory pattern (as shown by the change in minute ventilation) throughout the trial in response to $etCO_2$ values while achieving and maintaining a ventilatory pattern that matched the desired ventilatory profile as shown by the low iRMSE values (9.1 ± 3.4%).

Figure 15(D) shows average $etCO_2$ for all left C2 spinal cord hemisected animals after onset of entrainment to pacing and prior to the end of the trial. Across all animals, the elevated $etCO_2$ resulting from reduced tidal volume decreased towards normocapnia after the PG/PS controller was turned on (7.1 ± 0.8% to 6.05 ± 0.4%). While iRMSE, Figure 15(E), was above that observed in the anesthesia-induced hypoventilation group, controller performance was still deemed acceptable (17.5 ± 8.2%). This demonstrates that the adaptive controller is still able to provide adequate respiratory pacing despite differences in body weight and tidal volume after injury.

4.4 Discussion

The adaptive PG, adaptive PS closed-loop controller for respiratory pacing developed here was able to maintain adequate arterial CO_2 levels despite dynamic changes in metabolic demand, impaired ventilatory control, and reduced inspiratory capacity. The adaptive PG/PS controller was able to accomplish this by implementing a two-stage approach. The controller first generated an adequate ventilatory pattern in response to $PaCO_2$ through a mathematical model of the

biological rCPG and then, through the use of an artificial neural network, adapted stimulation parameters to elicit this desired pattern. This allowed the controller to both define and elicit a desired ventilatory pattern on a breath-by-breath basis regardless of metabolic, physiological, or mechanical changes.

A computational testbed was used to test its ability to respond to a dynamic alteration in $PaCO_2$ prior to *in vivo* assessment. In simulations, the controller demonstrated its ability to respond to dynamic changes in $PaCO_2$ levels, maintained stable performance despite sudden changes in $PaCO_2$, and proved its efficiency in maintaining normocapnia in contrast to a version of the controller with a fixed PG and adaptive PS. In experimental trials, hypoventilation was induced in two groups of rats, one through anesthesia-induced respiratory depression and another through reduced inspiratory capacity as a result of diaphragm hemiparesis caused by left C2 spinal cord hemisection. Both groups showed an overall decrease in $etCO_2$ towards normocapnia after the adaptive closed-loop controller was initiated during diaphragmatic pacing. The controller's ability to respond to $etCO_2$ on a breath-by-breath basis allowed for an automated physiological-like response to $PaCO_2$ throughout the trials, restoring normocapnia despite ventilatory impairments. The results obtained from these studies suggest that the proposed controller could be used in respiratory pacing applications to restore adequate ventilatory function and thus maintain normocapnia after hypoventilation regardless of changes in metabolic demand and biomechanical properties.

4.4.1 Use of a computational testbed allowed for controller development and assessment prior to *in vivo* studies

Prior to *in vivo* testing, the PG/PS controller was developed through a software-in-loop (SIL) approach, allowing for rapid development and assessment of the control algorithm. A previous implementation of the controller utilized a computational model of the rat's ventilatory biomechanics to characterize the PS controller parameters and assess its behavior (Chapter 3). Aside from decreasing development time, this SIL approach allowed for the development of the PG/PS controller in a controlled and predictable environment, particularly for the development of the chemoreceptor response algorithm. Furthermore, by simulating the effects of a sudden change in CO_2 production and apneic events in the computational testbed, it was also possible to assess controller behavior and develop approaches that would minimize their effect on controller stability. This led to a more robust closed-loop controller that could then be evaluated in an *in vivo* setting.

The use of this SIL approach also allows for exploring future changes to the PG/PS controller that might lead to additional functionality of the PG/PS controller without having to undergo extensive *in vivo* assessment. Such functionalities could include addition of abdominal muscle for control of active expiration. Active expiration allows for shortening of the cycle period by decreasing expiratory time, thus increasing minute ventilation. Active expiration could be accomplished by replacing the rCPG model used here with one that includes active expiration, such

as that proposed by Molkov et al. (Molkov et al., 2014a). This would require an additional PS module dedicated to control of abdominal musculature; similar to how the PG/PS controller approach has been applied for closed-loop agonist/antagonist muscle control (Fairchild et al., 2010; Kim et al., 2009). A SIL approach allows for rapid development and implementation of this expiratory functionality in a convenient and cost-effective environment.

The rCPG model used placed limitations on the range of acceptable CO_2 chemoreceptor neural input. This led to the need to impose bounds on the linear response of the chemoreceptor. This, however, increased safety by limiting the controller such that apnea or lung damage from excessive tidal volumes did not occur. Another limitation is that the rCPG model used was based off a cat rCPG, thus the ventilatory pattern generated did not directly match that found in rats. However, after scaling of the breath cycle duration to that of rats and through use of the rat biomechanical model, the ventilatory pattern generated by the controller was similar enough to be considered adequate for use in the rat model. The rCPG used was also limited in its functionality in that it was not able to replicate ventilatory behaviors such as active expiration, sighing, and coughing. While the current PG/PS controller would not have been able to elicit these behaviors due to limitations imposed by lack of additional muscle support, future iterations of the controller could address this issue and extend controller functionality.

4.4.2 Closed-loop control of $PaCO_2$ achieves and maintains normocapnia after respiratory depression and after spinal cord injury *in vivo*

In both sets of animal experiments, the PG/PS controller was able to generate a desired ventilatory pattern in response to dynamic alterations in $PaCO_2$ levels and adapt stimulation parameters to elicit this ventilatory pattern, leading to a ventilatory response similar to that observed physiologically. However, the resulting ventilatory pattern matched the desired ventilatory pattern more closely in the anesthesia-induced hypoventilation group than in the hemiparesis-induced hypoventilation group. In the latter, the reduced inspiratory capacity was not able to accomplish the elevated tidal volumes generated by the PG after some time after pacing initiation. This could be attributed to onset of diaphragm fatigue and reduced contribution from the external intercostal muscles, which would also be paralyzed after left C2hX. Thus, as reduced tidal volume results in lower minute ventilation, the rate at which excess CO_2 would be removed would also decrease. Reduced efficacy in CO_2 removal could lead to the controller being unable to achieve normocapnia. This could be addressed through several approaches in future versions of the controller. Studies have shown that co-activation of intercostal muscles and diaphragm muscle leads to the production of a breath that is larger than the additive sum of their individual activations (DiMarco et al., 2005; Walter et al., 2011). Thus, co-stimulation of these additional muscle sets might be able to elicit the higher tidal volumes that the PG module generates during elevated hypercapnia. Furthermore, addition of external intercostal pacing could reduce the total amount of work required from the diaphragm, reducing the amount of stimulation received and thus mitigating diaphragm muscle fatigue. Muscle fatigue could also be mitigated by implementing spinal cord stimulation rather than

diaphragm or phrenic nerve stimulation. Unlike neuromuscular or neural stimulation approaches, spinal cord stimulation has shown to elicit physiological recruitment of muscle fibers (DiMarco and Kowalski, 2013; Hachmann et al., 2017; Kowalski et al., 2013). By reducing diaphragm fatigue, it might then be possible to elicit higher tidal volumes than those evoked through other approaches. In addition, spinal cord stimulation could also synergistically stimulate the external intercostal muscles (DiMarco and Kowalski, 2013; Hachmann et al., 2017), further increasing likelihood that elevated tidal volumes could be achieved.

The interplay between an intrinsic neural ventilatory drive and respiratory pacing becomes much more significant when control of $PaCO_2$ is involved. This was seen in several trials when the controller was able to reduce $etCO_2$ to normocapnic values of 5% or lower. In these cases, loss of entrainment occurred more often than when $etCO_2$ was above normocapnia. This could be due to the combined effect of a decrease in respiratory drive leading to lower respiratory rate and reduced stimulation as a result of reduced desired tidal volume. Studies have shown that higher respiratory frequencies, within a certain percent difference, are able to better entrain to mechanical ventilation (Graves et al., 1986; Petrillo and Glass, 1984). It is likely that the same mechanism is at play here, causing a decrease in likelihood of entrainment between the intrinsic breathing and the pacing. As discussed in Chapter 3, reduced stimulation may also lead to increased rate of loss of entrainment, as entrainment was usually recovered when the controller increased stimulation. Both aspects can be seen when loss of entrainment causes a rise in $PaCO_2$. As $PaCO_2$ increases, desired tidal volume

and respiratory rate increase, strengthening the link between the intrinsic respiratory drive and increasing likelihood of entrainment. This could be addressed by modifying the PG module within the rCPG model such that breath volume remains above a tidal volume conducive to entrainment. By allowing the controller to create ventilatory patterns with larger tidal volumes and compensating by decreasing respiratory rate to maintain an equivalent minute ventilation, it would be possible to elicit ventilation that remains physiologically relevant, but with improved likelihood of entrainment. Alternatively, it may be possible to improve entrainment by periodically evoking sighs. The elevated volumes elicited during sighing would ensure entrainment is maintained. Additionally, sighing has been shown to improve oxygenation and reduce regional lung strain (Mauri et al., 2015), thus improving overall patient health.

4.5 Clinical Significance

While mechanical ventilation is the “gold-standard” for ventilatory support, respiratory pacing has gained traction recently as it is able to overcome many of the drawbacks of mechanical ventilation such as muscle atrophy due to respiratory muscle inactivity, lung tissue damage due to excessive pressure, and improved ambulatory capabilities. However, there is a lack of closed-loop respiratory pacing paradigms, due in large part to the reasonably extensive safety requirements for such a life-sustaining technology. The adaptive controller presented here attempts to deliver a robust and safe control approach for respiratory pacing that does not rely on subjective measures or clinician expertise to determine appropriate

stimulation and ventilatory parameters. This adaptive controller is able to control ventilation to maintain normocapnic $PaCO_2$ in a similar manner as physiological ventilatory control does. By being able to control ventilation in such a manner, this controller allows the user to engage in activities that could lead to elevated metabolic demand, such as during a physically demanding rehabilitation session after spinal cord injury, without risking hypoventilation. Conversely, it would prevent hyperventilation under activities that have low metabolic demand, such as during sleep. By being able to adequately ventilate the user, this controller is likely to lead to an improvement in the user's quality of life and overall health.

4.6 Overall conclusion

A closed-loop adaptive controller with a neuromorphic architecture has been developed through the use of a computational testbed and assessed both computationally and through *in vivo* experimentation. The adaptive controller was able to restore normocapnia in rats with depressed ventilation due to anesthesia and in rats with reduced inspiratory capacity due to respiratory muscle hemiparesis. While further optimization is required to increase controller robustness and reliability prior to clinical use, the work presented here serves as an important step in the development of a clinically feasible controller for treatment of chronic hypoventilation.

Table 1. Controller parameters and computational model constants

r =	1.1	W_{EI} =	1.371	W_{PI} =	1.719	W_{LI} =	5.0	W_{II} =	0.7
W_{IL} =	1.361	W_{EL} =	0.793	W_{RL} =	2.056	W_{LL} =	2.3	W_{vL} =	10.5
W_{EP} =	1.351	W_{RP} =	2.254	W_{PP} =	1.540	W_{IE} =	0.729	W_{RE} =	2.254
W_{EE} =	1.550	W_{IR} =	1.80	W_{PR} =	2.150	W_{RR} =	0.650	W_{vR} =	1.05
K =	0.6	k_d =	7 gcm^3/s	m_L =	1.8 g	B_L =	8.4 g/s	K_L =	11.5 g/s^2
n_a =	17	n_p =	6	η =	0.001	T =	0.014 s	V_T =	297.72
V_B =	2.28	M_T =	0.49	Q =	1.2875 ml/s			Q_T =	1.2512 ml/s
Q_B =	0.0363 ml/s	C_{in} =	0.01	τ_{AT} =	0.027 s	τ_{AB} =	0.01 s		
τ_{VT} =	0.1 s	τ_{VB} =	0.02 s						

Figures

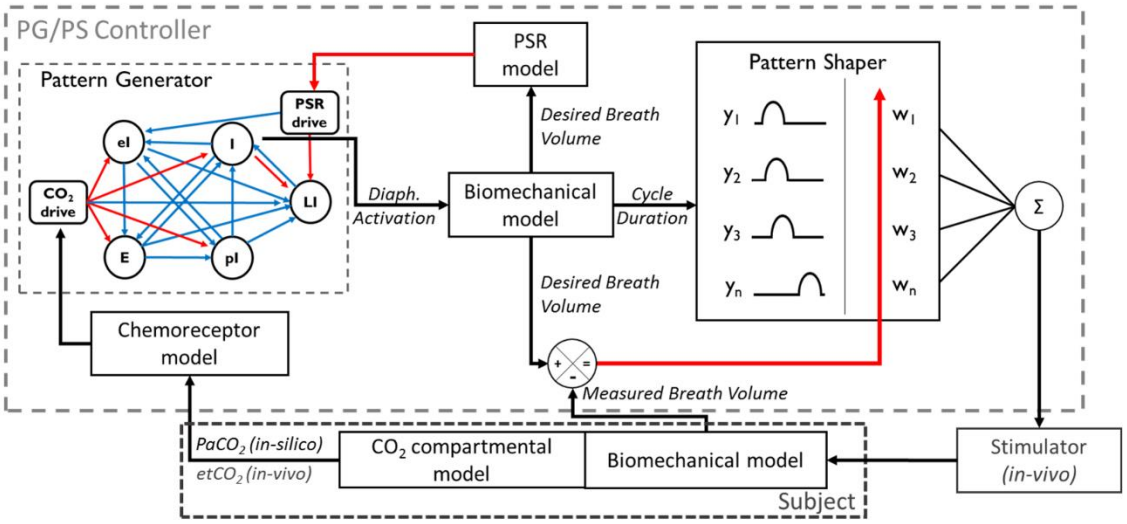

Figure 11. Architecture and design of the Pattern Generator / Pattern Shaper adaptive controller. A computational neural network model of the respiratory central pattern generator generates a ventilatory activity pattern based on input from pulmonary stretch receptor model and a CO_2 chemo-transducer which converts a measure of CO_2 into neural drive. The output of the inspiratory neuronal population serves as input into a biomechanical model of the chest to provide a “desired” breath volume profile. This desired profile is then compared to the measured breath volume profile within the Pattern Shaper module to derive an error measure which is used to modulate output weights in a single layer artificial neural network with time-shifted activation profiles. The output of each neuron is summed and serves as input to a programmable stimulator interfaced with the diaphragm. A change in ventilation due to pacing then drives a change in CO_2, closing the control loop.

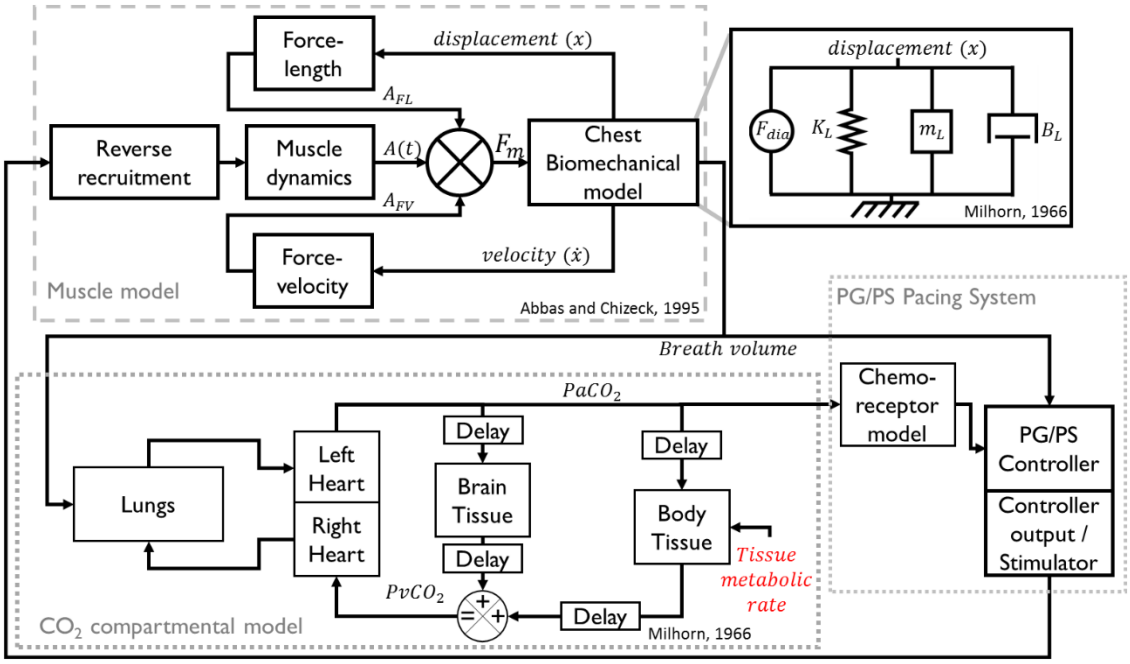

Figure 12. Organization of the computational testbed of the PG/PS controller using a rat model of chest biomechanics and CO_2 dynamics. A muscle model drives the force generated in a one-dimensional model of chest biomechanics. The ventilation elicited by this model drives changes in $PaCO_2$ in the compartmental model of CO_2 dynamics. $PaCO_2$ is sampled by the controller which then drives force generated by the muscle model. Changes in rate of CO_2 production were used to assess the controller's ability to maintain normocapnia. Parameters and values have been obtained from literature or scaled to match rat proportions.

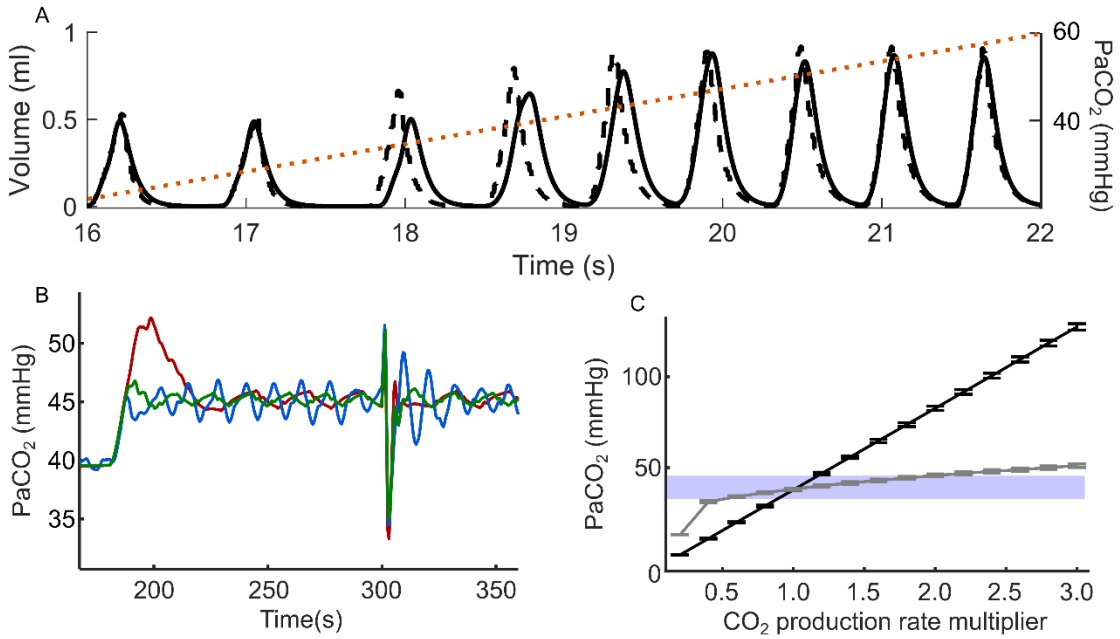

Figure 13. Adaptive PG/PS controller behavior in a computational testbed. **(A)** Open-loop PG, adaptive PS response to increased $PaCO_2$ values. The PG module generates a desired ventilatory profile (dashed) in response to $PaCO_2$ levels (dashed). The PS module responds by adapting stimulation to elicit a breath volume (solid) matching that of the pattern dictated by the PG. **(B)** Evaluation of the PG/PS response to $PaCO_2$ under various chemo-transducer time constants of 2 sec (blue), 8 sec (green), and 30 sec (red). Across all values assessed (1 – 30 sec), a time constant of 8 sec provided the best stability and robustness to perturbations. **(C)** Comparison between a fixed PG adaptive PS (solid black) and an adaptive PG/PS controller's (solid grey) ability to maintain normocapnia from 20% to 200% of the baseline CO_2 production rate. The adaptive PG/PS showed a much wider normocapnic range than the fixed PG adaptive PS, resulting from the controller's ability to substantially increase ventilation in response to $PaCO_2$.

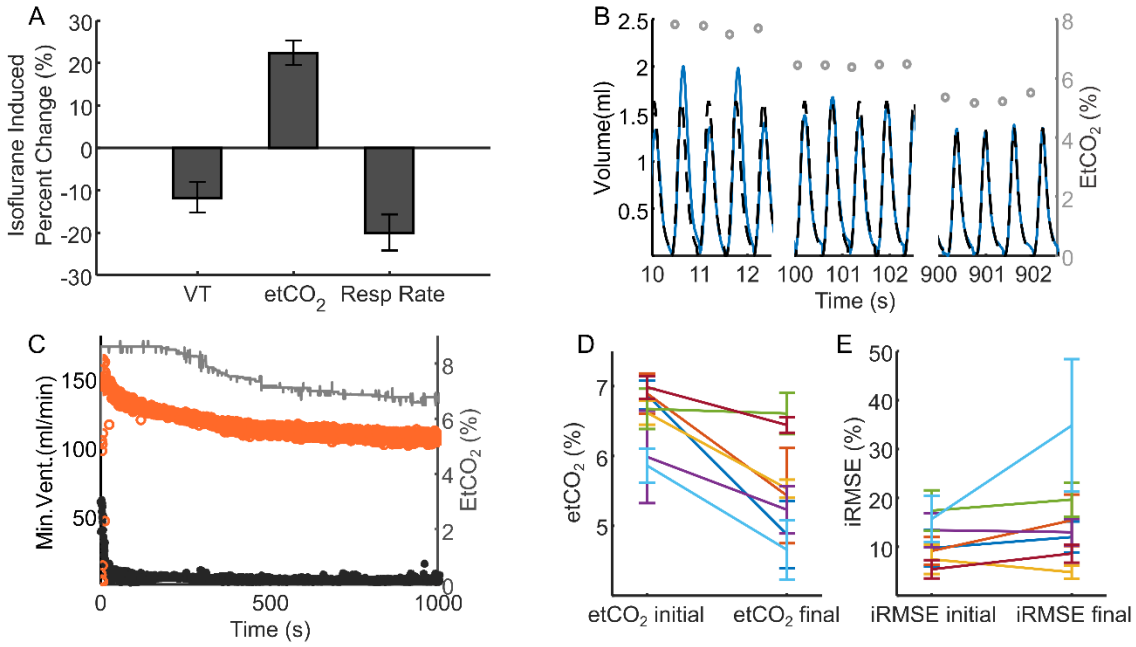

Figure 14. Adaptive PG/PS controller use *in vivo* after anesthesia-induced hypoventilation. (A) Supplemental isoflurane (+1.5%, 100% O_2) caused hypoventilation via a decrease in both tidal volume and respiratory rate after 10 min, which led to an increase in $etCO_2$. **(B)** Adaptive PG/PS controller response following ventilatory entrainment, 100 sec, and 900 sec after controller initiation. The adaptive PG/PS was able to respond to the elevated peak $etCO_2$ (circles) by eliciting a hypoventilatory pattern (dashed line) and adapting stimulation to match the measured volume (solid line) to the desired pattern. After 900 sec, $etCO_2$ is within acceptable levels and thus the ventilatory pattern elicited shows a decreased tidal volume and respiratory rate. **(C)** Adaptive PG/PS controller response throughout a 1000 sec trial. The adaptive PG/PS controller responds to an elevated $etCO_2$ (orange, empty circle) by dictating a ventilatory pattern with a high minute ventilation (grey). This in turn causes a decrease in $etCO_2$ towards normocapnia. Throughout the trial, iRMSE (black, solid circles) remains low (<10%) showing that the PS controller is able to match the pattern dictated by the PG. **(D)** The adaptive PG/PS controller was able to significantly decrease $etCO_2$ in 6 rats after anesthesia-induced hypoventilation. **(E)** Across all rats, iRMSE remained within 20%. One trial showed elevated iRMSE at the end of the trial due to loss of entrainment. A low tidal volume resulted from low $etCO_2$, decreasing likelihood of entrainment.

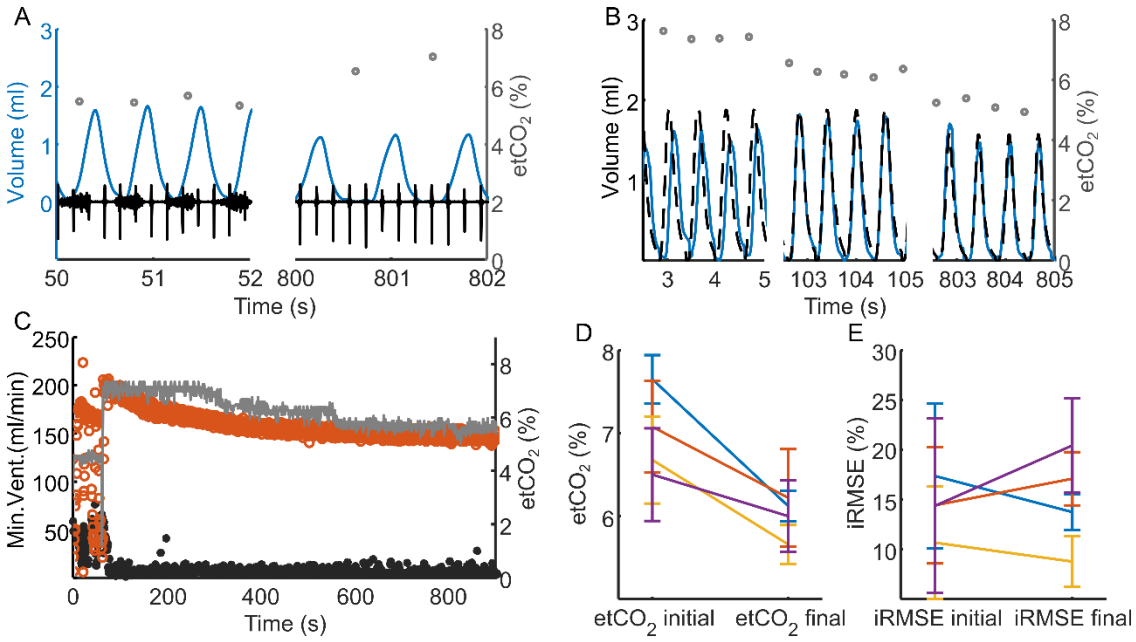

Figure 15. Adaptive PG/PS use *in vivo* after hypoventilation following C2 spinal cord hemisection. (A) Hemisection of the C2 spinal cord leads to hypoventilation due to paralysis of the hemidiaphragm ipsilateral to the injury as seen by lack of bursts of EMG activity (black) following C2 spinal hemisection. This leads to hypoventilation and consequently, to an increase in $etCO_2$ (empty circles). **(B)** The adaptive PG/PS controller initially generates a desired ventilatory pattern (dashed line) with elevated breath volume and respiratory rate due to elevated $etCO_2$. The PS then attempts to match the measured volume (solid line) to the desired ventilatory pattern. At 100 sec, the PS was able to match the measured breath volume to the elevated ventilatory profile, causing a decrease from the initial $etCO_2$ (empty circles). By the end of the trial at 800 sec, $etCO_2$ has been reduced to normocapnic ranges and thus the desired ventilatory pattern is one with reduced tidal volume and respiratory rate. **(C)** Throughout the trial, the PG/PS controller is able to autonomously modulate stimulation parameters, as shown by the low iRMSE (black, solid circle), to elicit sufficient minute ventilation (grey) to reduce $etCO_2$ (orange, empty circle) to normocapnic values. After $etCO_2$ has achieved normocapnia, ventilation is reduced such that normocapnia is maintained for the rest of the trial. **(D)** The adaptive PG/PS controller was able to restore ventilatory function and reduce $etCO_2$ significantly across all C2 spinal cord hemisected animals. **(E)** iRMSE across all animals before and after PG/PS controller intervention.

CHAPTER 5

ADAPTIVE CONTROL OF VENTILATION THROUGH THE USE OF AN ADAPTIVE CLOSED-LOOP PATTERN GENERATOR PATTERN SHAPER CONTROLLER IN AN INTEGRATED HUMAN COMPUTATIONAL TESTBED OF CHEST BIOMECHANICS AND CO_2 DYNAMICS

5.1 Introduction

Currently, respiratory pacing serves as an alternative to mechanical ventilation for treatment of hypoventilation after spinal injury, in congenital central hypoventilation syndrome, in central sleep apnea, or other conditions in which the phrenic nerve and the innervation of the diaphragm are intact, but the respiratory control center or pathways are impaired. Respiratory pacing electrically stimulates respiratory muscle(s) or their respective innervating nerves to cause a contraction and thus elicit a functional breath (DiMarco, 2018; Garara et al., 2016; Onders, 2012). This prevents issues regarding muscle atrophy, damage due to excessive positive pressure, and improves mobility and speech (DiMarco, 1999; Onders, 2012). However, all currently available respiratory pacing systems utilize open-loop control. Open-loop systems require modulation of stimulation parameters by trained professionals whenever changes to the ventilatory system occur, such as changes in CO_2 production or onset of fatigue. Additionally, each patient will possess different muscle activation requirements due to differences in biomechanical properties such as differences in muscle mass or fiber distribution, body weight, and pulmonary resistance and compliance. This leads to each patient

requiring long sessions to calibrate the system and set appropriate stimulation parameters during their first system setup. Implementation of closed-loop strategies for respiratory pacing can lead to avoidance of these issues, which may lead to an improvement in quality of life for users of respiratory pacing systems.

A neuromorphic closed-loop adaptive controller has been developed that can elicit appropriate ventilation despite changes in CO_2 production, respiratory depression, and presence of diaphragm hemiparesis in rats. This adaptive controller follows a Pattern Generator Pattern Shaper (PG/PS) approach first developed and assessed for control of locomotion of the lower limb (Abbas and Chizeck, 1991; Abbas and Triolo, 1997; Fairchild et al., 2010; Kim et al., 2009; Riess and Abbas, 2000) and then adapted for ventilatory control use as described in Chapters 3 and Chapters 4 of this dissertation. The PG/PS controller mimics the physiological control of ventilation by implementation of a PG module that defines a model-based ventilatory pattern based on a measure of arterial partial pressure of CO_2 ($PaCO_2$) and a PS module that adapts stimulation parameters to elicit a ventilatory profile that matches the ventilatory profile provided by the PG. This approach leads to adaptive closed-loop control of ventilation for regulation of $PaCO_2$ regardless of changes that might occur as a result of biomechanical, physiological, or metabolic factors.

Previous work concerning the closed-loop adaptive control for respiratory pacing assessed its performance in computational models and experimental *in vivo* rat models. While technology validation in animals is considered a critical step in the

translational pathway, differences in physiology between human and animal models can lead to results that differ from those found in preclinical studies (Kwon et al., 2010; Mak et al., 2014; Siddiqui et al., 2016). Factors such as respiratory rate range and CO_2 dynamics influence how controller parameters are defined and as such, how it will respond. Hence, a transitional stage is necessary to properly adapt the controller to match human physiology. Here, a computational testbed served as a developmental platform in which the controller could be converted for use in diaphragmatic pacing in people and as a platform to assess the adapted controller's performance in comparison to earlier animal studies.

Previously, the adaptive PG/PS controller was developed and assessed in a two-stage process. The first stage addressed development and assessment of the PS module. The PS module was evaluated based on its ability to adapt to achieve and maintain a desired breath volume regardless of changes in ventilatory biomechanics. Animal studies were able to demonstrate that the PS module could adapt stimulation parameters to maintain the desired breath volume, despite onset of diaphragm muscle fatigue (Siu et al., 2019). Thus, assessment of the controller's ability to account for diaphragm fatigue can be considered a viable test to validate the PS module. The second stage concerned the development and assessment of the PG module of the adaptive controller as well as its integration with the PS module. In Chapter 4, the PG/PS controller was evaluated based on its ability to achieve and maintain normocapnia after hypercapnia had been induced. Studies in hypercapnic rats showed that the adaptive controller could generate a model-based ventilatory pattern in response to changes in $PaCO_2$ and elicit this pattern

through adaptation of the stimulation parameters in order to attain normocapnia. Thus, assessment of the controller's response to changes in CO_2 production rate, which would result after changes in metabolic activity, can be used to test the controller's ability to respond to changes in metabolic demand. Finally, subject-to-subject variability was inherently present in all animal studies. By evaluating controller performance in a computational testbed with randomized model parameter sets, it is possible to demonstrate that the closed-loop PG/PS controller is able to provide personalized pacing to maintain normocapnia.

A computational testbed with integrated models of ventilatory biomechanics and CO_2 dynamics was used to transition the PG/PS controller to a human implementation and to carry out the above-mentioned assessments in a computational environment. These computational studies demonstrated that the adaptive controller was able to be translated for human implementation in a manner that preserves or improves the performance observed in previous pre-clinical trials. While additional validation is required prior to clinical use of this neuromorphic control algorithm, these computational trials serve to inform future clinical studies and serve as a platform in which the controller can be optimized to deliver a safer, more robust adaptive closed-loop controller for respiratory pacing.

5.2 Methods

5.2.1 PG/PS controller design

The PG/PS controller utilizes the architecture similar to that of the human ventilatory control scheme. This allows the controller to elicit a physiological-like

ventilatory response. The structure of the PG/PS controller has been defined previously in Chapter 3 and 4 and will thus only be described briefly here. The PG consists of a mathematical model based on that of the respiratory central pattern generator (rCPG) developed by Botros and Bruce (Botros and Bruce, 1990). The rCPG network model consists of five interconnected neuronal populations that generate a ventilatory pattern in response to chemoreceptor input and mechanoreceptor feedback. Each population is maximally activated at a particular phase of the respiratory cycle. Chemoreceptor and mechanoreceptor inputs modulate the output of the rCPG. The chemoreceptor input, n_{CO2}, is given by a linear stepwise function of $PaCO_2$ given below.

$$n_{CO_2} = \begin{cases} P_aCO_2 < 35 & n_{CO_2} = 0.2 \\ 53 < P_aCO_2 < 35 & n_{CO_2} = (PaCO_2 \cdot 0.072) - 2.32 \\ P_aCO_2 > 53 & n_{CO_2} = 1.5 \end{cases} \quad (23)$$

To represent the mechanoreceptor input, a one-dimensional model of chest biomechanics was used (Milhorn, 1966). The output from the “inspiratory” neuronal population of the rCPG drives the diaphragm muscle within the biomechanical model, creating a contractile force which drives diaphragm displacement. This displacement is then scaled to average human parameters to represent breath volume. This output contains information on the timing and shape of the breath as dictated by the PG and the biomechanical model and serves as the “desired” ventilatory pattern that the PS module described below is set to follow. The PG continuously generates a ventilatory pattern in response to alterations in $PaCO_2$

values, updating the desired ventilatory pattern used by the PS module within breaths.

The PS module's role is to adapt stimulation parameters to evoke the ventilatory pattern generated by the PG module. The PS module is composed of a single-layer neural network with neuronal outputs shifted by 0.05 s along the respiratory cycle, as described in Chapter 3 (Siu et al., 2019) and Chapter 4. Distribution of the neurons across the respiratory cycle allows for activation of specific neurons during specific respiratory phases. The total number of neurons within the network is based off a maximal breath duration of 6 seconds, resulting in a total of 120 artificial neurons. Shortening of the breathing cycle inactivates neurons that are active during the early expiratory phase of the breathing cycle. Neurons found elsewhere in the cycle remain active to ensure they can contribute to the controller output during elevated respiratory rates. Briefly, each neuronal output, or activation, consists of a weighted raised cosine function maximal at equally distributed discrete points throughout the breath cycle. At each time step, weights for each neuronal output is continuously modulated based on an error value, a learning rate, and previous neuronal outputs. The error is calculated from differences between the desired volume profile and the evoked volume at each time step. A learning rate value increases or decreases the magnitude by which the weights are updated. Previous activations, up to a certain past activation value, are averaged to distribute the error of previous activations into the current activation to account for biomechanical delays in muscle activation. The controller

parameters are given in Table 1. Figure 16 depicts a PG/PS controller design and its integration with the computational testbed described below.

5.2.2 Computational testbed for controller development

The PG/PS controller was developed and tested in Simulink (Mathworks Inc., MA) using a computational model of the human respiratory biomechanics paired with a reverse recruitment model of the diaphragm (Hillen et al., 2014), and a CO_2 compartmental model (Batzel and Tran, 2000).

The biomechanical model consists of a Hill-type muscle model with reverse recruitment behavior, chest resistance and compliance, and a pulley system representing diaphragm and central tendon mechanics (Hillen et al., 2014). The muscle model implemented here has been described previously (Cheng et al., 2000; Song et al., 2008) and adapted to the diaphragm muscle using parameters reported elsewhere (Gorman et al., 2002). Here, the muscle is divided into two hemidiaphragms, with identical stimulation being delivered to both hemidiaphragms. The biomechanical model is represented by the mathematical model listed below,

$$F_{Lhdia} + F_{Rhdia} = B_{L2}\dot{x} + K_{L2}x \quad (24)$$

With F_{Lhdia} and F_{Rhdia} representing the force elicited by the left and right hemidiaphragms, respectively. The PG/PS controller is paired with this biomechanical model by replacing the neural activation with the controller output.

The CO_2 2-compartment model is based off a model developed for analysis of respiratory dynamics (Batzel and Tran, 2000). This adapted model consists of a lung compartment in which transport of CO_2 between ambient air and blood occurs, and a tissue model in which blood collects the CO_2 produced by a tissue volume. The original model also consists of a brain compartment for CO_2 feedback to a central controller; however, that aspect was ignored in the current implementation as the adaptive controller is to serve as a substitute for the intrinsic central controller. Production of CO_2 within the tissue compartment is used to represent overall CO_2 production in the body.

Concentration of CO_2 in the lung compartment is defined by

$$V_{A,CO_2}\dot{F}_{A,CO_2} = Q\left(C_{v,CO_2} - C_{a,CO_2}\right) + \dot{V}_A\left(F_{i,CO_2} - F_{A,CO_2}\right) \quad (25)$$

Where $F_{A,\,CO2}$ and $F_{i,\,CO2}$ represent the fractional concentration of CO_2 in the alveoli and inspired air, respectively. Effective CO_2 volume in the lung compartment is given by $V_{A,CO2}$. $C_{V,CO2}$ and $C_{a,CO2}$, refer to concentration of CO_2 in venous blood and arterial blood respectively. Q refers to cardiac output, or pulmonary flow, and V_A refers to alveolar ventilation, which is provided by the biomechanical model controlled by the PG/PS controller.

The tissue compartment where CO_2 is produced is given by

$$V_{T,CO_2}\dot{C}_{v,CO_2} = Q\left(C_{a,CO_2} - C_{v,CO_2}\right) + MR_{CO_2} \quad (26)$$

Where $V_{T,CO2}$ is the volume of the tissue in which CO_2 is produced, $C_{v,CO2}$ is the venous concentration of CO_2, $C_{a,CO2}$ is the arterial CO_2 concentration, and MR_{CO2}

is the rate at which CO_2 is produced. The transport delays this CO_2 compartmental model and other constants can be found in Table 1.

5.2.3 Simulations

The controller was integrated into the Simulink computational testbed by utilizing $PaCO_2$ output from the CO_2 compartmental model as the input to the PG and using the biomechanical model output as the measured volume input to the PS module. A scheme of this computational setup is shown in Figure 17. Simulations were done to assess the adaptive controller's performance when presented with changes in production rate of CO_2, in the presence of severe fatigue, and on models with randomized biomechanical properties. Performance in all of these simulations was assessed by deviation of $PaCO_2$ from the normocapnic range to assess ability to control $PaCO_2$ and by evaluation of iRMSE values across the simulation to assess ability to match the elicited ventilatory pattern to the desired ventilatory pattern.

Simulations in which CO_2 production rate was varied from 20% to 200% of the baseline CO_2 production rate to represent changes in metabolic activity were carried out to assess the controller's ability to maintain $PaCO_2$ levels within normocapnic range. The PG/PS controller was initiated at $t = 0$ and left to perform under a nominal CO_2 production rate for 500 sec, after which the change in CO_2 production occurred. These simulations were designed to determine the range over which normocapnia can be maintained by the PG/PS controller. For comparison, the same set of simulations were carried out utilizing a version of the

controller with an open-loop PG that is unable to respond to $PaCO_2$ and thus maintains a constant ventilatory pattern throughout the simulated trials.

To assess the controller's ability to account for fatigue, changes in fiber properties were made to the muscle model (Hillen et al., 2014). The non-fatigued model had a fractional physiological cross area (PCSA) of 0.37 for slow fibers and 0.63 for fast fatigable fibers (Polla et al., 2004; Stubbings et al., 2008). In the fatigued model, the fractional PCSA was changed to 0.99 for slow fibers and 0.01 for fast fatigable fibers to represent the shift in the ratio of fiber contribution to force production after onset of fatigue. Moreover, muscle mass was reduced from 213 g to 150 g to simulate a 50% reduction in force after fatigue to match experimental data (Gorman et al., 2002). Simulations consisted of trials under both non-fatigued and fatigued conditions. Changes in iRMSE and charge delivered were assessed to observe how the controller responded to these fatigue-related changes.

Lastly, to assess the PG/PS controller's ability to deliver personalized pacing to achieve and maintain normocapnia, simulations with randomized model parameters within the computational testbed of human ventilatory biomechanics and CO_2 dynamics were carried out. The parameters that were changed were diaphragm muscle mass, chest compliance, effective CO_2 volume within the lungs, cardiac output, and volume of tissue in which CO_2 is produced. These parameters were randomized following a normal distribution to values within 20% of the normative values found in Table 1. A total of five randomized sets of parameters were used. The model parameters used in each testbed are listed in Table 2. Each

trial consisted of a 50% increase in CO_2 production rate after 500 sec of controller initiation.

5.3 Results

5.3.1 The adaptive PG/PS controller is capable of maintaining normocapnia after changes in CO_2 production rate

The adaptive PG/PS controller was able to determine a proper ventilatory pattern based on the change in CO_2 production, modulate stimulation parameters to match and maintain this ventilatory pattern, and then elicit a proper response again when CO_2 production rate returned to baseline. This response can be seen in Figure 18(A) across different time periods in a simulated trial lasting 2000 sec. As $PaCO_2$ increased due to a 40% increase in CO_2 production rate, the PG responded by eliciting a new ventilatory profile with a higher minute ventilation, transitioning from one of 119.1 L/min to 135.05 L/min. This increase in minute ventilation was sufficient to maintain $PaCO_2$ within normocapnic levels. Despite the PG generating different ventilatory profiles as it responded to changes in $PaCO_2$, the PS module was able to fine-tune stimulation parameters to elicit a ventilatory profile that matched that of the desired ventilatory profile. Figure 18(B) depicts the same trial as in Figure 18(A) but shows $PaCO_2$ and iRMSE throughout the entirety of the trial. CO_2 production rate was increased by 40% at 500 sec and remained elevated for the remaining duration of the trial. Throughout the trial, iRMSE was consistently low, showing that the PG/PS controller was able to match the desired ventilatory profile consistently as seen in Figure 18(A). Additionally, it is worth highlighting that

the rate of change in $PaCO_2$ due to change in CO_2 production was slower than the rate of change in $PaCO_2$ due to ventilation, allowing for an adequately damped response to changes in $PaCO_2$, reducing risk of instability and/or oscillatory behavior.

Figure 18(C) compares $PaCO_2$ between the fixed PG, adaptive PS and the fully adaptive PG/PS controllers at the end of trials in which CO_2 production rate was varied from 20% to 200% of the baseline rate. The adaptive PG/PS controller was able to maintain normocapnia within a range of 20% to 180% of the baseline rate of CO_2 production. This is a much wider range when compared to when a fixed PG, adaptive PS controller is used (90 to 110% of baseline). Figure 18(D) shows $PaCO_2$ and minute ventilation in trials where CO_2 production rate was altered to 20%, and 180% of the baseline rate using both a fixed PG, adaptive PS and an adaptive PG/PS approach. The adaptive PG/PS controller has a clear effect on $PaCO_2$ as it is able to significantly reduce the effects of the change in CO_2 production rate.

5.3.2 The adaptive controller is able to adapt to account for fatigue

The presence of muscle fatigue did not adversely affect the controller's ability to elicit a desired ventilatory pattern to achieve and maintain normocapnia. Figure 19(A) and Figure 19(B) show the first 40 sec of trials in which, respectively, no fatigue is present and with fatigue. During fatigue, a markedly larger PG/PS controller output amplitude is observed. This is caused by the reduced force capacity of the muscle, prompting the adaptive PS to provide a compensatory

increase in output to elicit a ventilatory pattern that matches the desired ventilatory profile given by the PG.

Figure 19(C) shows that here was no difference in iRMSE between both conditions, inferring that the controller was able to achieve the desired ventilatory profile regardless of fatigue. However, as expected, peak controller output differed greatly as the trial with fatigue showed a large increase in output to account for the reduced force capacity of the diaphragm. The resulting PG/PS output profile in both trials shows how differences in muscle condition can lead to differences in controller output. Figure 19(D) shows the PG/PS controller output profile of the last cycle of each trial. Other than an elevated amplitude, differences in the controller output profile are present. This is most likely due to differences in activation properties as a result of difference in fiber fractional PCSA rather than differences in force capacity. This highlights the benefits of implementing a controller that is able to autonomously decide the stimulation parameters in a closed-loop manner to account for changes in muscle fiber properties as a result of muscle fatigue or muscle atrophy.

5.3.3 The PG/PS controller is capable of providing individualized respiratory pacing to achieve and maintain adequate ventilation

All previous simulations assessed controller response in a single computational model with the same model parameters. To verify that the PG/PS controller is able to achieve the normocapnia regardless of differences in individual properties, the controller was implemented in computational testbeds of human ventilatory

biomechanics and CO_2 dynamics with randomized model parameters. Regardless of these differences, the controller was able to modulate stimulation to match the ventilatory pattern given by the PG module of the controller, resulting in normocapnic $PaCO_2$ (Figure 20(A)) and low iRMSE (Figure 20(B)). While iRMSE and $PaCO_2$ were very similar for all sets of parameters, there were expected differences found in the PG/PS controller output. Figure 20(C) shows that PG/PS controller output per cycle differed more between each set of parameters compared to iRMSE and $PaCO_2$. This can be attributed to the PG/PS controller being able to account for differences in biomechanical properties between the parameter sets resulting in differences in PG/PS controller output profiles.

5.4 Discussion

A human computational model served as a testbed to evaluate performance of an adaptive closed-loop controller for ventilatory control after transition from a rat model implementation. This adaptive controller was able to respond to a measure of $PaCO_2$, determine an appropriate ventilatory response, and adapt stimulation to elicit this response, successfully mimicking physiological control of $PaCO_2$ in a human computational model of ventilatory biomechanics and CO_2 dynamics. Simulations showed that the adaptive controller was able to adequately control $PaCO_2$ to maintain normocapnia within a wide range of CO_2 production rates, despite presence of fatigue, and when varying model parameters in the computational testbed. This computational study serves as an important transition between pre-clinical studies and future clinical trials, addressing some of the

questions and concerns that would be present during clinical implementation of the closed-loop adaptive controller.

5.4.1 The adaptive controller is able to determine an appropriate ventilatory response to maintain normocapnia

The PG/PS adaptive controller is designed to respond to changes in $PaCO_2$ continuously to ensure normocapnia is maintained. However, similarly to physiological ventilatory control, the PG/PS controller is only able to maintain normocapnia within a certain range. In the simulations carried out, normocapnia was not maintained when the CO_2 production rate was less than 20% and more than 180% of the baseline value, respectively leading to slight hypocapnia and hypercapnia, respectively. However, when a controller unable to account for $PaCO_2$ was assessed at these limits, the resulting values were those that suggest cerebral damage (Marhong and Fan, 2014; Roussos and Koutsoukou, 2003), demonstrating the advantage of the adaptive closed-loop control approach over an open-loop control approach. It is, however, possible to further optimize the controller to expand this range. While the inspiratory breath volume elicited by the PG did approach the suggested inspiratory capacity for adult males, respiratory rate could still be maximized by reducing expiratory time through active expiration. This could be accomplished through control of expiratory muscles and by replacing the current rCPG model used to one that exhibits active expiration, such as one proposed by Molkov et al (Molkov et al., 2014a). A separate PS module would need to be included to control the additional expiratory muscles in a similar manner

as shown in earlier studies concerning flexor/extensor muscle PG/PS control (Abbas and Triolo, 1997; Fairchild et al., 2010; Jung et al., 2009; Kim et al., 2009). Instead of activating off the inspiratory neuronal population, this additional PS module would be based off the expiratory neuronal population; providing the desired activation for the abdominal muscles.

While the ventilatory pattern provided by the PG was limited due to physiological constraints, the ventilatory changes elicited by the controller were comparable to physiological limits. Hence, it is possible that metabolic conditions leading to a rate of CO_2 production that exceeds that of CO_2 removal would be due to more critical and severe issues that are beyond the capabilities of the PG/PS controller. However, for conditions where CO_2 production remains within the limits of the controller, such as during increased physical activity or sleep, the PG/PS controller presented here can provide sufficient ventilatory control to maintain normocapnia.

5.4.2 The adaptive controller adapts stimulation to account for onset of muscle-related changes

Electrical stimulation of skeletal muscle has been shown to increase onset of muscle fatigue (Ratkevičius et al., 1998). This is mostly due to fast fatigable fibers being activated at lower current amplitudes than the slow fatigue-resistant fibers, causing reverse recruitment of muscle fiber types (Peckham and Knutson, 2005). As the fatigable fibers are recruited more often than usual, onset of muscle fatigue occurs. Recruitment of additional fatigue resistant fibers is then required to account for the loss of the fatigable fibers if the same amount of force is required to be

produced by the muscle. This would translate to a wider current spread, which can be accomplished by increasing stimulation amplitude. Simulations assessing PG/PS controller performance under a fatigued state showed that the controller was able to elicit the desired ventilatory pattern by autonomously increasing amplitude of the stimulation delivered, leading to a wider current spread, recruiting more fibers and thus increasing force generated.

The diaphragm muscle has a relatively even distribution of fatigue-resistant and fatigable fibers compared to other skeletal muscles (Polla et al., 2004; Stubbings et al., 2008). During eupnic breathing, slow fatigue-resistant fibers are mostly active, with the fast-fatigable fibers being active during behaviors requiring a stronger contractile force such as sighing, coughing, and sneezing (Seven et al., 2014). Since these fast-fatigable fibers elicit a strong contractile force with low stimulation, the stimulation profile required to elicit a eupneic breath is low in amplitude and narrow. Meanwhile, during fatigue, when these fatigable fibers are exhausted, the stimulation waveform required is one that shows a ramping increase in amplitude to recruit more fibers, leading to a longer lasting stimulation profile with a higher peak amplitude. The PG/PS controller is able to autonomously modulate stimulation shape which resulted in stimulation waveforms with these characteristics, suggesting that it has the ability to overcome the effects of fatigue to maintain a desired ventilatory pattern.

5.4.3 Individualized pacing for respiratory rehabilitation

One of the benefits of a closed-loop approach to respiratory pacing is that the adaptive controller can figure out how best to achieve a desired ventilatory pattern regardless of the state or properties of respiratory biomechanics. This is a critical function of the controller, particularly for clinical implementation, as between subject variations are bound to be present. Simulations showed that, despite randomized differences in muscle mass, chest compliance, and chest resistance, the controller was still able to modulate stimulation to achieve the desired ventilatory pattern. This suggests that the controller will be able to adapt to individualized pacing in a clinical setting regardless of disease or conditions affecting chest biomechanics.

These simulations also highlighted how the controller can account for effects of muscle condition on ventilatory mechanics. This is clinically relevant as most chronically ventilated individuals will display some degree of diaphragm muscle atrophy. The reduced muscle mass due to atrophy severely limits the contractile force capacity of the diaphragm, reducing inspiratory capacity. When encountering these situations, the controller would increase stimulation to increase muscle recruitment and thus elicit sufficient force to produce adequate breath volume. If the PG/PS controller is used chronically or periodically, recovery from atrophy may occur due to activation of muscle fibers (Ayas et al., 1999). This would lead to progressive increments in intrinsic muscle force, which the controller would

account for by reducing stimulation required to elicit a breath, leading to eventual weaning from respiratory pacing in an autonomous manner.

Respiratory pacing has been used in respiratory rehabilitation following cervical spinal cord injury to restore ventilatory independence. Currently, before dependence on pacing, patients with implanted respiratory pacers must undergo a conditioning period to increase the diaphragm muscle's resistance to stimulation-induced fatigue (Glenn et al., 1984; Pavlovic and Wendt, 2003). During this period, mechanical ventilation is still used to support ventilation, which may attenuate the beneficial effects of the pacing sessions. The structure of the PG/PS controller is such that it is possible to create a synergistic effect with mechanical ventilation to overcome these limitations. If the PG module is set such that it follows the respiratory frequency of the mechanical ventilator and the mechanical ventilator is set to provide a substantial fraction of the desired breath volume, the PS module would be able to adapt in order to provide only the stimulation required to achieve the remaining fraction of the desired breath volume. This approach would likely reduce the time required for diaphragm conditioning as the pacing would be continuous, rather than intermittent, and also minimize the risk of hypoventilation as mechanical ventilation is still present.

In the current study, each of the assessments was performed exclusive to one another. However, in clinical implementation, all the simulated conditions are likely to be encountered within individual patients. Future computational studies that explore the interactions between these parameters in more detail are suggested.

These studies would help define the patient demographic that most likely will respond positively to adaptive pacing, improving patient outcomes and reducing risk to those that do not fall within this demographic. Furthermore, other situations likely to be encountered clinically could also be explored. Among these are presence of muscle atrophy, response to diaphragm pacing conditioning, interaction with residual muscle activity, and effect of postural load.

The work presented here aims to not only serve as a step for use of the adaptive PG/PS controller clinically, but also to serve as one example of use of computational modeling to support clinical assessment of new control algorithms beyond what is possible clinically. With the development of clinically relevant models and increase in computational power and availability, the feasibility of implementing these computational testbeds for development and assessment of control schemes is magnified. This can lead to a reduction in time across all the translational steps of new technology, from development to approval for clinical use. While pre-clinical and clinical trials are still required to account for factors not included in the computational models, computational clinical assessment can still serve an important role.

Here, a computational testbed of human ventilatory biomechanics and CO_2 dynamics has been implemented to assess the performance of an adaptive closed-loop controller for respiratory pacing under the presence of clinically relevant conditions. Results indicate that the adaptive controller is able to elicit a ventilatory profile capable of achieving and/or maintaining normocapnia regardless of any of

the conditions assessed in a testbed based on human biomechanics and CO_2 dynamics. This serves as an important step towards clinical assessment of the adaptive PG/PS controller. Furthermore, implementation of a computational testbed allows for the development, optimization, and implementation of new controller features without requiring extensive pre-clinical assessment, reducing time spent in the development cycle; thus, delivering essential technology to market and users at a faster pace.

Tables

Table 1. Adaptive PG/PS controller parameters and computational model constants

a_E =	1.409	a_I =	3.091	a_L =	1.568	a_P =	0.7	a_R =	0.591
W_{EI} =	1.371	W_{PI} =	1.719	W_{LI} =	2.5	W_{II} =	0.85	W_{IL} =	1.361
W_{EL} =	0.793	W_{RL} =	2.056	W_{PL} =	6.0	W_{LL} =	1.15	W_{vL} =	10.5
W_{EP} =	1.351	W_{RP} =	2.254	W_{PP} =	1.540	W_{IE} =	0.729	W_{RE} =	2.25
W_{EE} =	1.550	W_{IR} =	1.80	W_{PR} =	2.150	W_{RR} =	0.650	W_{vR} =	1.05
B_E =	4.14	B_I =	5.044	B_L =	-2.2	B_P =	3.989	B_R =	2.193
K =	0.6	m_{bm} =	600 g	k_{bm} =	2.8×10^6 gcm^3/s^2	B_{bm} =	2800 g/s		
K_{bm} =	3500 g/s^2			B_{dia} =	250 g/s	m_{dia} =	312 g	n_a =	15
n_p =	30	η =	0.0001	T =	0.05 s	V_T =	15 L	M_{CO2} =	3.667
V_{CO2} =	*3.2 L*	Q =	100 ml/	τ_{LT} =	19.8 s	τ_{TL}=	4.6 s		

Table 2. Parameter sets used to assess controller performance computationally with different ventilatory biomechanics and CO_2 dynamics.

Testbed	Cardiac output (ml/s)	Effective CO_2 volume (ml)	Muscle mass (g)	Compliance (g/s)	Tissue volume (ml)
1	110.3	3511.2	203.8	265.5	13027.1
2	108.2	2600.7	194.0	204.6	12582.8
3	112.9	3449.4	197.4	295.0	12206.7
4	97.6	3048.4	235.6	279.5	13121.2
5	99.6	3130.4	225.5	270.9	16528.1

Figures

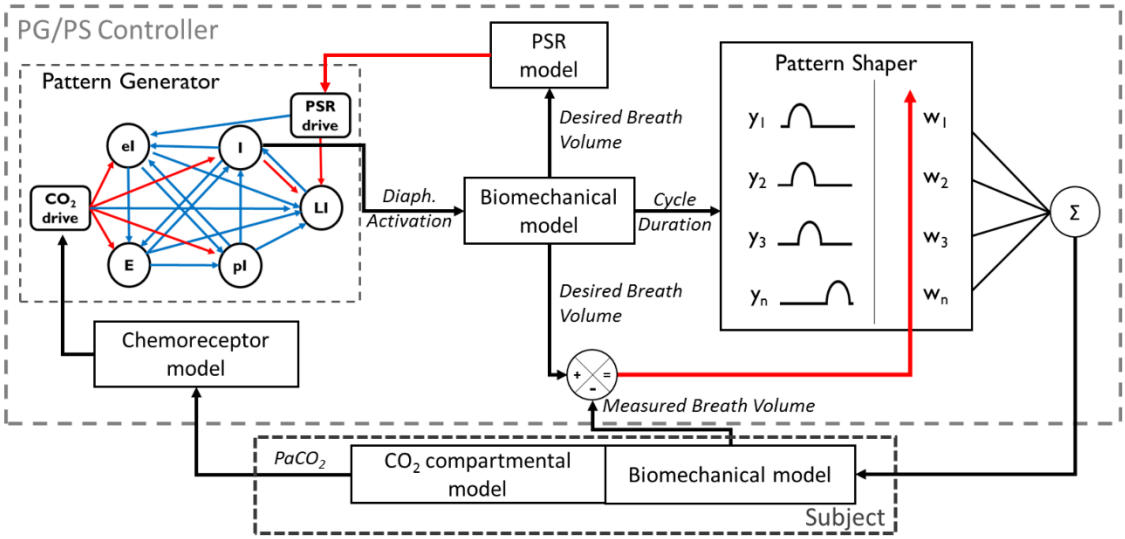

Figure 16. Architecture and design of the Pattern Generator / Pattern Shaper adaptive controller for use in computational human studies for control of $PaCO_2$. A modeled CO_2 chemoreceptor converts $PaCO_2$ into neural drive which serves as an input to a model of the respiratory central pattern generator neural network. The Patten Generator output is used in a biomechanical model of the chest to determine a “desired” breath volume profile. This volume profile is compared against the measured breath volume throughout the respiratory cycle within the Pattern Shaper. The derived error drives changes in neuronal weights in an artificial neural network. The summation of the weighted neuronal outputs serves as the controller output which then dictates stimulation delivered to the diaphragm muscle model. A change in ventilation due to pacing then drives a change in $PaCO_2$, closing the control loop.

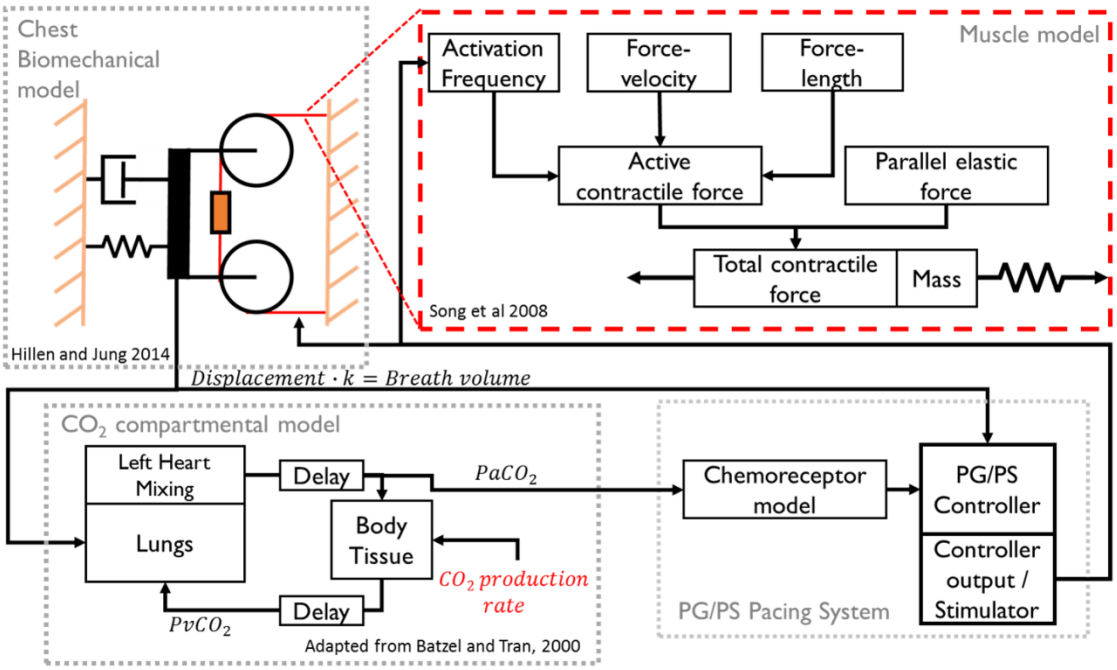

Figure 17. Organization of the computational testbed of the PG/PS controller using a human model of chest biomechanics and CO_2 dynamics. A Hill-type muscle model drives the force generated in a one-dimensional model of chest biomechanics. Displacement caused by force is linearly transformed to breath volume. The ventilation elicited affects $PaCO_2$ concentration in a compartmental model of CO_2 dynamics. The controller generates a ventilatory pattern based on $PaCO_2$ sampled and adapts to match this pattern via stimulation of the diaphragm. Changes in CO_2 production rate were used to assess controller's ability to maintain normocapnia.

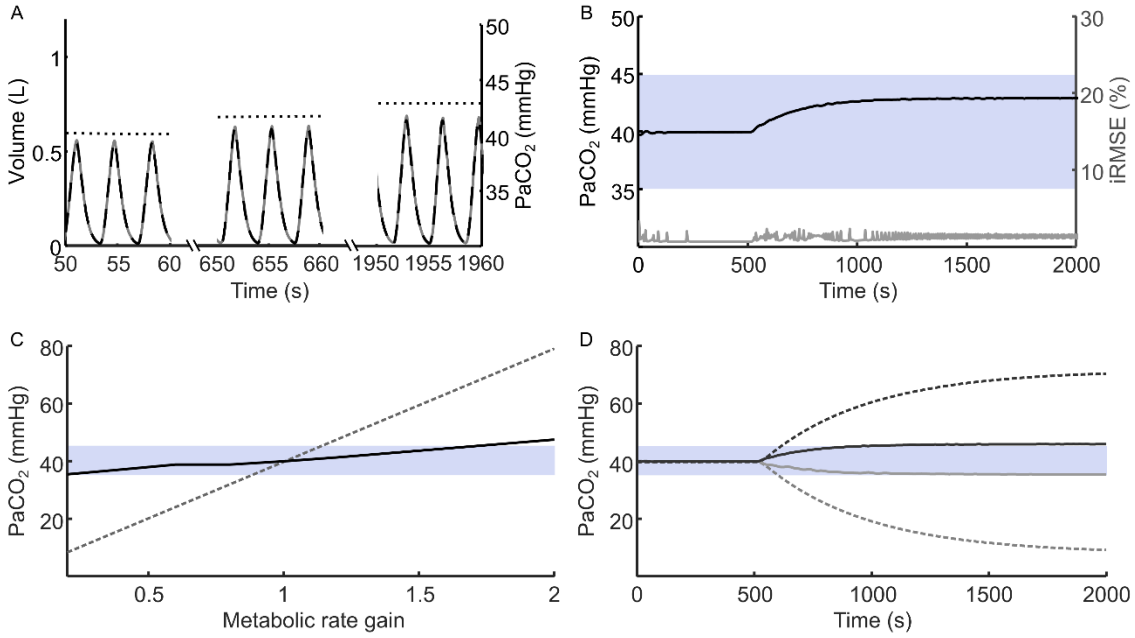

Figure 18. Adaptive PG/PS controller effect on $PaCO_2$ after changes in CO_2 production rates. (A) Example of a simulated trial showing the ventilatory pattern generated by the adaptive PG/PS controller (dashed) in response to changes in $PaCO_2$ (dotted) and its ability to match the elicited breath volume (solid, grey) to this pattern early in the trial, 150 sec after increasing CO_2 production rate, and shortly before end of trial. **(B)** $PaCO_2$ (black) and iRMSE (grey) throughout the 2000 sec trial in which CO_2 was increased by 40% at 500 sec. The pale blue shaded region indicates normocapnia (35 – 45 mmHg). **(C)** Comparison of final $PaCO_2$ levels between a fixed PG, adaptive PS controller (dotted) and an adaptive PG/PS controller (solid) in trials where CO_2 production was varied from 20% to 200% of the baseline production rate. **(D)** The adaptive PG/PS controller is able to maintain $PaCO_2$ levels within a normocapnic range in trials in which the rate of CO_2 produced due to metabolic processes was reduced to 20% of baseline (grey) or increased to 180% of baseline (black) using a fixed PG, adaptive PS controller (dashed) and an adaptive PG/PS controller (solid).

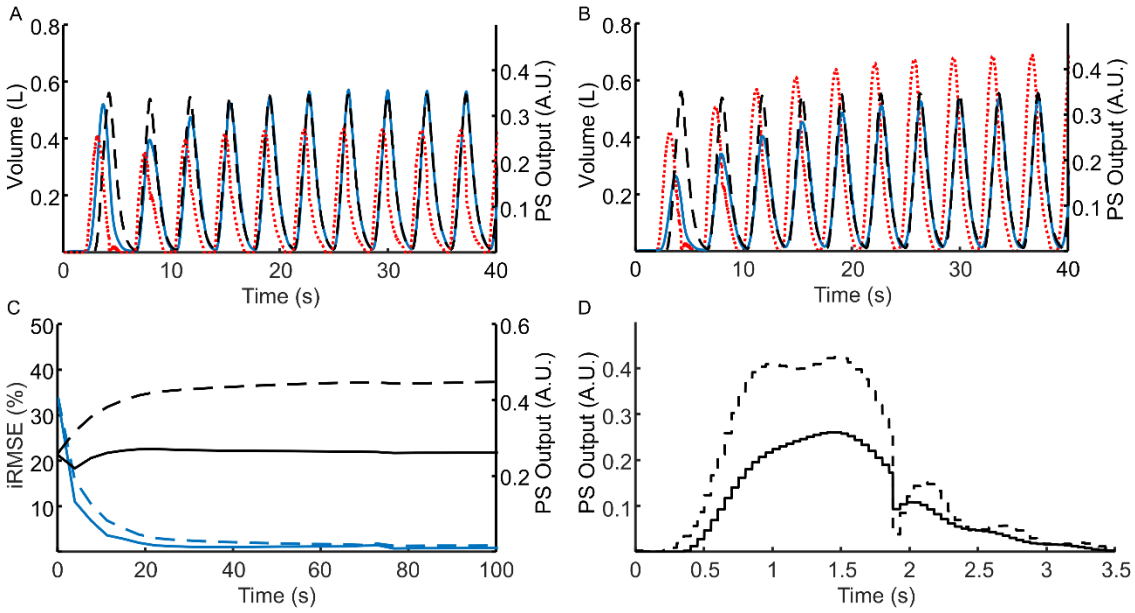

Figure 19. Adaptive PG/PS controller response in a non-fatigued and fatigued diaphragm muscle. (A) Measured breath volume (solid), desired breath volume (dashed), and PG/PS controller output (dotted) in a trial in a non-fatigued diaphragm muscle compared to **(B)** a trial in which the diaphragm muscle exhibits severe muscular fatigue. **(C)** PG/PS controller output (black) and iRMSE (blue) in a non-fatigued diaphragm (solid) and a fatigued diaphragm (dashed) during the initial 100 sec of the trials. **(D)** PG/PS controller output profile in a non-fatigued diaphragm (solid) and a fatigued diaphragm (dashed) 2000 sec after controller initiation.

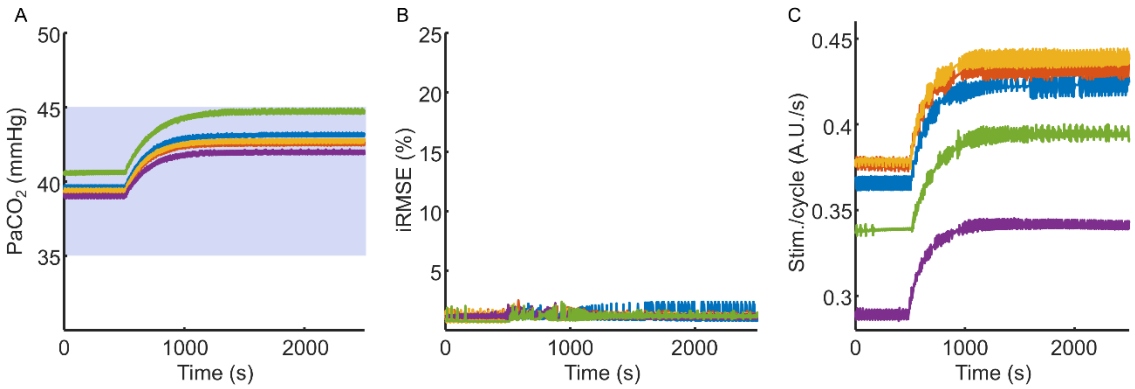

Figure 20. Adaptive PG/PS controller performance across multiple sets of randomized testbed parameters after a 50% increase in CO_2 production. Each color represents a different testbed. **(A)** After increasing CO_2 production by 50% at 500 sec, $PaCO_2$ was able to remain within normocapnia for all testbeds. Pale blue shaded region depicts normocapnic range. **(B)** A low iRMSE for all testbeds indicated that the PG/PS controller was able to finely modulate controller output to achieve the desired ventilatory profile. **(C)** PG/PS controller output per cycle, analogous to charge per cycle, varied between testbeds to account for differences in the biomechanical properties of each testbed.

CHAPTER 6

DISSERTATION CONCLUSIONS

6.1 Summary

An adaptive closed-loop control system for ventilatory support through respiratory pacing of the diaphragm has been developed and assessed. This control system follows a pattern generator/pattern shaper architecture, where a mathematical model of the respiratory central pattern generator (rCPG) neural network responds to a measure of $PaCO_2$ by generating an adequate model-based ventilatory pattern while a single-layer adaptive neural network with error driven neuronal weights define the stimulation amplitude throughout the duration of the respiratory cycle. The PG/PS design leads to breath-by-breath feedforward control of $PaCO_2$ and within breath feedback control of stimulation to achieve a desired breath volume profile. This allows for the controller to maintain ventilation regardless of changes to CO_2 production, ventilatory biomechanics, muscle activation properties, or tissue-electrode interface conditions.

The PG/PS respiratory control system was assessed computationally and experimentally. Computational models of both rat and human respiratory mechanics and CO_2 dynamics served as testbeds for controller development and characterization prior to *in vivo* implementation. Animal experiments in spinal cord-intact rats and spinal cord hemisected animals permitted assessment of the Pattern Shaper in a complex biological setting. Two models of hypoventilation, respiratory depression due to anesthesia and reduced inspiratory capacity due to

respiratory muscle hemiparesis, were used for assessment of the PG/PS system's ability to control $PaCO_2$. Both the computational and experimental studies showed that the controller is able to respond adequately to $PaCO_2$ by generating an appropriate ventilatory response and by modulating stimulation to achieve this desired ventilatory pattern to normalize $PaCO_2$ levels.

6.2 Conclusions

The following conclusions on the performance and abilities of the PG/PS respiratory control system have been drawn based on the research presented in the previous chapters.

- *The Pattern Shaper was able to autonomously adapt to determine stimulation parameters that could evoke and maintain a desired breath volume profile*. Adaptation to the difference between the evoked breath volume and the desired breath volume allowed the controller to adapt to the subject's biomechanics, providing personalized pacing to achieve the desired breath volume profile without the need for an extensive calibration process. Once the desired breath profile was achieved, the controller was able to maintain it through continuous adaptation despite changes that might affect the stimulation's ability to achieve the desired breath volume profile, such as muscle fatigue. Furthermore, it is possible for the Pattern Shaper to serve as an approach for automatic weaning from respiratory pacing. As the intrinsic diaphragm contribution to breath volume increases as a result of recovery, a positive error would occur. The controller would

compensate for this by decreasing stimulation. As this gradual change occurs, stimulation would gradually decrease until it ceases when the diaphragm is able to elicit a breath without assistance. This would effectively wean the patient from assisted ventilation without the need for clinician intervention.

- *The implementation of the Pattern Generator showed that it is possible to dynamically modulate cycle duration and breath volume in response to $PaCO_2$ while adapting stimulation parameters through the Pattern Shaper to elicit this ventilatory pattern.* The Pattern Generator mimics the physiological ventilatory response by generating a model-based ventilatory pattern in response to dynamic $PaCO_2$ levels. The resulting response then serves as the ventilatory profile that the Pattern Shaper attempts to attain by adapting stimulation. By responding to $PaCO_2$ in a physiological-like manner, the PG/PS respiratory control system could allow users to enjoy activities that increase or decrease metabolic demand without fear of inadequate ventilation. This has implications in daily life as well as during rehabilitation, where physically intensive activities that may not have been possible otherwise may lead to improved recovery outcomes.

- *The PG/PS respiratory pacing controller was able to elicit appropriate ventilation to maintain normocapnia in an integrated model of human ventilatory biomechanics and CO_2 dynamics in multiple clinically-relevant scenarios*. After adaptation for human use, the PG/PS controller was able

to achieve and/or maintain normocapnia under conditions where CO_2 production increased due to increased metabolic demand, after severe diaphragm muscle fatigue, and when implemented in testbeds with different model parameters. These simulated trials represent conditions that are likely to be found during chronic clinical use and thus serve as preliminary proof that the controller is a viable approach for control of respiratory pacing. These computational studies thus serve to further the development of the controller and to advance the translational pathway for future clinical studies.

The Pattern Shaper proved to be a viable strategy for control of diaphragmatic contraction for respiratory support thanks to its ability to adapt stimulation to provide complementary electrical activation of the diaphragm. In the presence of residual ventilatory function, the controller was able to modulate stimulation such that the summation of the intrinsic and electrical activation of the diaphragm muscle led to the matching of the desired ventilatory pattern, delivering only the necessary amount of charge. As changes in the intrinsic contractile force generated by the diaphragm occurred, likely due to muscle fatigue, the PS was able to compensate by increasing stimulation delivered and thus was able to achieve and maintain the desired breath volume profile. This implies that other changes that affect muscle force may also be able to be accounted for, such as changes due to atrophy or hypertrophy of the diaphragm. One of the benefits of an adaptive closed-loop approach to respiratory pacing is that the adaptive controller can figure out how best to achieve a desired ventilatory pattern regardless of the

state or properties of respiratory biomechanics. This is a critical function of the controller, particularly for clinical implementation, as between subject variations are bound to be present.

Implementation of this neuromorphic respiratory control system shows that it is possible to control an autonomic biological function while also adapting to residual function. Intrinsic ventilatory function is present in both spinal cord intact and C2 spinal cord hemisected rats, albeit reduced in the latter. This requires entrainment between the intrinsic respiratory drive and the PG/PS respiratory control system for proper adaptation and modulation of stimulation parameters. The PG/PS controller was able to establish a link with the biological rCPG to achieve respiratory entrainment, likely through vagal pathways. Additionally, when loss of entrainment occurred, the PG/PS controller's intrinsic characteristics increased stimulation delivered. This led to re-establishing of intrinsic ventilation entrainment to the pacing. By properly taking advantage of the interaction between the intrinsic biological control and the neurostimulation pacing technology, it may be possible to develop control strategies that are able to not only restore function of other autonomic processes but also improve their existing function. These may include control of visceral organ function, such as gastrointestinal control to improve motility or control of spleen function for modulation of autoimmune function.

The development of a closed-loop control strategy for the respiratory system is significant in that it may allow for more extensive use of respiratory pacing, leading to improved clinical outcomes for the system's users. The control system's ability

to determine an adequate ventilatory pattern and modulate stimulation to match the given ventilatory pattern ensures that the patient will maintain normocapnia without the need for constant supervision or manipulation of controller and/or stimulation parameters.

6.3 Limitations

While the work presented here showed adequate PG/PS controller performance, all control applications rely heavily on the accuracy and precision of the input signals to the controller. Currently, a robust and reliable method for continuous $PaCO_2$ sensing is not available for clinical use. While end-tidal CO_2 measurement is common in hospital settings, it is not a reliable measure of $PaCO_2$ as its accuracy can be severely impacted by respiratory disorders, cardiac disorders, and any other factor affecting the ventilation/perfusion relationship (Huttmann et al., 2014). Other approaches for continuous $PaCO_2$ monitoring are available, such as transcutaneous CO_2 sensors, but these require continuous application of heat to improve transcutaneous CO_2 diffusion and reconditioning of the electrode after several hours (Janssens et al., 1998). These factors prevent transcutaneous CO_2 sensing from being a reliable chronic approach to $PaCO_2$ sensing. Similarly, wearable breath volume sensing approaches have been developed for respiratory monitoring (Caretti et al., 1994; Lonbe et al., 1999; Wolf and Arnold, 2005). Most rely on inductive plethysmography of chest expansion and have been proven to be reliable in differentiating between apnea (Lonbe et al., 1999) and show reliable estimation of volumetric respiratory measures during tasks of everyday life

(Grossman et al., 2010), and during exercise (Clarenbach et al., 2005). However, these approaches have yet to be validated for chronic assessment of respiratory volume; a necessary step prior to integration with a life-sustaining closed-loop control application.

Another limitation of the work presented here was lack of respiratory pacing of respiratory muscles other than the diaphragm muscle. The diaphragm muscle accounts for only 65% of inspiratory force produced during eupnic breathing, with the other 35% attributed to external intercostal muscles and accessory muscles (Jarosz et al., 2012). Being able to elicit only 65% of total inspiratory force limits the range of respiratory maneuvers that may be achievable while on pacing support. This includes inability to fully elicit ventilatory profiles requiring very high inspiratory volumes due to elevated $PaCO_2$ values. This limitation was observable in experimental studies after spinal cord hemisection, where the reduced intrinsic activation of the ipsilateral respiratory muscles led to difficulties in attaining the desired tidal volume. Even though with increase in respiratory rate, a reduction in $etCO_2$ was still possible, albeit at a slower rate. As mentioned in previous chapters this could be addressed by modifying the rCPG model used such that the change in ventilation relies more on respiratory rate than on tidal volume.

6.4 Future work

The work presented here aimed to develop and implement a closed-loop control system for respiratory pacing that was capable of regulating $PaCO_2$ through modulation and control of respiratory rate and breath volume in a physiological-

like manner. The eventual goal of the work presented here is to deliver a closed-loop respiratory control system that is robust enough and safe enough for chronic clinical use. Assessing controller performance in computational simulations using a human model of ventilatory dynamics did further this goal. However, extensive work is still required to achieve clinical implementation of the control system. This section will discuss possible future work that may lead to increased robustness, performance, and functionality of the PG/PS control system. Additionally, proper validation of this control algorithm will be discussed; especially since the controller offers a life-sustaining technology, failure of which could lead to death.

All experimental studies performed here controlled ventilation through electrical stimulation of the diaphragm muscle. However, other techniques such as phrenic nerve stimulation and spinal cord stimulation are currently implemented clinically or have been explored pre-clinically (DiMarco, 2005; Hachmann et al., 2017; Jarosz et al., 2012; Khong et al., 2010; Kowalski et al., 2013; Le Pimpec-Barthes et al., 2016; Mercier et al., 2017; Onders, 2012). While the design of the PG/PS controller suggests that performance will not be negatively impacted when implemented in other stimulation modalities, it is possible that performance may improve. In the case of phrenic nerve stimulation, there would be no need for mapping of the diaphragm motor point. This would reduce risk of erroneous electrode placement and provide a more widespread activation of the diaphragm with sufficient stimulation than is possible via diaphragmatic stimulation (Onders, 2012). Spinal cord stimulation suggests further benefits in exchange for a riskier electrode implantation process. If spinal cord stimulation stimulates the premotor

phrenic pathways, the intrinsic muscle activation dynamics are preserved, avoiding the issue of reverse recruitment (Hachmann et al., 2017; Kowalski et al., 2013). This may lead to a more natural diaphragm muscle contraction, finer control of diaphragm muscle contraction, and increased time before onset of muscle fatigue. Furthermore, spinal cord stimulation takes advantage of the intrinsic spinal connectivity between phrenic motor pools and other inspiratory muscles, mainly the external intercostals. Spinal cord stimulation of the phrenic motor pools has been shown to cause activation of external intercostal muscles (Dimarco et al., 1997; DiMarco et al., 2005; DiMarco and Kowalski, 2013). This can thus lead to further reduction in muscle fatigue as the mechanical work of breathing can be distributed between the diaphragm and external intercostal muscles, reducing the workload on the diaphragm.

Other than reducing the respiratory workload of the diaphragm, respiratory pacing of additional respiratory muscles can lead to other benefits. Addition of intercostal muscles would lead to an overall increase in elicited inspiratory capacity, allowing for the production of non-ventilatory behaviors that require high inspiratory volumes, such as sighing. Meanwhile, addition of expiratory muscle control would allow for forceful expiration, allowing behaviors such as active expiration and coughing. Control of external intercostal muscles by applying the same stimulation pattern given by the PS module that is controlling the diaphragm muscle has shown some promise in ongoing experiments (not reported). However, control of expiratory muscles would require an additional PS module that controls expiratory activity. This expiratory PS would need to be linked to the expiratory neuronal

population within the PG module through an appropriate expiratory muscle model in a similar manner as is currently done for the inspiratory PS. Implementation of these behaviors in the controller could be done by expanding the intrinsic capabilities of the PG to include additional responses (as for active expiration), or by including subroutines into the PG module that are activated either as a timed response (for sighing), or a triggered response (as for coughing).

Pre-clinical validation of the adaptive PG/PS controller in chronic models is also suggested prior to clinical implementation. Acute studies do not address factors that may be present in chronic animal studies such as electrode encapsulation, spinal shock due to injury, respiratory neuroplasticity, and chronic changes in diaphragm muscle fiber properties. Carrying out chronic studies would allow for assessment of the controller's response to these factors and other factors that may be present but have not been accounted for. Through chronic studies, the controller would not only be further optimized to ensure robustness, reliability, and safety but also lead to evaluation of the controller's long-term effect on muscular and neural tissue.

Finally, early feasibility clinical trials would need to be performed in order to transition to extensive clinical trials. Early feasibility clinical trials could possibly be carried out under clinician supervision within operating rooms during procedures when maintenance of existing diaphragm pacers is performed. This would not require an extensive acclimatization period to pacing nor require additional surgical procedures. The existing leads could either be interfaced with an external

stimulator controlled by the adaptive controller or the adaptive controller could be linked with the implanted stimulator. Either way would take advantage of electrodes already implanted in the diaphragm or on the phrenic nerve, minimizing risk and cost of the study.

In conclusion, an adaptive closed-loop controller for respiratory pacing was developed and assessed in acute pre-clinical models. The adaptive controller was able to respond to changes in $PaCO_2$ to generate a proper ventilatory response and was able to adapt stimulation pulses delivered to the diaphragm to elicit this ventilatory response. While extensive work is still required prior to clinical implementation of the system, the work presented here serves as an important step towards use of a technology that can allow patients with chronic hypoventilation to lead a more independent and healthier lifestyle.

REFERENCES

Abbas, J. J., and Chizeck, H. J. (1991). A neural network controller for functional neuromuscular stimulation systems. in *Proceedings of the Annual International Conference of the IEEE Engineering in Medicine and Biology Society Volume 13: 1991* (IEEE), 1456–1457. doi:10.1109/IEMBS.1991.684544.

Abbas, J. J., and Chizeck, H. J. (1995). Neural network control of functional neuromuscular stimulation systems: Computer simulation studies. *IEEE Trans. Biomed. Eng.* 42, 1117–1127. doi:10.1109/10.469379.

Abbas, J. J., and Triolo, R. J. (1997). Experimental evaluation of an adaptive feedforward controller for use in functional neuromuscular stimulation systems. *IEEE Trans. Rehabil. Eng.* 5, 12–22.

Abu-Shaweesh, J. M., Dreshaj, I. A., Thomas, A. J., Haxhiu, M. A., Strohl, K. P., and Martin, R. J. (1999). Changes in respiratory timing induced by hypercapnia in maturing rats. *J. Appl. Physiol.* 87, 484–90. doi:10.1152/jappl.1999.87.2.484.

Akers, J. M., Peckham, P. H., Keith, M. W., and Merritt, K. (1997). Tissue response to chronically stimulated implanted epimysial and intramuscular electrodes. *IEEE Trans. Rehabil. Eng.* 5, 207–220. doi:10.1109/86.593301.

Amirjani, N., Kiernan, M. C., McKenzie, D. K., Butler, J. E., and Gandevia, S. C. (2012). Is there a case for diaphragm pacing for amyotrophic lateral sclerosis patients? *Amyotroph. Lateral Scler.* doi:10.3109/17482968.2012.673169.

Andrew Shanely, R., Zergeroglu, M. A., Lennon, S. L., Sugiura, T., Yimlamai, T., Enns, D., et al. (2002). Mechanical ventilation-induced diaphragmatic atrophy is associated with oxidative injury and increased proteolytic activity. *Am. J. Respir. Crit. Care Med.* 166, 1369–1374. doi:10.1164/rccm.200202-088OC.

Ayas, N. T., McCool, F. D., Gore, R., Lieberman, S. L., and Brown, R. (1999). Prevention of human diaphragm atrophy with short periods of electrical stimulation. *Am. J. Respir. Crit. Care Med.* 159, 2018–2020. doi:10.1164/ajrccm.159.6.9806147.

Barnett, W. H., Abdala, A. P., Paton, J. F. R., Rybak, I. A., Zoccal, D. B., and Molkov, Y. I. (2017). Chemoreception and neuroplasticity in respiratory circuits. *Exp. Neurol.* 287, 153–164. doi:10.1016/j.expneurol.2016.05.036.

Batzel, J. J., and Tran, H. T. (2000). Stability of the human respiratory control system: I. Analysis of a two-dimensional delay state-space model. *J. Math. Biol.* 41, 45–79. doi:10.1007/s002850000044.

Berry-Kravis, E. M., Zhou, L., Rand, C. M., and Weese-Mayer, D. E. (2006). Congenital Central Hypoventilation Syndrome. *Am. J. Respir. Crit. Care Med.* 174, 1139–1144. doi:10.1164/rccm.200602-305OC.

Botros, S. M., and Bruce, E. N. (1990). Neural network implementation of a three-phase model of respiratory rhythm generation. *Biol. Cybern.* 63, 143–153. doi:10.1007/BF00203037.

Brouillette, R. T., and Thach, B. T. (1980). Control of genioglossus muscle inspiratory activity. *J. Appl. Physiol.* 49, 801–808.

Brown, E. B. (1953). Physiological effects of hyperventilation. *Physiol. Rev.* 33, 445–71. doi:10.1152/physrev.1953.33.4.445.

Brown, R., DiMarco, A. F., Hoit, J. D., and Garshick, E. (2006). Respiratory dysfunction and management in spinal cord injury. *Respir. Care* 51, 853-68;discussion 869-70. doi:10.1016/j.surg.2006.10.010.Use.

Burnet, H., and Hilaire, G. (1999). Pulmonary stretch receptor discharges and vagal regulation of respiration differ between two mouse strains. *J. Physiol.* 519, 581–590. doi:10.1111/j.1469-7793.1999.0581m.x.

Caretti, D. M., Pullen, P. V., Premo, L. A., and Kuhlmann, W. D. (1994). Reliability of respiratory inductive plethysmography for measuring tidal volume during exercise. *Am. Ind. Hyg. Assoc. J.* 55, 918–923. doi:10.1080/15428119491018411.

Castelli, J., Kolbl, F., Siu, R., N'Kaoua, G., Bornat, Y., Mangalore, A., et al. (2017). An IC-based controllable stimulator for respiratory muscle stimulation investigations. in *Proceedings of the Annual International Conference of the IEEE Engineering in Medicine and Biology Society, EMBS* (IEEE), 1970–1973. doi:10.1109/EMBC.2017.8037236.

Cheng, E. J., Brown, I. E., and Loeb, G. E. (2000). Virtual muscle: A computational approach to understanding the effects of muscle properties on motor control. *J. Neurosci. Methods* 101, 117–130. doi:10.1016/S0165-0270(00)00258-2.

Chervin, R. D., and Guilleminault, C. (1994). Diaphragm pacing: Review and reassessment. *Sleep* 17, 176–187. doi:10.1093/sleep/17.2.176.

Cienfuegos, P. J., Shoemaker, A., Grange, R. W., Abaid, N., and Leonessa, A. (2017). Classical and adaptive control of ex vivo skeletal muscle contractions using functional electrical stimulation (FES). *PLoS One* 12, 1–29. doi:10.1371/journal.pone.0172761.

Clarenbach, C. F., Senn, O., Brack, T., Kohler, M., and Bloch, K. E. (2005). Monitoring of ventilation during exercise by a portable respiratory inductive plethysmograph. *Chest* 128, 1282–1290. doi:10.1378/chest.128.3.1282.

Claxton, A. R., Wong, D. T., Chung, F., and Fehlings, M. G. (1998). Predictors of hospital mortality and mechanical ventilation in patients with cervical spinal cord injury. *Can. J. Anaesth.* 45, 144–149. doi:10.1007/BF03013253.

Cnaan, A., Laird, N., and Slasor, P. (1997). Using the general linear mixed model to analyse unbalanced repeated measures and longitudinal data. *Stat. Med.* 16, 2349–2380. doi:10.1002/(SICI)1097-0258(19971030)16:20<2349::AID-SIM667>3.0.CO;2-E [pii].

Cragg, P. A., and Drysdale, D. B. (1983). Interaction of hypoxia and hypercapnia on ventilation, tidal volume and respiratory frequency in the anaesthetized rat. *J. Physiol.* 341, 477–93. doi:10.1113/jphysiol.1983.sp014818.

Dahan, A., and Teppema, L. J. (2003). Influence of anaesthesia and analgesia on the control of breathing. *Br. J. Anaesth.* 91, 40–49. doi:10.1093/bja/aeg150.

Dardai, E., and Heavner, J. E. (1987). Respiratory and cardiovascular effects of halothane, isoflurane and enflurane delivered via a Jackson-Rees breathing system in temperature controlled and uncontrolled rats. *Methods Find. Exp. Clin. Pharmacol.*

Davoodi, R., and Andrews, B. J. (1998). Computer simulation of FES standing up in paraplegia: A self-adaptive fuzzy controller with reinforcement learning. *IEEE Trans. Rehabil. Eng.* 6, 151–161. doi:10.1109/86.681180.

De Troyer, A., and Estenne, M. (1984). Coordination between rib cage muscles and diaphragm during quiet breathing in humans. *J. Appl. Physiol.* 57, 899–906. doi:10.1152/jappl.1984.57.3.899.

De Troyer, A., Kirkwood, P. A., and Wilson, T. A. (2005). Respiratory action of the intercostal muscles. *Physiol. Rev.* 85, 717–56. doi:10.1152/physrev.00007.2004.

DiMarco, A. F. (1999). Diaphragm pacing in patients with spinal cord injury. *Top. Spinal Cord Inj. Rehabil.* 5, 6–20. doi:10.1310/71JT-5H5H-81WR-FWL0.

DiMarco, A. F. (2005). Restoration of respiratory muscle function following spinal cord injury: Review of electrical and magnetic stimulation techniques. *Respir. Physiol. Neurobiol.* 147, 273–287. doi:10.1016/j.resp.2005.03.007.

DiMarco, A. F. (2009). Phrenic nerve stimulation in patients with spinal cord injury. *Respir. Physiol. Neurobiol.* 169, 200–209. doi:10.1016/j.resp.2009.09.008.

DiMarco, A. F. (2018). Diaphragm pacing. *Clin. Chest Med.* 39, 459–471. doi:10.1016/j.ccm.2018.01.008.

DiMarco, A. F., Geertman, R. T., Tabbaa, K., and Kowalski, K. E. (2018). Complete Restoration of Respiratory Muscle Function in Three Subjects with Spinal Cord Injury Pilot Interventional Clinical Trial. *Am. J. Phys. Med. Rehabil.*, 1. doi:10.1097/PHM.0000000000001018.

DiMarco, A. F., and Kowalski, K. E. (2013). Spinal pathways mediating phrenic activation during high frequency spinal cord stimulation. *Respir. Physiol. Neurobiol.* doi:10.1016/j.resp.2012.12.003.

DiMarco, A. F., Onders, R. P., Kowalski, K. E., Miller, M. E., Ferek, S., and Mortimer, T. J. (2002). Phrenic nerve pacing in a tetraplegic patient via intramuscular diaphragm electrodes. *Am. J. Respir. Crit. Care Med.* 166, 1604–1606. doi:10.1164/rccm.200203-175CR.

Dimarco, A. F., Romaniuk, J. R., Kowalski, K. E., and Supinski, G. S. (1997). Efficacy of combined inspiratory intercostal and expiratory muscle pacing to maintain artificial ventilation. *Am. J. Respir. Crit. Care Med.* 156, 122–126. doi:10.1164/ajrccm.156.1.9609103.

DiMarco, A. F., Takaoka, Y., and Kowalski, K. E. (2005). Combined intercostal and diaphragm pacing to provide artificial ventilation in patients with tetraplegia. *Arch. Phys. Med. Rehabil.* 86, 1200–1207. doi:10.1016/j.apmr.2004.11.027.

Doperalski, N. J., Sandhu, M. S., Bavis, R. W., Reier, P. J., and Fuller, D. D. (2008). Ventilation and phrenic output following high cervical spinal hemisection in male vs. female rats. *Respir. Physiol. Neurobiol.* 162, 160–167. doi:10.1016/j.resp.2008.06.005.

dos Santos, E. da L., Gelain, M. C., Krueger, E., Nogueira-Neto, G. N., and Nohama, P. (2016). Artificial motor control for electrically stimulated upper limbs of plegic or paretic people. *Rev. Bras. Eng. Biomed.* 32, 199–211. doi:10.1590/2446-4740.03415.

Dougherty, B. J., Lee, K.-Z., Lane, M. A., Reier, P. J., and Fuller, D. D. (2012a). Contribution of the spontaneous crossed-phrenic phenomenon to inspiratory tidal volume in spontaneously breathing rats. *J. Appl. Physiol.* 112, 96–105. doi:10.1152/japplphysiol.00690.2011.

Dougherty, B. J., Lee, K. Z., Gonzalez-Rothi, E. J., Lane, M. A., Reier, P. J., and Fuller, D. D. (2012b). Recovery of inspiratory intercostal muscle activity following high cervical hemisection. *Respir. Physiol. Neurobiol.* 183, 186–192. doi:10.1016/j.resp.2012.06.006.

Eikermann, M., Malhotra, A., Fassbender, P., Zaremba, S., Jordan, A. S., Gautam, S., et al. (2008). Differential effects of isoflurane and propofol on upper airway dilator muscle activity and breathing. *Anesthesiology* 108, 897–906. doi:10.1097/ALN.0b013e31816c8a60.

Fairchild, M. D., Kim, S. J., Iarkov, A., Abbas, J. J., and Jung, R. (2010). Repetetive hindlimb movement using intermittent adaptive neuromuscular electrical stimulation in an incomplete spinal cord injury rodent model. *Exp. Neurol.* 223, 623–633. doi:10.1016/j.expneurol.2010.02.011.

Faul, F., Erdfelder, E., Lang, A.-G., and Buchner, A. (2007). G*Power: A flexible statistical power analysis program for the social, behavioral, and biomedical sciences. *Behav. Res. Methods* 39, 175–191. doi:10.3758/BF03193146.

Feldman, J. L., and Kam, K. (2015). Facing the challenge of mammalian neural microcircuits: Taking a few breaths may help. *J. Physiol.* 593, 3–23. doi:10.1113/jphysiol.2014.277632.

Feng Wang, and Andrews, B. J. (1994). Adaptive fuzzy logic controller for FES-computer simulation study. in *Proceedings of 16th Annual International Conference of the IEEE Engineering in Medicine and Biology Society* (IEEE). doi:10.1109/IEMBS.1994.411981.

Ferrante, S., Bejarano, N. C., Ambrosini, E., Nardone, A., Turcato, A. M., Monticone, M., et al. (2016). A personalized multi-channel FES controller based on muscle synergies to support gait rehabilitation after stroke. *Front. Neurosci.* 10, 425. doi:10.3389/fnins.2016.00425.

Ferrarin, M., Palazzo, F., Riener, R., and Quintern, J. (2001). Model-based control of FES-induced single joint movements. *IEEE Trans. Neural Syst. Rehabil. Eng.* 9, 245–257. doi:10.1109/7333.948452.

Freeman, C. T., Hughes, A. M., Burridge, J. H., Chappell, P. H., Lewin, P. L., and Rogers, E. (2009). Iterative learning control of FES applied to the upper extremity for rehabilitation. *Control Eng. Pract.* 17, 368–381. doi:10.1016/j.conengprac.2008.08.003.

Fregosi, R. F., and Fuller, D. D. (1997). Respiratory-related control of extrinsic tongue muscle activity. *Respir. Physiol.* 110, 295–306. doi:10.1016/S0034-5687(97)00095-9.

Fuller, D. D., ElMallah, M. K., Smith, B. K., Corti, M., Lawson, L. A., Falk, D. J., et al. (2013). The respiratory neuromuscular system in Pompe disease. *Respir. Physiol. Neurobiol.* doi:10.1016/j.resp.2013.06.007.

Garara, B., Wood, A., Marcus, H. J., Tsang, K., Wilson, M. H., and Khan, M. (2016). Intramuscular diaphragmatic stimulation for patients with traumatic high cervical injuries and ventilator dependent respiratory failure: A systematic review of safety and effectiveness. *Injury* 47, 539–544. doi:10.1016/j.injury.2015.12.020.

Gardner, B. P., Watt, J. W., and Krishnan, K. R. (1986). The artificial ventilation of acute spinal cord damaged patients: a retrospective study of forty-four patients. *Paraplegia* 24, 208–20. doi:10.1038/sc.1986.30.

Gill, L. C., Ross, H. H., Lee, K. Z., Gonzalez-Rothi, E. J., Dougherty, B. J., Judge, A. R., et al. (2014). Rapid diaphragm atrophy following cervical spinal cord hemisection. *Respir. Physiol. Neurobiol.* 192, 66–73. doi:10.1016/j.resp.2013.12.006.

Glenn, W. W., Hogan, J. F., Loke, J. S., Ciesielski, T. E., Phelps, M. L., and Rowedder, R. (1984). Ventilatory support by pacing of the conditioned diaphragm in quadriplegia. *N. Engl. J. Med.* 310, 1150–5. doi:10.1056/NEJM198405033101804.

Glenn, W. W. L., Brouillette, R. T., Dentz, B., Fodstad, H., Hunt, C. E., Keens, T., et al. (1988). Fundamental considerations in pacing of the diaphragm for chronic ventilatory insufficiency: a multi-center study. *Pacing Clin. Electrophysiol.* 11, 2121–7. Available at: http://www.ncbi.nlm.nih.gov/pubmed/2463598.

Glenn, W. W. L., Holcomb, W. G., Shaw, R. K., Hogan, J. F., and Holschuh, K. R. (1976). Long term ventilatory support by diaphragm pacing in quadriplegia. *Ann. Surg.* 183, 566–577. doi:10.1097/00000658-197605000-00014.

Goligher, E. C., Fan, E., Herridge, M. S., Murray, A., Vorona, S., Brace, D., et al. (2015). Evolution of diaphragm thickness during mechanical ventilation: Impact of inspiratory effort. *Am. J. Respir. Crit. Care Med.* 192, 1080–1088. doi:10.1164/rccm.201503-0620OC.

Gonzalez-Bermejo, J., LLontop, C., Similowski, T., and Morélot-Panzini, C. (2015). Respiratory neuromodulation in patients with neurological pathologies: For whom and how? *Ann. Phys. Rehabil. Med.* 58, 238–244. doi:10.1016/j.rehab.2015.07.001.

Gonzalez-Bermejo, J., Morélot-Panzini, C., Tanguy, M. L., Meininger, V., Pradat, P. F., Lenglet, T., et al. (2016). Early diaphragm pacing in patients with amyotrophic lateral sclerosis (RespiStimALS): a randomised controlled triple-blind trial. *Lancet Neurol.* 15, 1217–1227. doi:10.1016/S1474-4422(16)30233-2.

Gorman, R. B., McKenzie, D. K., Pride, N. B., Tolman, J. F., and Gandevia, S. C. (2002). Diaphragm length during tidal breathing in patients with chronic obstructive pulmonary disease. *Am. J. Respir. Crit. Care Med.* 166, 1461–1469. doi:10.1164/rccm.200111-087OC.

Graves, C., Glass, L., Laporta, D., Meloche, R., and Grassino, A. (1986). Respiratory phase locking during mechanical ventilation in anesthetized human subjects. *Am. J. Physiol.* 250, R902–R909. Available at: http://www.ncbi.nlm.nih.gov/pubmed/3706575.

Grill, W. M., and Mortimer, T. J. (1994). Electrical properties of implant encapsulation tissue. *Ann. Biomed. Eng.* 22, 23–33. doi:10.1007/BF02368219.

Grossman, P., Wilhelm, F. H., and Brutsche, M. (2010). Accuracy of ventilatory measurement employing ambulatory inductive plethysmography during tasks of everyday life. *Biol. Psychol.* 84, 121–128. doi:10.1016/j.biopsycho.2010.02.008.

Guyenet, P. G. (2014). Regulation of breathing and autonomic outflows by chemoreceptors. *Compr. Physiol.* 4, 1511–1562. doi:10.1002/cphy.c140004.

Gwo-Ching Chang, Jer-Junn Lub, Gon-Der Liao, Jin-Shin Lai, Cheng-Kung Cheng, Bor-Lin Kuo, et al. (1997). A neuro-control system for the knee joint position control with quadriceps stimulation. *IEEE Trans. Rehabil. Eng.* 5, 2–11. doi:10.1109/86.559344.

Hachmann, J. T., Grahn, P. J., Calvert, J. S., Drubach, D. I., Lee, K. H., and Lavrov, I. A. (2017). Electrical Neuromodulation of the Respiratory System After Spinal Cord Injury. *Mayo Clin. Proc.* 92, 1401–1414. doi:10.1016/j.mayocp.2017.04.011.

Harris, M. B., and St John, W. M. (2003). Tonic pulmonary stretch receptor feedback modulates both eupnea and gasping in an in situ rat preparation. *Am. J. Physiol. Regul. Integr. Comp. Physiol.* 285, R215-21. doi:10.1152/ajpregu.00112.2003.

Hillen, B. K., Jung, R., and B.K., H. (2014). Computational model of human ventilation for electrical stimulation following cervical spinal cord injury. *BMC Neurosci.* 15, 1–2. doi:10.1186/1471-2202-15-s1-p133.

Huttmann, S. E., Windisch, W., and Storre, J. H. (2014). Techniques for the measurement and monitoring of carbon dioxide in the blood. *Ann. Am. Thorac. Soc.* 11, 645–652. doi:10.1513/AnnalsATS.201311-387FR.

Ibrahim, B. S. K. K., Tokhi, M. O., Huq, M. S., and Gharooni, S. C. (2011). Fuzzy logic based cycle-to-cycle control of FES-induced swinging motion. *InECCE 2011 - Int. Conf. Electr. Control Comput. Eng.*, 60–64. doi:10.1109/INECCE.2011.5953850.

Ichihara, K., Venkatasubramanian, G., Abbas, J. J., and Jung, R. (2009). Neuromuscular electrical stimulation of the hindlimb muscles for movement therapy in a rodent model. *J. Neurosci. Methods* 176, 213–224. doi:10.1016/j.jneumeth.2008.09.015.

Imai, A., Steffey, E. P., Farver, T. B., and Ilkiw, J. E. (1999). Assessment of isoflurane-induced anesthesia in ferrets and rats. *Am. J. Vet. Res.*

Janssens, J. P., Howarh-Frey, C., Chevrolet, J. C., Abajo, B., and Rochat, T. (1998). Transcutaneous PCO2 to monitor noninvasive mechanical ventilation in adults: Assessment of a new transcutaneous PCO2 device. *Chest* 113, 768–773. doi:10.1378/chest.113.3.768.

Jarosz, R., Littlepage, M. M., Creasey, G., and McKenna, S. L. (2012). Functional electrical stimulation in spinal cord injury respiratory care. *Top. Spinal Cord Inj. Rehabil.* 18, 315–21. doi:10.1310/sci1804-315.

John, J., Fiona Bailey, E., and Fregosi, R. F. (2005). Respiratory-related discharge of genioglossus muscle motor units. *Am. J. Respir. Crit. Care Med.* 172, 1331–1337. doi:10.1164/rccm.200505-790OC.

Jung, R. (2018). System and method for neuromorphic controlled adaptive pacing of respiratory muscles and nerves. doi:US9872989B2.

Jung, R., Ichihara, K., Venkatasubramanian, G., and Abbas, J. J. (2009). Chronic neuromuscular electrical stimulation of paralyzed hindlimbs in a rodent model. *J. Neurosci. Methods* 183, 241–254. doi:10.1016/j.jneumeth.2009.06.043.

Kacmarek, R. M. (2011). The mechanical ventilator: Past, present, and future. *Respir. Care* 56, 1170–1180. doi:10.4187/respcare.01420.

Kam, K., Worrell, J. W., Janczewski, W. A., Cui, Y., and Feldman, J. L. (2013). Distinct inspiratory rhythm and pattern generating mechanisms in the preBötzinger complex. *J. Neurosci.* 33, 9235–45. doi:10.1523/JNEUROSCI.4143-12.2013.

Kasi, A., Perez, I., Kun, S., and Keens, T. (2016). Congenital central hypoventilation syndrome: Diagnostic and management challenges. *Pediatr. Heal. Med. Ther.* Volume 7, 99–107. doi:10.2147/PHMT.S95054.

Khong, P., Lazzaro, A., and Mobbs, R. (2010). Phrenic nerve stimulation: The Australian experience. *J. Clin. Neurosci.* 17, 205–208. doi:10.1016/j.jocn.2009.06.012.

Kim, S. J., Fairchild, M. D., Iarkov, A., Abbas, J. J., and Jung, R. (2009). Adaptive control of movement for neuromuscular stimulation-assisted therapy in a rodent model. *IEEE Trans. Biomed. Eng.* 56, 452–461. doi:10.1109/TBME.2008.2008193.

Kimura, M., Sugiura, T., Fukui, Y., Kimura, T., and Harada, Y. (1992). Heart rate and body temperature sensitive diaphragm pacing. *Med. Biol. Eng. Comput.* 30, 155–61. Available at: http://www.ncbi.nlm.nih.gov/pubmed/1453780.

Kishnani, P. S., Steiner, R. D., Bali, D., Berger, K., Byrne, B. J., Case, L., et al. (2006). Pompe disease diagnosis and management guideline. *Genet. Med.* 8, 267–288. doi:10.1097/01.gim.0000218152.87434.f3.

Kowalski, K. E., Hsieh, Y. H., Dick, T. E., and DiMarco, A. F. (2013). Diaphragm activation via high frequency spinal cord stimulation in a rodent model of spinal cord injury. *Exp. Neurol.* 247, 689–693. doi:10.1016/j.expneurol.2013.03.006.

Kwon, B. K., Hillyer, J., and Tetzlaff, W. (2010). Translational research in spinal cord injury: a survey of opinion from the SCI community. *J. Neurotrauma* 27, 21–33. doi:10.1089/neu.2009.1048.

Lane, M. A., Lee, K.-Z., Fuller, D. D., and Reier, P. J. (2009). Spinal circuitry and respiratory recovery following spinal cord injury. *Respir. Physiol. Neurobiol.* 169, 123–132. doi:10.1016/j.resp.2009.08.007.

Le Pimpec-Barthes, F., Gonzalez-Bermejo, J., Hubsch, J. P., Duguet, A., Morélot-Panzini, C., Riquet, M., et al. (2011). Intrathoracic phrenic pacing: A 10-year experience in France. *J. Thorac. Cardiovasc. Surg.* 142, 378–383. doi:10.1016/j.jtcvs.2011.04.033.

Le Pimpec-Barthes, F., Legras, A., Arame, A., Pricopi, C., Boucherie, J. C., Badia, A., et al. (2016). Diaphragm pacing: The state of the art. *J. Thorac. Dis.* 8, S376–S386. doi:10.21037/jtd.2016.03.97.

Lepore, A. C., Tolmie, C., O'Donnell, J., Wright, M. C., Dejea, C., Rauck, B., et al. (2010). Peripheral hyperstimulation alters site of disease onset and course in SOD1 rats. *Neurobiol. Dis.* doi:10.1016/j.nbd.2010.03.021.

Lessard, C. S. (2009). *Basic feedback controls in biomedicine*. 1st ed. , ed. J. D. Enderle Morgan & Claypool doi:10.220/S00157ED1V01Y200812BME027.

Levine, S., Nguyen, T., Taylor, N., Friscia, M. E., Budak, M. T., Rothenberg, P., et al. (2008). Rapid disuse atrophy of diaphragm fibers in mechanically ventilated humans. *N. Engl. J. Med.* 358, 1327–35. doi:10.1056/NEJMoa070447.

Linn, W. S., Adkins, R. H., Gong, H., and Waters, R. L. (2000). Pulmonary function in chronic spinal cord injury: a cross-sectional survey of 222 southern California adult outpatients. *Arch. Phys. Med. Rehabil.* 81, 757–763. doi:10.1016/S0003-9993(00)90107-2.

Lonbe, D. I., Amlrada, T., and Howard, M. R. S. (1999). Accuracy of respiratory inductive plethysmography for the diagnosis of upper airway resistance syndrome. *Chest* 115, 1333–1337. doi:10.1378/chest.115.5.1333.

Lucangelo, U., Pelosi, P., Zin, W. A., and Aliverti, A. (2008). *Respiratory system and artificial ventilation*. 1st ed. Milan, Itally: Springer doi:10.1007/978-88-470-0765-9.

MacLeod, J. J. R. (1925). The chemical control of respiration. *Anesth. Analg.* 4, 112???117. doi:10.1213/00000539-192501000-00027.

Mak, I. W., Evaniew, N., and Ghert, M. (2014). Lost in translation: animal models and clinical trials in cancer treatment. *Am. J. Transl. Res.* 6, 114–8. Available at: http://www.ncbi.nlm.nih.gov/pubmed/24489990%0Ahttp://www.pubmedcentral.nih.gov/articlerender.fcgi?artid=PMC3902221.

Mantilla, C. B., Seven, Y. B., Zhan, W. Z., and Sieck, G. C. (2010). Diaphragm motor unit recruitment in rats. *Respir. Physiol. Neurobiol.* 173, 101–106. doi:10.1016/j.resp.2010.07.001.

Marhong, J., and Fan, E. (2014). Carbon Dioxide in the Critically Ill: Too Much or Too Little of a Good Thing? *Respir. Care* 59, 1597–1605. doi:10.4187/respcare.03405.

Masmoudi, H., Persichini, R., Cecchini, J., Delemazure, J., Dres, M., Mayaux, J., et al. (2017). Corrective effect of diaphragm pacing on the decrease in cardiac output induced by positive pressure mechanical ventilation in anesthetized sheep. *Respir. Physiol. Neurobiol.* 236, 23–28. doi:10.1016/j.resp.2016.10.009.

Mauri, T., Eronia, N., Abbruzzese, C., Marcolin, R., Coppadoro, A., Spadaro, S., et al. (2015). Effects of Sigh on Regional Lung Strain and Ventilation Heterogeneity in Acute Respiratory Failure Patients Undergoing Assisted Mechanical Ventilation. *Crit. Care Med.* 43, 1823–1831. doi:10.1097/CCM.0000000000001083.

McDermott, C. J., Shaw, P. J., Cooper, C. L., Dixon, S., Baird, W. O., Bradburn, M. J., et al. (2015). Safety and efficacy of diaphragm pacing in patients with respiratory insufficiency due to amyotrophic lateral sclerosis (DiPALS): A multicentre, open-label, randomised controlled trial. *Lancet Neurol.* 14, 883–892. doi:10.1016/S1474-4422(15)00152-0.

Mercier, L. M., Gonzalez-Rothi, E. J., Streeter, K. A., Posgai, S. S., Poirier, A. S., Fuller, D. D., et al. (2017). Intraspinal microstimulation and diaphragm activation after cervical spinal cord injury. *J. Neurophysiol.* 117, 767–776. doi:10.1152/jn.00721.2016.

Milhorn, H. T. (1966). “The respiratory system,” in *Application of control theory to physiological systems* (Philadelphia, PA: WB Saunders), 230–254.

Molkov, Y. I., Rubin, J. E., Rybak, I. A., and Smith, J. C. (2017). Computational models of the neural control of breathing. *Wiley Interdiscip. Rev. Syst. Biol. Med.* 9, 1–22. doi:10.1002/wsbm.1371.

Molkov, Y. I., Shevtsova, N. A., Park, C., Ben-Tal, A., Smith, J. C., Rubin, J. E., et al. (2014a). A closed-loop model of the respiratory system: Focus on hypercapnia and active expiration. *PLoS One* 9, e109894. doi:10.1371/journal.pone.0109894.

Molkov, Y. I., Zoccal, D. B., Baekey, D. M., Abdala, A. P., Machado, B. H., Dick, T. E., et al. (2014b). Physiological and pathophysiological interactions between the respiratory central pattern generator and the sympathetic nervous system. *Prog. Brain Res.* 212, 1–23. doi:10.1016/B978-0-444-63488-7.00001-X.

Muzzin, S., Baconnier, P. F., and Benchetrit, G. (1992). Entrainment of respiratory rhythm by periodic lung inflation: effect of airflow rate and duration. *Am. J. Physiol.* 263, R292-300. Available at: http://www.ncbi.nlm.nih.gov/pubmed/1510169.

Nagels, J., Làndsér, F. J., van der Linden, L., Clément, J., and Van de Woestijne, K. P. (1980). Mechanical properties of lungs and chest wall during spontaneous breathing. *J. Appl. Physiol.* 49, 408–16. doi:10.1152/jappl.1980.49.3.408.

Nair, J., Streeter, K. A., Turner, S. M. F., Sunshine, M. D., Bolser, D. C., Fox, E. J., et al. (2017). Anatomy and physiology of phrenic afferent neurons. *J. Neurophysiol.* 118, 2975–2990. doi:10.1152/jn.00484.2017.

National Spinal Cord Injury Statistical Center (2018). The 2018 Annual Statistical Report for the Spinal Cord Injury Model Systems.

Nochomovitz, M. L., Dimarco, A. F., Mortimer, T. J., and Cherniack, N. S. (1983). Diaphragm activation with intramuscular stimulation in dogs. *Am. Rev. Respir. Dis.* 127, 325–329. doi:10.1164/arrd.1983.127.3.325 [doi].

Ogilvie, M. D., Gottschalk, A., Anders, K., Richter, D. W., and Pack, A. I. (1992). A network model of respiratory rhythmogenesis. *Am. J. Physiol.* 263, R962-75. Available at: http://www.ncbi.nlm.nih.gov/pubmed/7831394%5Cnhttp://www.ncbi.nlm.nih.gov/pubmed/1415810.

Onders, R. P. (2012). *Functional electrical stimulation: Restoration of respiratory function*. 1st ed. Elsevier B.V. doi:10.1016/B978-0-444-52137-8.00017-6.

Onders, R. P., Elmo, M. J., and Ignagni, A. R. (2007). Diaphragm pacing stimulation system for tetraplegia in individuals injured during childhood or adolescence. *J. Spinal Cord Med.* 30 Suppl 1, S25-9. doi:10.1080/10790268.2007.11753965.

Onders, R. P., Ponsky, T. A., Elmo, M., Lidsky, K., and Barksdale, E. (2011). First reported experience with intramuscular diaphragm pacing in replacing positive pressure mechanical ventilators in children. *J. Pediatr. Surg.* 46, 72–76. doi:10.1016/j.jpedsurg.2010.09.071.

Pavlovic, D., and Wendt, M. (2003). Diaphragm pacing during prolonged mechanical ventilation of the lungs could prevent from respiratory muscle fatigue. *Med. Hypotheses* 60, 398–403. doi:10.1016/S0306-9877(02)00413-9.

Peckham, P. H., and Knutson, J. S. (2005). Functional electrical stimulation for neuromuscular applications. *Annu. Rev. Biomed. Eng.* 7, 327–60. doi:10.1146/annurev.bioeng.6.040803.140103.

Peterson, D. K., Nochomovitz, M. L., DiMarco, A. F., and Mortimer, T. J. (1986). Intramuscular electrical activation of the phrenic nerve. *IEEE Trans. Biomed. Eng.* 33, 342–351. doi:10.1109/TBME.1986.325720.

Petrillo, G. A., and Glass, L. (1984). A theory for phase locking of respiration in cats to a mechanical ventilator. *Am. J. Physiol.* 246, R311-20. Available at: http://www.ncbi.nlm.nih.gov/pubmed/6584038.

Plantier, L., Cazes, A., Dinh-Xuan, A.-T., Bancal, C., Marchand-Adam, S., and Crestani, B. (2018). Physiology of the lung in idiopathic pulmonary fibrosis. *Eur. Respir. Rev.* 27, 170062. doi:10.1183/16000617.0062-2017.

Polla, B., D'Antona, G., Bottinelli, R., and Reggiani, C. (2004). Respiratory muscle fibres: Specialisation and plasticity. *Thorax* 59, 808–817. doi:10.1136/thx.2003.009894.

Posluszny, J. A., Onders, R. P., Kerwin, A. J., Weinstein, M. S., Stein, D. M., Knight, J., et al. (2014). Multicenter review of diaphragm pacing in spinal cord injury: Successful not only in weaning from ventilators but also in bridging to independent respiration. *J. Trauma Acute Care Surg.* 76, 303–310. doi:10.1097/TA.0000000000000112.

Powers, S. K., Shanely, R. A., Coombes, J. S., Koesterer, T. J., McKenzie, M., Van Gammeren, D., et al. (2002). Mechanical ventilation results in progressive contractile dysfunction in the diaphragm. *J. Appl. Physiol.* 92, 1851–1858. doi:10.1152/japplphysiol.00881.2001.

Ratkevičius, A., Skurvydas, A., Povilonis, E., Quistorff, B., and Lexell, J. (1998). Effects of contraction duration on low-frequency fatigue in voluntary and electrically induced exercise of quadriceps muscle in humans. *Eur. J. Appl. Physiol. Occup. Physiol.* 77, 462–468. doi:10.1007/s004210050361.

Resquín, F., Gonzalez-Vargas, J., Ibáñez, J., Brunetti, F., and Pons, J. L. (2016). Feedback error learning controller for functional electrical stimulation assistance in a hybrid robotic system for reaching rehabilitation. *Eur. J. Transl. Myol.* 26, 6164. doi:10.4081/ejtm.2016.6164.

Reynolds, S., Ebner, A., Meffen, T., Thakkar, V., Gani, M., Taylor, K., et al. (2017). Diaphragm activation in ventilated patients using a novel transvenous phrenic nerve pacing catheter. *Crit. Care Med.* 45, e691–e694. doi:10.1097/CCM.0000000000002366.

Ricard, J. D., Dreyfuss, D., and Saumon, G. (2003). Ventilator-induced lung injury. *Eur. Respir. J.* 42, 2s-9s. doi:10.1183/09031936.03.00420103.

Richter, D. W., and Smith, J. C. (2014). Respiratory rhythm generation in vivo. *Physiology (Bethesda).* 29, 58–71. doi:10.1152/physiol.00035.2013.

Riess, J., and Abbas, J. J. (2000). Adaptive neural network control of cyclic movements using functional neuromuscular stimulation. *IEEE Trans. Rehabil. Eng.* 8, 42–52. doi:10.1109/86.830948.

Roussos, C., and Koutsoukou, A. (2003). Respiratory failure. *Eur. Respir. J.* 22, 3s-14s. doi:10.1183/09031936.03.00038503.

Rubin, J. E., Bacak, B. J., Molkov, Y. I., Shevtsova, N. A., Smith, J. C., and Rybak, I. A. (2011). Interacting oscillations in neural control of breathing: Modeling and qualitative analysis. *J. Comput. Neurosci.* 30, 607–632. doi:10.1007/s10827-010-0281-0.

Rybak, I. A., Paton, J. F. R., and Schwaber, J. S. (1997). Modeling neural mechanisms for genesis of respiratory rhythm and pattern. II. Network models of the central respiratory pattern generator. *J. Neurophysiol.* 77, 2007–2026. doi:0022-3077/97.

Sandhu, M. S., Dougherty, B. J., Lane, M. A., Bolser, D. C., Kirkwood, P. A., Reier, P. J., et al. (2009). Respiratory recovery following high cervical hemisection. *Respir. Physiol. Neurobiol.* 169, 94–101. doi:10.1016/j.resp.2009.06.014.

Sauleda, J., Gea, J., Orozco-Levi, M., Corominas, J., Minguella, J., Aguar, C., et al. (1998). Structure and function relationships of the respiratory muscles. *Eur. Respir. J.* 11, 906–911. doi:10.1183/09031936.98.11040906.

Seven, Y. B., Mantilla, C. B., and Sieck, G. C. (2014). Recruitment of rat diaphragm motor units across motor behaviors with different levels of diaphragm activation. *J. Appl. Physiol.* 117, 1308–1316. doi:10.1152/japplphysiol.01395.2013.

Sharp, J. T., Henry, J. P., Sweany, S. K., Meadows, W. R., and Pietras, R. J. (1964). Total Respiratory Inertance and Its Gas and Tissue Components in Normal and Obese Men *. *J. Clin. Invest.* 43, 503–509. doi:10.1172/JCI104936.

Siddiqui, E. A., Jagdale, P., Ahire, K., Jadhav, S., Khan, S. A., Bhosle, S., et al. (2016). Relevance of small laboratory animals as models in translational research: Challenges and road ahead. *J. Appl. Pharm. Sci.* 6, 198–209. doi:10.7324/JAPS.2016.60531.

Simon, P. M., Habel, A. M., Daubenspeck, J. A., and Leiter, J. C. (2000). Vagal feedback in the entrainment of respiration to mechanical ventilation in sleeping humans. *J. Appl. Physiol.* 89, 760–9. Available at: http://hinarilogin.research4life.org/uniquesigjap.physiology.org/uniquesig0/content/89/2/760.abstract.

Simon, P. M., Zurob, A. S., Wies, W. M., Leiter, J. C., Hubmayr, R. D., Jensen, M. L., et al. (1999). Entrainment of respiration in humans by periodic lung inflations: Effect of state and CO2. *Am. J. Respir. Crit. Care Med.* 160, 950–960. doi:10.1164/ajrccm.160.3.9712057.

Siu, R., Abbas, J. J., Hillen, B. K., Gomes, J., Coxe, S., Castelli, J., et al. (2019). Restoring Ventilatory Control Using an Adaptive Bioelectronic System. *J. Neurotrauma*, neu.2018.6358. doi:10.1089/neu.2018.6358.

Slutsky, A. S. (1993). ACCP Consensus Conference - Mechanical Ventilation. *Chest*. doi:10.1378/chest.110.3.866-a.

Smith, B. K., Fuller, D. D., Martin, A. D., Lottenberg, L., Islam, S., Lawson, L. A., et al. (2016). Diaphragm pacing as a rehabilitative tool for patients with Pompe Disease who are ventilator-dependent: case series. *Phys. Ther.* 96, 696–703. doi:10.2522/ptj.20150122.

Smith, J. C., Abdala, A. P., Rybak, I. A., and Paton, J. F. R. (2009). Structural and functional architecture of respiratory networks in the mammalian brainstem. *Philos. Trans. R. Soc. B Biol. Sci.* 364, 2577–2587. doi:10.1098/rstb.2009.0081.

Smith, J. C., Butera, R. J., Koshiya, N., Del Negro, C. A., Wilson, C. G., and Johnson, S. M. (2000). Respiratory rhythm generation in neonatal and adult mammals: The hybrid pacemaker-network model. *Respir. Physiol.* 122, 131–147. doi:10.1016/S0034-5687(00)00155-9.

Smith, J. C., Ellenberger, H. H., Ballanyi, K., Richter, D. W., and Feldman, J. L. (1991). Pre-Bötzinger complex: a brainstem region that may generate respiratory rhythm in mammals. *Science* 254, 726–9. doi:10.1126/science.1683005.

Sollevi, A., and Lindahl, S. G. E. (1995). Hypoxic and hypercapnic ventilatory responses during isoflurane sedation and anaesthesia in women. *Acta Anaesthesiol. Scand.* doi:10.1111/j.1399-6576.1995.tb04200.x.

Song, D., Raphael, G., Lan, N., and Loeb, G. E. (2008). Computationally efficient models of neuromuscular recruitment and mechanics. *J. Neural Eng.* 5, 175–184. doi:10.1088/1741-2560/5/2/008.

Stites, E. C., and Abbas, J. J. (2000). Sensitivity and versatility of an adaptive system for controlling cyclic movements using functional neuromuscular stimulation. *IEEE Trans. Biomed. Eng.* 47, 1287–1292. doi:10.1109/10.867965.

Stubbings, A. K., Moore, A. J., Dusmet, M., Goldstraw, P., West, T. G., Polkey, M. I., et al. (2008). Physiological properties of human diaphragm muscle fibres and the effect of chronic obstructive pulmonary disease. *J. Physiol.* 586, 2637–2650. doi:10.1113/jphysiol.2007.149799.

Teixeira, E., Jayaraman, G., Shue, G., Crago, P. E., Loparo, K., and Chizeck, H. J. (1991). Feedback control of nonlinear multiplicative systems using neural networks: an application to electrically stimulated muscle. in *IEEE International Conference on Systems Engineering*, 218–220. doi:10.1109/ICSYSE.1991.161117.

Tiruvoipati, R., Pilcher, D., Buscher, H., Botha, J., and Bailey, M. (2017). Effects of Hypercapnia and Hypercapnic Acidosis on Hospital Mortality in

Mechanically Ventilated Patients. *Crit. Care Med.* 45, e649–e656. doi:10.1097/CCM.0000000000002332.

Topor, Z. L., Vasilakos, K., Younes, M., and Remmers, J. E. (2007). Model based analysis of sleep disordered breathing in congestive heart failure. *Respir. Physiol. Neurobiol.* 155, 82–92. doi:10.1016/j.resp.2006.04.016.

Trang, H., Dehan, M., Beaufils, F., Zaccana, I., Amiel, J., and Gaultier, C. (2005). The French congenital central hypoventilation syndrome registry: General data, phenotype, and genotype. *Chest* 127, 72–79. doi:10.1378/chest.127.1.72.

Ursino, M., and Magosso, E. (2002). A theoretical analysis of the carotid body chemoreceptor response to O2 and CO2 pressure changes. *Respir. Physiol. Neurobiol.* 130, 99–110. doi:10.1016/S0034-5687(01)00335-8.

Vassilakopoulos, T. (2012). Ventilator-induced diaphragm dysfunction: The clinical relevance of animal models. *Appl. Physiol. Intensive Care Med. 2 Physiol. Rev. Ed.*, 197–206. doi:10.1007/978-3-642-28233-1_20.

Walter, J. S., Wurster, R. D., Zhu, Q., and Laghi, F. (2011). Respiratory muscle pacing with chronically implanted intramuscular Permaloc electrodes: A feasibility study. *J. Rehabil. Res. Dev.* 48, 103. doi:10.1682/JRRD.2010.05.0086.

Wassink, R., and Keller, T. (2004). Sliding Mode Closed-Loop Control of FES: Controlling the Shank Movement. *IEEE Trans. Biomed. Eng.* 51, 263–272. doi:10.1109/TBME.2003.820393.

Weese-Mayer, D. E., Berry-Kravis, E. M., Zhou, L., Maher, B. S., Silvestri, J. M., Curran, M. E., et al. (2003). Idiopathic congenital central hypoventilation syndrome: Analysis of genes pertinent to early autonomic nervous system embryologic development and identification of mutations in PHOX2b. *Am. J. Med. Genet.* 123A, 267–278. doi:10.1002/ajmg.a.20527.

Weese-Mayer, D. E., Rand, C. M., Berry-Kravis, E. M., Jennings, L. J., Loghmanee, D. A., Patwari, P. P., et al. (2009). Congenital central hypoventilation syndrome from past to future: Model for translational and transitional autonomic medicine. *Pediatr. Pulmonol.* 44, 521–535. doi:10.1002/ppul.21045.

Weese-Mayer, D. E., Shannon, D. C., Keens, T. G., and Silvestri, J. M. (1999). Idiopathic Congenital Central Hypoventilation Syndrome. *Am. J. Respir. Crit. Care Med.* 160, 368–373. doi:10.1164/ajrccm.160.1.16010.

West, J. B., and Luke, A. M. (2016). *West's Respiratory Physiology - The Essentials*.

Whitehead, G. S., Kimmel, E. C., Reboulet, J. E., and Still, K. R. (1999). Pulmonary Function in Normal Rats. Wright-Patterson Air Force Base, Ohio, USA Available at: http://www.stormingmedia.us/56/5687/A568763.html.

Wilhelm, F. H., Trabert, W., and Roth, W. T. (2001). Characteristics of sighing in panic disorder. *Biol. Psychiatry*. doi:10.1016/S0006-3223(00)01014-3.

Winslow, C., and Rozovsky, J. (2003). Effect of spinal cord injury on the respiratory system. *Am. J. Phys. Med. Rehabil.* 82, 803–14. doi:10.1097/01.PHM.0000078184.08835.01.

Wolf, G. K., and Arnold, J. H. (2005). Noninvasive assessment of lung volume: Respiratory inductance plethysmography and electrical impedance tomography. *Crit. Care Med.* 33, S163–S169. doi:10.1097/01.CCM.0000155917.39056.97.

Zambon, M., Beccaria, P., Matsuno, J., Gemma, M., Frati, E., Colombo, S., et al. (2016). Mechanical ventilation and diaphragmatic atrophy in critically ill patients: An ultrasound study. *Crit. Care Med.* 44, 1347–1352. doi:10.1097/CCM.0000000000001657.

Zbrzeski, A., Bornat, Y., Hillen, B. K., Siu, R., Abbas, J. J., Jung, R., et al. (2016). Bio-inspired controller on an fpga applied to closed-loop diaphragmatic stimulation. *Front. Neurosci.* 10, 14. doi:10.3389/fnins.2016.00275.

Zimmer, M. B., Nantwi, K., and Goshgarian, H. G. (2007). Effect of spinal cord injury on the respiratory system: basic research and current clinical treatment options. *J. Spinal Cord Med.* 30, 319–30. doi:10.1016/j.expneurol.2007.05.015.

VITA

RICARDO SIU

Born, San Pedro Sula, Cortes, Honduras

2006-2008	A.A., Biology Miami Dade Community College Miami, Florida
2008-2012	B.S, Biomedical Engineering Florida International University Miami, Florida
2012-2013	Research Technician Adaptive Neural Systems Laboratory Florida International University Miami, Florida
2013-2019	Doctoral Candidate Florida International University Miami, Florida
2017-2018	Teaching Assistant Florida International University Miami, Florida
2018	Neuroplasticity Symposium Scholar University of Florida Gainesville, Florida

PUBLICATIONS AND PRESENTATIONS

Castelli, J., Kolbl, F., Siu, R., N'Kaoua, G., Bornat, Y., Mangalore, A., Hillen, B., Abbas J., Renaud S., Jung R., Lewis, N. (2017). *An IC-based controllable stimulator for respiratory muscle stimulation investigations*. In 2017 39th Annual International Conference of the IEEE/EMBS: Smarter Technology for a Healthier World, EMBC 2017 Proceedings (pp. 1970-1973). DOI: 10.1109/EMBC.2017.8037236

Siu R, Hillen B, Thota A, Abbas J, Renaud S, Jung R. *Closed-loop adaptive controller for respiratory pacing in a rodent model*. 2016 UM Neural Engineering Symposium, Miami, FL.

Siu R, Hillen BK, Thota A, Renaud S, Abbas J, Jung R. *Parametrization of a closed-loop adaptive controller for respiratory pacing in a rodent model*. Program No. 249.18. 2016 Neuroscience Meeting Planner. Society for Neuroscience, 2016. San Diego, CA.

Siu R, Abbas J, Hillen B, Renaud S, Jung R. *A neuromorphic system for adaptive closed-loop control of ventilation after spinal cord injury*. 2017 CRCNS PI Meeting, Providence, RI.

Siu R, Abbas J, Hillen BK, Jung R. A *neuromorphic system for adaptive closed-loop control of ventilation after spinal cord injury*. 2017 Biomedical Engineering Society Meeting. Phoenix, AZ.

Siu R, Abbas J, Hillen BK, Jung R. *Adaptive control of ventilation through respiratory pacing following spinal cord injury*. Program No. 779.04. 2017 Neuroscience Meeting Planner. Society for Neuroscience, 2017. Washington, D.C.

Siu R, Abbas J, Hillen B, Renaud S, Jung R. *Adaptive control of ventilation through ventilatory pacing*. 2018 Annual Neuromuscular Plasticity Symposium. Gainesville, FL.

Siu R, Abbas J, Hillen BK, Jung R. *Adaptive closed-loop control of ventilation.* Conference of Florida Graduate Schools 2018. Tallahassee, FL.

Siu R, Abbas J, Hillen BK, Renaud S, Jung R. *Computational validation of a closed-loop neuromorphic controller for ventilatory control*. Computational Neuroscience 2018. Seattle, WA.

Siu R, Abbas J, Hillen BK, Jung R. *Computational assessment of a neuromorphic closed-loop controller for ventilatory pacing*. Biomedical Engineering Society Conference 2018. Atlanta, GA.

Siu, R., Abbas, J.J., Hillen, B.K., Gomes, J., Coxe, S., Castelli, J., Renaud, S., and Jung, R. (2019). *Restoring ventilatory control using an adaptive bioelectronic system*. J. Neurotrauma , neu.2018.6358.

Zbrzeski A, Siu R, Bornat Y, Hillen B, Jung R, Renaud S. *A versatile fast-development platform applied to closed-loop diaphragmatic pacing*. Proceedings of 7th International IEEE/EMBS Conference on Neural Engineering, 2015. Pg.791-794. Doi:10.1109/NER.2015.7146742

Zbrzeski A, Bornat Y, Hillen B, Siu R, Abbas J, Jung R. *Bio-inspired Controller on an FPGA applied to Closed-loop Diaphragmatic Stimulation*. Front Neurosci 2016;10:275. http://dx.doi.org/10.3389/FNINS.2016.00275.